A Geophysical Study of Active Faulting in Fort Bend County, Texas

---

A Thesis Presented to the Faculty of the

Department of Earth and Atmospheric Science

University of Houston

In Partial Fulfillment

of the Requirements for the Degree

Master of Science

BY

Kevin Wayne Schmidt

May 2013

A Geophysical Study of Active Faulting In Fort Bend County, Texas

---

Kevin Wayne Schmidt

Approved:

Dr. Shuhab Khan, Chairman

Dr. Robert Stewart, Member

Dr. Richard Engelkemeir, Member

Dean, College of Natural Sciences and Mathematics

Acknowledgements

My Family

Dr. Shuhab Khan, Dr. Robert Stewart, Dr. Richard Engelkemeir

GeoMap, Neuralog, ElPaso, EP Energy, Seitel, SEI Exchange

George Ranch, Schultz, Fort Bend County, Needville Cemetary

Li Chang, Ady Geda, Jeff Sposato, Anoop William

GEORS Group at University of Houston

A Geophysical Study of Active Faulting in Fort Bend County, Texas

---

An Abstract of a Thesis Presented to the Faculty of the

Department of Earth and Atmospheric Science

University of Houston

In Partial Fulfillment

of the Requirements for the Degree

Master of Science

BY

Kevin Wayne Schmidt

May 2013

Abstract

Several active faults are reported from southeast Texas. These faults have been studied in great detail in Harris County, but little work has been done in Fort Bend County where there are at least four known fault systems. These are the Long Point, Needville, Arcola, and the Addicks fault systems. This study focuses on the Needville and Arcola fault systems in an effort to determine the continuity and displacement along these two fault systems. The purpose of this study is to build on the previous work with the use of the latest tools to identify and understand the faulting mechanisms in the Fort Bend County. This study used Light Detection and Ranging (LiDAR), aerial photographs, Ground Penetrating Radar (GPR), 2D Seismic, Global Positioning System (GPS), gravity, and well logs which proved to be complementary, and work very efficiently together. The LiDAR produced a comprehensive surface model that revealed four faults never reported before, and extended previously recognized faults. The GPR data show disturbance in the fault zone, and provided a link of LiDAR to 2D Seismic data. The 2D Seismic stacked profile displayed a comprehensive vertical section that allowed the Needville Fault to be interpreted to approximately 800 meters. The Well logs provided a source of information to produce a subsurface model that helped identification of the fault locations. The gravity data confirmed that there is a low gravity anomaly in the Needville Fault Zone. GPS suggested movement of 9 cm over 4 years for the Arcola Fault. All these complementary datasets helped create a comprehensive 3D model that demonstrates complex geology in this passive margin of the Gulf Coast.

Contents

Table of Figures

Table of Tables

Chapter 1

1.1 Introduction

Southeast Texas is known to have many normal faults that run parallel to the coast of the Gulf of Mexico, as can be seen in Figure 1-1(Chowdhury & Turco, 2006). Within southeast Texas lies the Houston area which has had multiple studies done that has revealed both regional and local faults. These studies include those of (Ruhl, 1991) and (Engelkemeir & Khan, 2008). These faults that have been found in the Houston area include three major faults through Fort Bend County. They are the Long Point Fault, Arcola Fault, and the Needville Fault, as can be seen in Figure 1-2. These faults cause different kinds of problems than many people consider when thinking of faults. The faults in Fort Bend County move in a relatively continuous sliding motion which can cause areas to slowly grow apart. Also due to this relatively slow continuous motion the faults can be unnoticeable which leads to people building such things as homes right on top of the fault. This relatively slow, continuous movement of the faults is due to the stratigraphy of this region comprising of clay-rich sediments. A surface map of the sediments can be seen in Figure 1-3. The sediments in the area with the lack of rock allows for the aseismic movement along the faults, since the faults have the ability to slide rather than develop strain on hard lithographic beds.

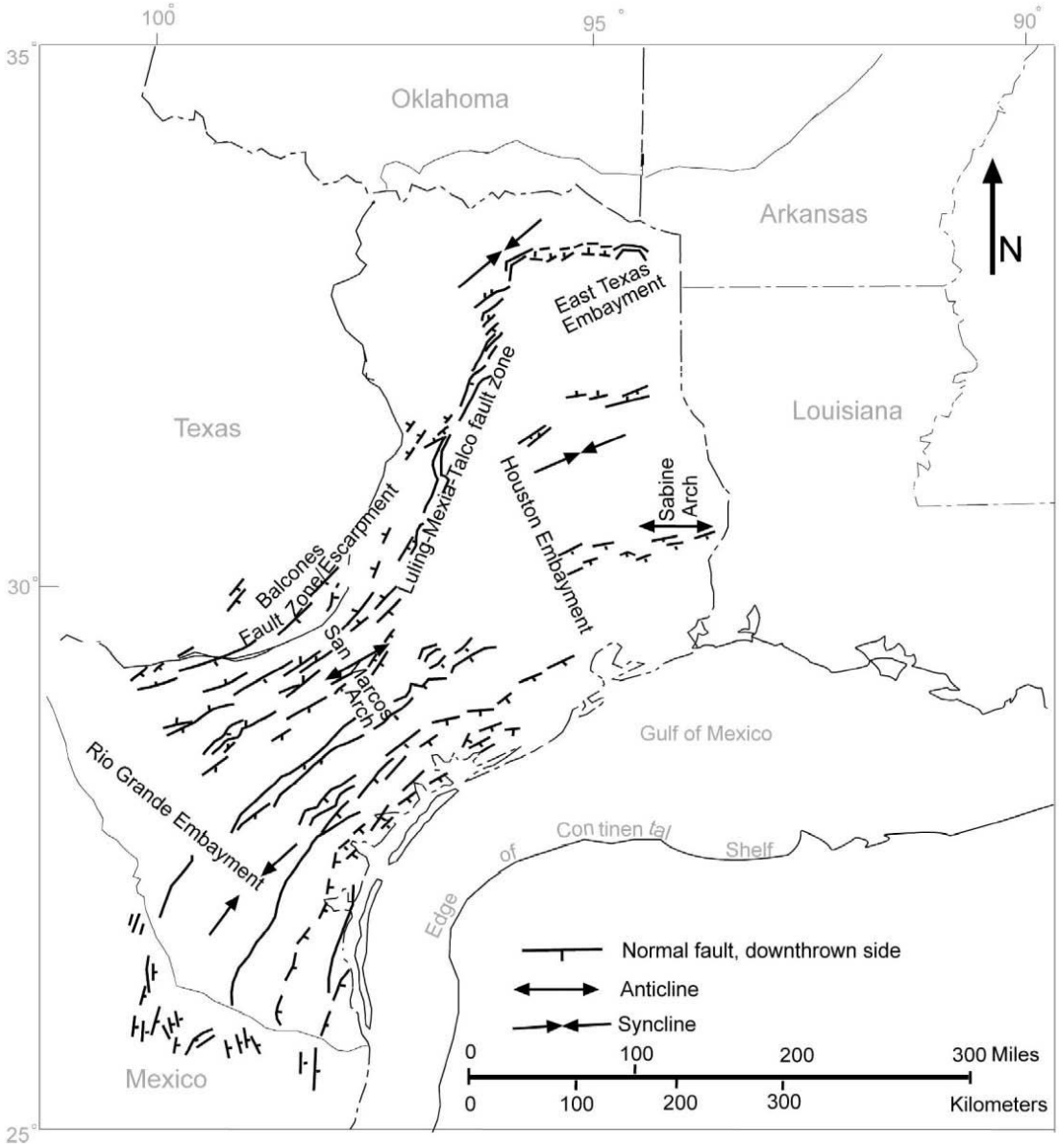

Figure 1-1: Fault location and orientation across southeast Texas. It is evident that there are a large number of normal faults that run parallel and are dipping toward the Texas Gulf Coast. There are also to a lesser extent antithetic faults that run parallel and are dipping away from the Texas Gulf Coast. (Chowdhury & Turco, 2006)

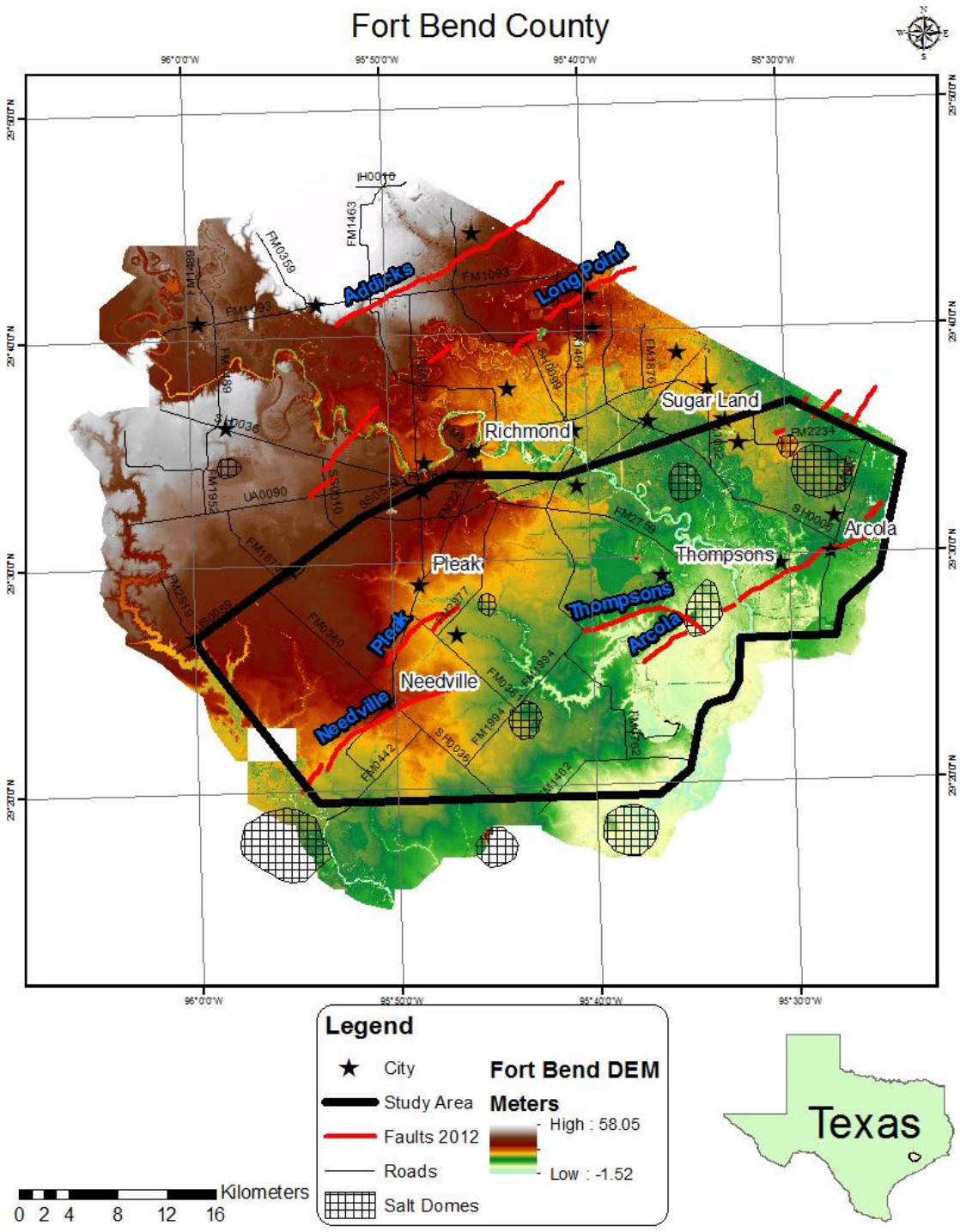

Figure 1-2: Digital Elevation Model (DEM) of study area with location of major faults and salt domes.

This lack of development of a pressure build up means that there will not be any sudden releases of strain, which is what people feel in earthquakes. For this reason most people that live in the Houston area do not even realize that faults are present all along the Texas Gulf Coast. This can be very costly to property owners, since some people or organizations buy their property on top of faults and construct homes, business buildings, and even schools. There have been previous studies done in Fort Bend County, such as Ruhl in 1991, but since the previous studies new technology has been developed that are better able to detect the faults (Ruhl, 1991). Recent studies have been conducted in Harris County using newer technology such as Light Detection and Ranging (LiDAR), Ground Penetrating Radar (GPR), and Global Positioning System (GPS). The use of LiDAR has led to a higher accuracy of mapping faults in the Houston area (Engelkemeir & Khan, 2008). GPS has been used in the Houston area to help monitor surface deformation (Engelkemeir, et al., 2010). For Fort Bend County, this new technology will allow for the faults to be better identified at the surface and then allow the faults to be better tracked through the subsurface. The current technology should be sufficient enough to produce a full cross sectional image of the faults. This will be done by combining multiple techniques to produce a better understanding of the subsurface in Fort Bend County including the mechanisms for why the faulting is occurring. The techniques that will be utilized in this study include LiDAR, GPR, GPS, seismic, gravity, and well logs.

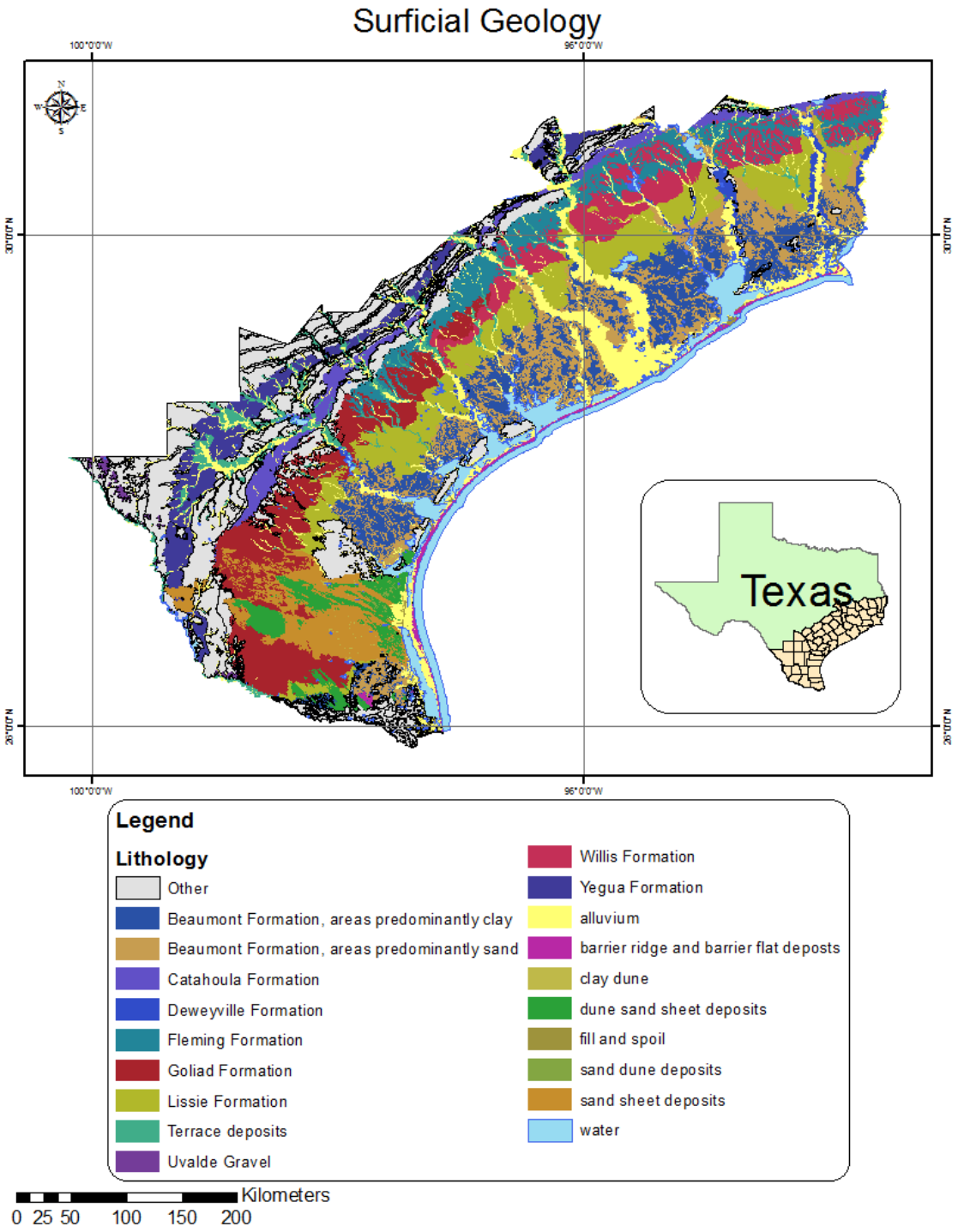

Figure 1-3: Surficial geology across southeast Texas. (TNRIS, 2012)

1.1.1 Attributes of Active Surface Faults

Active faults along the Texas Gulf Coast are different than what people typically think of when they consider faults. Normally when the word fault is brought up the first thing that pops into people's heads is earthquakes and immediate destruction. This however is not the case for the Texas Gulf Coast. Active surface faults have typically been most noticeable when people inadvertently build a structure on top of one. Even when this happens it can be five to ten years before anyone knows that the structure is on top of an active fault. This has to do with the relative slow continuous slip of the faults. Earthquakes are caused from a slow build up of pressure on hard rock formations that instantly break and give way to an abrupt movement. However in the Houston area there is none of these hard rock formations and thus the faulting is more like a very slow moving landslide into the Gulf of Mexico. With this slow movement of the faults there are no fault scarps to speak of in the Houston area, but rather fault inclinations or fault ramps. These fault inclinations occur do to the erosion of the higher fault block, as the lower fault block continues to slide down.

1.2 Objectives

The work focused on the surface and subsurface faulting in Fort Bend County. The primary area of Fort Bend County that was studied is the area south of the Brazos River through south of the city of Needville (Figure 1-2). The main objective was to find the faults on the surface. Then, depending on what data became attainable, it would be

determined how the faults are oriented in the subsurface, and how the subsurface correlates to the surface. This was handled through the use of LiDAR, aerial photographs, GPR, gravity, GPS, seismic, and well logs. Fort Bend County is very characteristic of the geology of the Texas Gulf Coast, and therefore the results from this study provide an idea for what may be found throughout other passive margin regions. This work also provides a methodology for future studies to improve on data integration, and therefore can lead to fewer misinterpretations. A more detailed outline of the objectives can be seen below.

1. Process LiDAR in order to reveal areas of surface faulting and use multiple LiDAR datasets to see rate of displacement along these faults
2. See change in surface faulting using aerial photographs
3. Acquire GPS data from Subsidence district on the up and down thrown sides of the faults and estimate rate of displacements
4. Acquire and process seismic data in order to map the faults at depth
5. Gravity numbers potentially show different content of the ground. This may include that salt uplifts in the area may be a cause or a mechanism for some of the faulting.

6. GPR was conducted perpendicular to a fault to image the faults in subsurface. The GPR helps to connect the surface image of the fault produced through the LiDAR processing and the subsurface image of the faults found through the seismic processing.

7. Obtained well logs and correlated them together in an effort to produce cross sections and structure maps of the area.

8. After all of the data was gathered and processed it was combined to reveal the neotectonic activity of the area. This produces a more understandable image of the area in an effort to bring greater knowledge about the geologic activity that has happened or is still happening in Fort Bend County.

Chapter 2

2.1 Background of Area

In the Houston area there are many active faults. Presently the location of the surface faulting is widely known in Harris County due to decades of mapping of the larger faults, and by more recent efforts of mapping of the smaller faults through the use of the latest technologies. The faulting in the Houston area is commonly believed to be the result of both subsidence and salt diapers throughout the area (Verbeek & Clanton, 1981).

Perhaps one of the most devastating examples of the effect of subsidence would be what happened to the Brownwood Subdivision. The Brownwood subdivision was developed in the late 1930's at about ten feet or less above sea level southeast of Houston. By the late 1970's the area had subsided more than eight feet and was subject to frequent flooding. The subdivision was eventually abandoned after Huricane Alicia in 1983 (Figure 2-1) and turned into a nature center (Coplin & Galloway, 1999).

With the amount of ground deformation that has been observed around the Brownwood Subdivision and places in Harris County it is only logical that Fort Bend County must be experiencing deformation also since it is located mainly southwest of Houston. Much of Fort Bend has been shaped by the Brazos River and the evolution of its meandering across the county as can be seen in Figure 2-2. This meandering history

is very prominent throughout the county with the presence of horseshoe lakes, and many creeks that at one point may have been the main channel for the Brazos River. This meandering has played a key factor in the urbanization of Fort Bend County as most neighborhoods are built behind levees to protect themselves from the Brazos. With Fort Bend County rapidly urbanizing the importance of understanding the geology is becoming greater every day in order to recognize the potential hazards.

Figure 2-1: Image from (Coplin & Galloway, 1999) which shows the Brownwood subdivision in 1983 after hurricane Alicia.

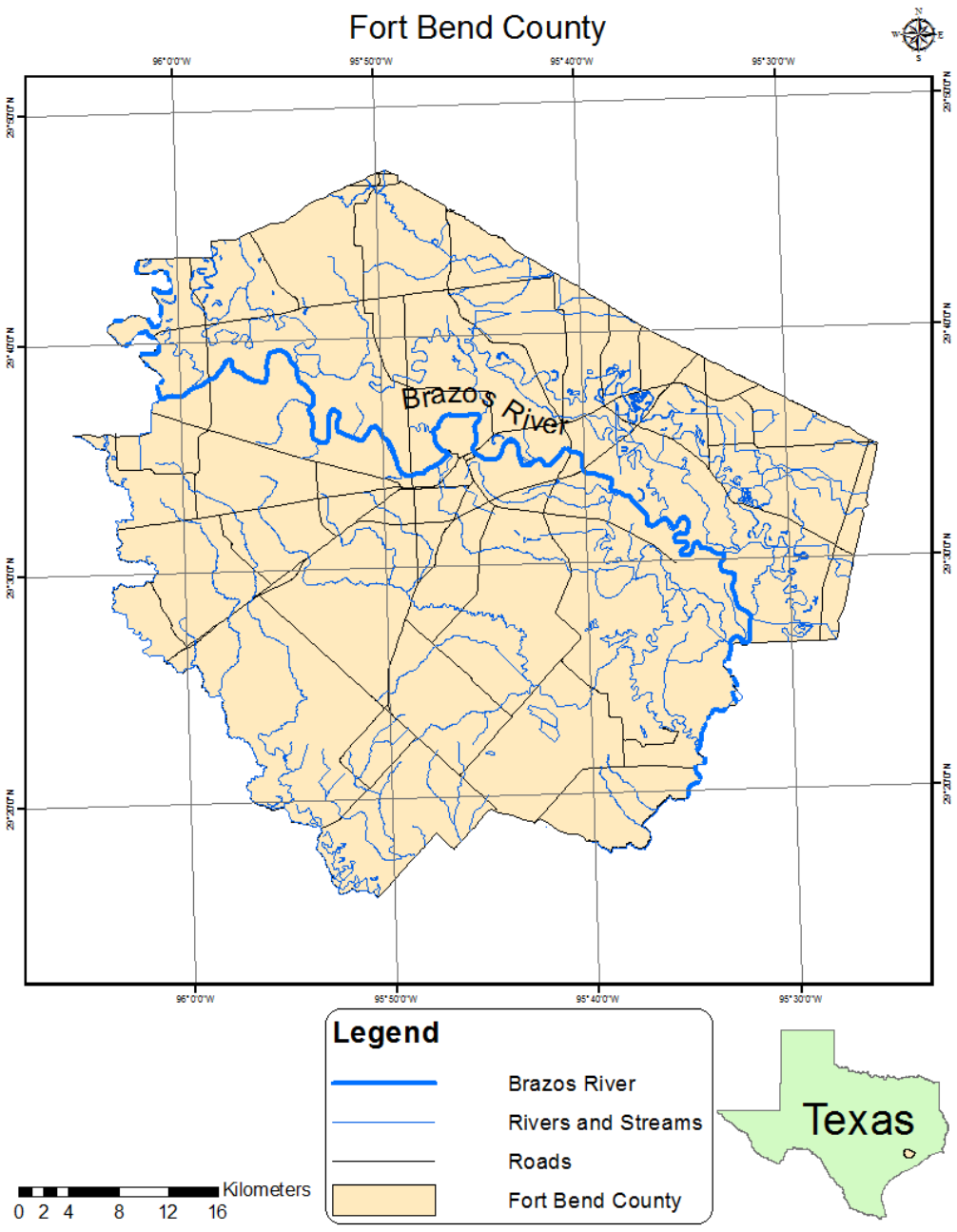

Figure 2-2: Map of Fort Bend County, Texas that shows the locations of rivers and creeks throughout the county.(TIGER, 2012)

2.2 Previous Studies

There have been many studies carried out across Southeast Texas in an effort to better understand the geomorphology of the region. However the largest focus of these studies has been in Harris County with fewer studies in the surrounding areas. Harris County is continuously studied with the newest technologies available. An example of these studies would be that of Engelkemeir (2008). However, Fort Bend County has not been thoroughly studied since 1991 when John Ruhl worked on his Masters thesis (Ruhl, 1991). There have been a lot of new technologies since 1991 that are able to more clearly distinguish the active faulting. Another study was conducted in Brazoria County in 1989 by Justine Boccanera (Boccanera, 1989).

2.2.1 Goldstone Oil Corporation

Greenman and Gustafson finished a study in 1953 on the startigrpahy of Fort Bend County. In this report there is a stratigraphic section correlated to a well log (Figure 2-3), a structure contour map of the top of the Frio Formation (Figure 2-4), and a cross section compiled from eleven well logs (Figure 2-5).

The stratigraphic section in Figure 2-3 ranges from approximately 1200 meters to 2100 meters in depth and reveals what is expected from a Gulf Coast setting. The section shows that there are undifferentiated formations of Miocene age from the top of the section to a depth of approximately 1375 meters. At this depth Oligocene age formations appear starting with the Anahuac, which is clay that ranges from

approximately 1375 meters to 1525 meters. Then the next named formation is the Frio, which is shale with interbedded sand that ranges from approximately 1525 meters to 2015 meters. Then the next formation is the Vicksburg, which is a lignitic shale that ranges from the base of the Frio to off the bottom of the statigraphic section.

The structure contour map of the Frio (Greenman & Gustafson, 1953) reveals that there are many faults passing though the Needville Field. All of these faults are trending in a northeast to southwest orientation, which is expected since this conforms to the regional scale faulting that is seen in Figure 1-1. One thing that is interesting to note is that there are both antithetic and normal faulting occurring through the Needville Field. This is important in that the regional scale normal and antithetic faulting in Figure 1-1 can also be seen in the much more local scale of Needville Field.

From the cross section that was created from the correlation of eleven well logs it becomes very clear of the complexity of the faulting through the Needville Field. There are numerous normal and antithetic faults that have produced significant offsets in the strata of what appears to be as much as 90 meters for the Anahuac, and as much as much as 240 meters for the Vicksburg.

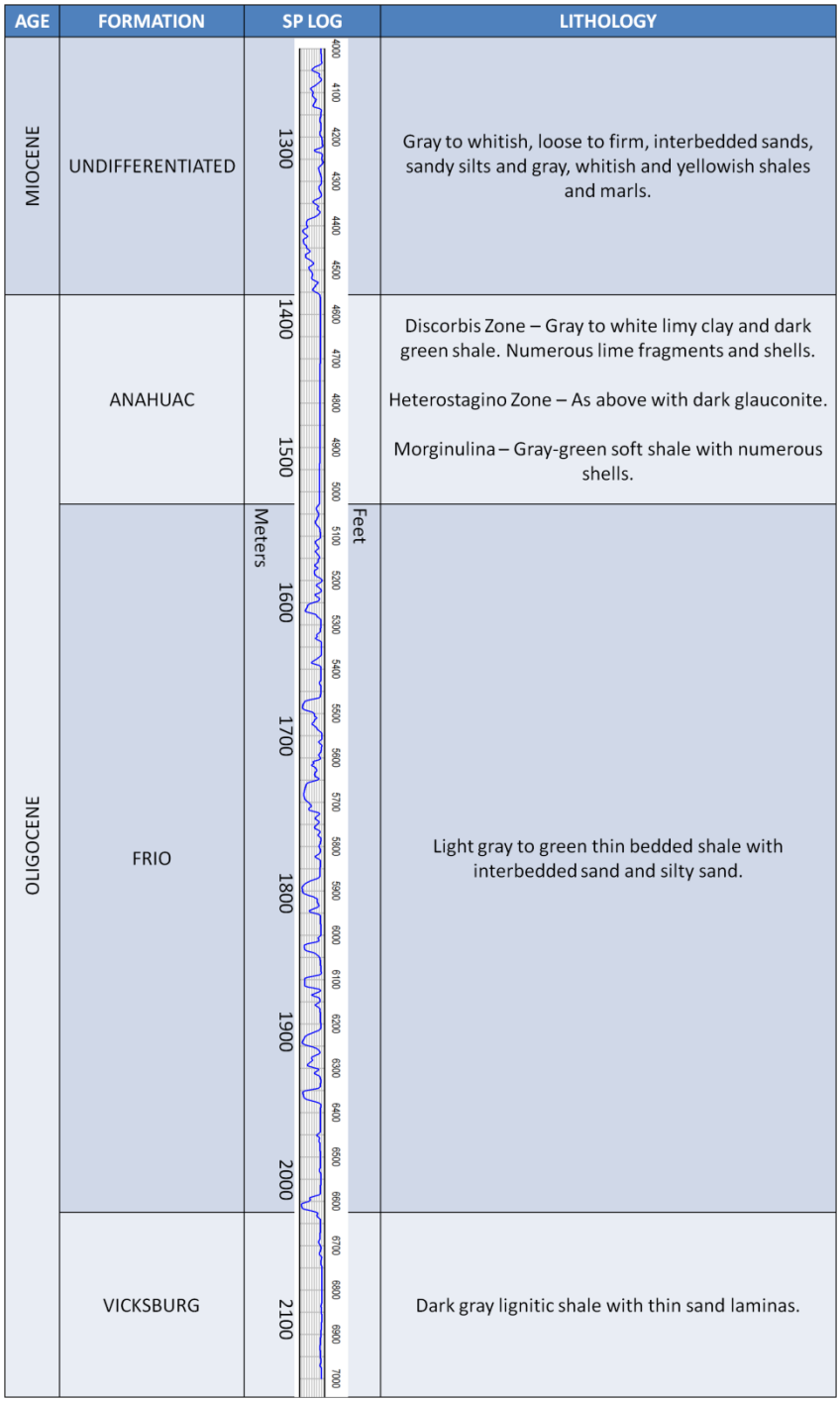

Figure 2-3: Typical stratigraphy in the Needville area. Figure modified from Greenman & Gustafson (1953).

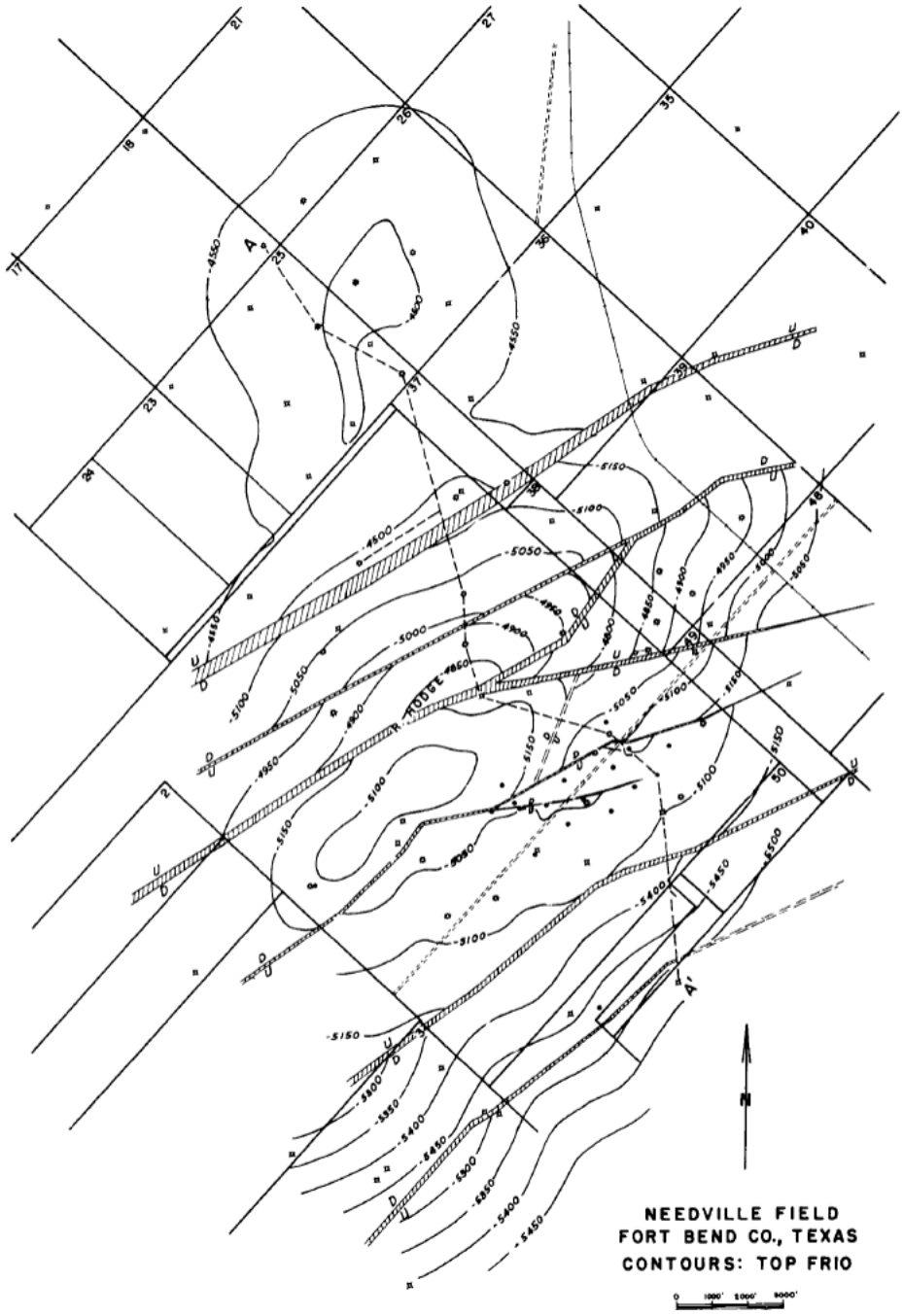

Figure 2-4: Structure contours of the top of the Frio formation with interpreted faulting.(Greenman & Gustafson, 1953)

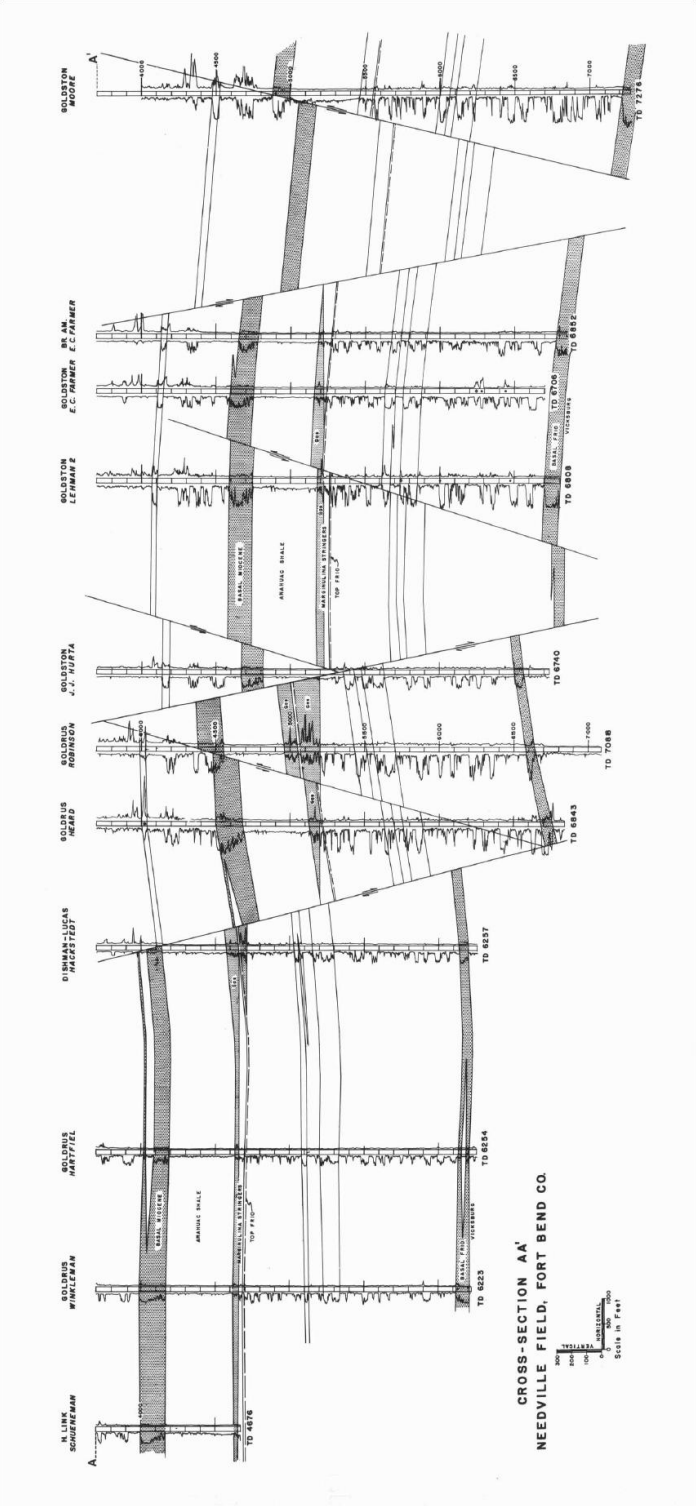

Figure 2-5: Cross section compiled from eleven well logs. (Greenman & Gustafson, 1953)

2.2.2 Engelkemeir

In 2008 Engelkemeir finished a PhD Dissertation on evaluating Houston area neotectonics using GIS and remote sensing techniques. In this dissertation Engelkemeir used LiDAR, seismic, GPR, and GPS in an effort to better identify the faulting throughout Houston. His study suggested that with the newer technologies the faults around the Houston area can be better identified and understood in relation to movement (Engelkemeir, 2008).

2.2.3 Boccanera

Boccanera (1989) finished a Masters Thesis on surface faulting through the use of aerial photograph reconnaissance, field investigations, interpretation of well log and seismic data, and application of predictive models to better identify the faulting throughout Brazoria County. This study provided evidence of 130 faults in Brazoria county. Of these faults approximately 70% were found to follow the regional faulting trend with the remaining 30% comprised of faulting associated with the radial faulting from salt tectonics (Boccanera, 1989).

2.2.4 Harris Galveston Subsidence District and Fort Bend Subsidence District

Subsidence plays a large role in faulting in the Houston area. Luckily the Harris Galveston Subsidence District (HGSD) conducts ongoing studies in Harris and Galveston Counties along with a partnership with the Fort Bend Subsidence District (FBSD). These two organizations use Continuously Operating Reference Stations (CORS) along with

Port-A-Measure (PAM) stations in order to monitor the subsidence around the Houston area. The CORS are permanent stations that have a permanent GPS located at them. A PAM is a permanent location that has a portable GPS stationed at the location on a rotating basis (Harris Galveston Subsidence District). From these stations along with other information the HGSD was able to produce a subsidence map of the Houston area as seen in Figure 2-6. From this figure it is noticeable that the largest amount of subsidence is to the east and southeast of Houston.

2.3 Importance of this Study

By combining the multiple technologies a clearer understanding of the area can be determined and therefore can help in understanding some of the mechanisms that are behind the faulting. This will also allow more knowledge for the area as it continues to urbanize and produce oil and gas. By having this knowledge it may lead to better city planning in order to avoid possible hazards or to allow for better engineering design of any structures that must be placed across a faulting zone.

One possible hazard is that of drilling through faults. This can cause multiple problems such as tension, lateral compression, axial compression, shear, and bending of the well bore and casing (Fjaer et al., 2008).

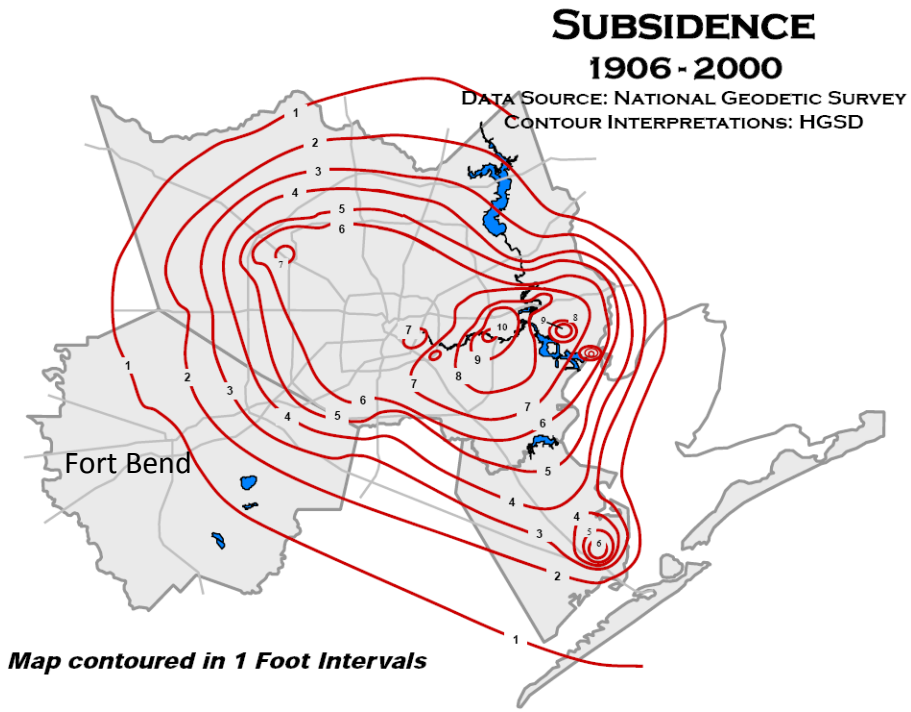

Figure 2-6: Subsidence map of the Houston area from the Harris Galveston Subsidence District.

Chapter 3

3.1 Techniques Used in this Study

The techniques used in this study include Aerial Photographs, LiDAR, GPS, well logs, seismic, gravity, and GPR. The reasoning for using so many different types of technologies all in one survey is to be able to obtain a greater understanding of what is happening. If only one type of technology is used you may think you know a great deal about what you are observing, when actually you are just seeing an illusion or noise. Think about seeing a huge fault scarp. You see it in person, with LiDAR, and aerial photographs so you may assume it to be a fault. Then you look at well logs and seismic and nothing is actually there, so who knows what you are actually looking at but at least you now know it may not be as straight forward as initially imagined.

LiDAR provides a very precise surface model of which aerial photographs can be draped over. GPR then provides information about the near subsurface. Seismic provides information deeper below what GPR can see. Well logs provide sparse horizontal data, but offer a complete vertical section at their locations. GPS can provide rate and directions of movement. Gravity can provide information about possible composition of the ground throughout the area on a large scale basis.

The techniques that were used in this study to confirm the presence of faulting for each fault system in Fort Bend County can be seen in the following Table 3-1. The

techniques used for each fault was dependant on multiple factors. These factors include data availability, computing capacity, land access, and time constraint of this study.

Fault	GPS	LiDAR	GPR	Seismic	Well Logs	Gravity	DOQQ	Field Observation
Needville		X	X	X	X	X	X	X
Arcola	X	X					X	X
Addicks		X						
Long Point		X						
Pleak		X						
Thompsons		X			X			

Table 3-1: Type of data used for each fault that was mentioned observed in this study.

3.1.1 GPS

GPS data from the Harris Galveston Subsidence District and the Fort Bend Subsidence District was used in order to visualize the ground movement in Fort Bend County. Rate of movement for faults is estimated from the difference of GPS data on the hanging wall and footwall of faults.

One unique aspect of the faulting along the Texas Gulf Coast is that typically both the hanging and footwalls are moving down in elevation. This is partially an effect of the relatively soft and looser sediments of the coastal areas that are constantly compacting. Another cause of this around urban areas is due to water withdrawal and to a lesser extent hydrocarbon withdrawal.

3.1.2 LiDAR

LiDAR is a fairly new technology that's potential is still being realized. The purpose of LiDAR in this study was to create a surface image of Fort Bend County in

order to reveal areas in which the faults are visible on the surface. The ideal place for LiDAR to work is in areas that are undisturbed by human activity, and that has no trees or vegetation. This is due to the nature of how LiDAR works in that the laser shot down to the first object it hits, and then reflects back to the sensor on the plane. This is great if a 3D elevation model of a city or trees is required, but bad for having a bare earth surface model. Also with the raw LiDAR data you will find that there are outliers that have to be removed. One reason for these outliers has to deal with the fact that when the laser hits an object on earth, the signal may not bounce directly back, but may be diffracted and bounce around a little before getting picked back up by the sensor on the plane. To help with all of this confusion and noise produced from the multiple problems is partially why the LiDAR data is quantified into multiple levels of returns. The ideal situation rarely occurs though, and therefore there are workarounds for producing a bare earth model in areas that have been altered from their natural state, or that have trees present. For this there are many filters you can create to classify the LiDAR data. These filters include such things that are based on geometric shape, earth's curvature, and elevation difference from one point to the nearest surrounding points. With all filters and processing comes a downside of reducing detail in data. For this reason it is very important to think of the scale at which the faulting is occurring in Fort Bend County. For people that are familiar with the Houston area it is obvious that there are no large scale cliff faces that have formed in the area due to the faulting. Most people

visiting or living in the Houston area would never even realize that a fault is present due to how small the surface deviations are between the up thrown and downthrown sides of the faults. This small deviations in the surface elevations produces a difficulty in that by looking at Fort Bend County as one bare earth DEM LiDAR image would reveal very little, since the topography changes in Fort Bend County range from close to sea level to around fifty eight meters above sea level, and the fault displacements that are trying to be identified are on the scale of centimeters.

The LiDAR used in this study was acquired by Merrick & Company in 2005 using the North American 1983 Harn state plane coordinate system. The metadata for the LiDAR notes that the data has a vertical positional accuracy of 0.27 feet or 8.23 cm. The LiDAR was obtained in LAS format, which in order for this to be a workable format in ArcGIS requires the repetition of a few steps, and much time. To simplify the process of converting from LAS to a more usable and manipulative format model builder was used to create a new ArcGIS tool as seen in Figure 3-1. This model took forty five hours and fifty minutes to complete for the 2005 Fort Bend LiDAR data.

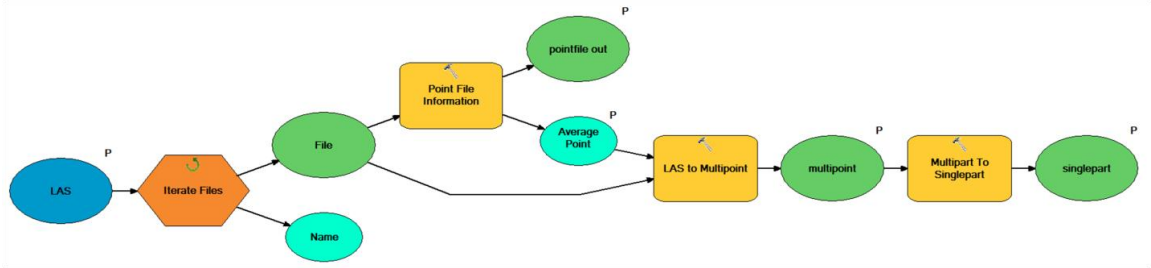

Figure 3-1: ArcGIS model builder model that converts LiDAR .las files to multipoint ArcGIS shapefiles, and then to singlepart ArcGIS shapefiles.

From the resulting file format the LiDAR data points can then be analyzed in a point cloud cluster. From doing this reveals that there are still many outliers in the data. To identify and remove these required the use of height information from each point. Another new tool was created using model builder as seen in Figure 3-2. This model took seventy hours and twelve minutes to complete for the 2005 Fort Bend LiDAR data.

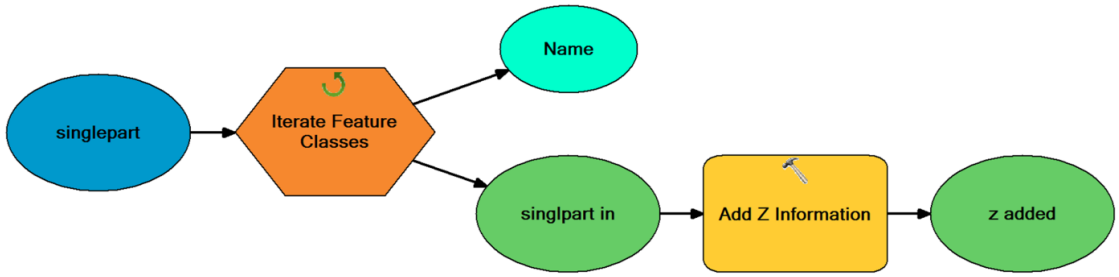

Figure 3-2: ArcGIS model builder model which adds z information to singlepart ArcGIS shapefiles.

Once the Z information was added it was necessary to create a tin and then a raster image of the data while excluding the outlier data points. To simplify the process the model in Figure 3-3 was created. This model took twenty five hours and nine minutes to complete for the 2005 Fort Bend LiDAR data.

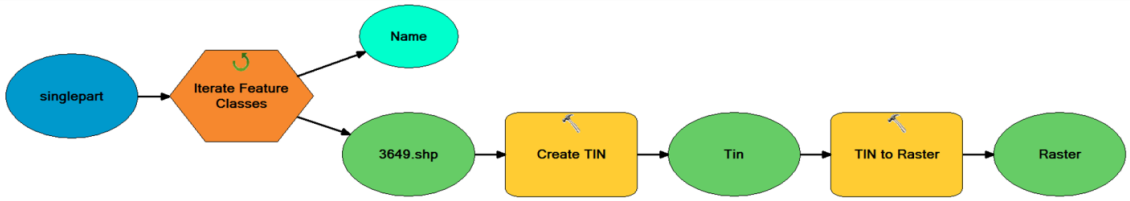

Figure 3-3: ArcGIS model builder model which converts singlepart ArcGIS shapefiles to triangulated irregular networks (TIN) and then to a raster.

A combined version of the models in Figure 3-1, Figure 3-2, and Figure 3-3 can be seen in Figure 3-4.

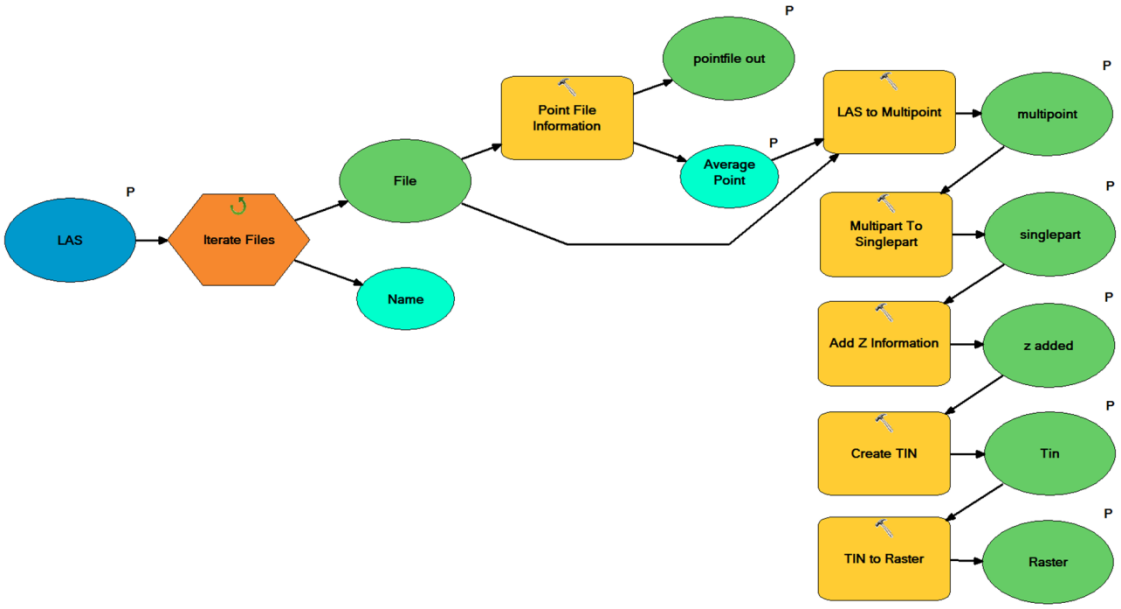

Figure 3-4: A combined version of the previously mentioned ArcGIS model builder tools which ultimately converts LiDAR in .las format to digital elevation models (DEM) in a raster format.

After creating the raster images it was found necessary to produce hillshades of the images. To simplify this process the model in Figure 3-5 was created. Unfortunately the time for running this model was not recorded for the 2005 Fort Bend LiDAR data.

The most useful hillshade parameters that can be used for Fort Bend County were found

to be using an azimuth of 315° and an altitude of 45°. This means that an image will be created that emulates the effect of a light being shined on the area from the northwest at an angle of 45° from the horizon. The azimuth of 315° is ideal for the faults that trend in a northeast to southwest orientation, but does nothing to help in the distinguishing of the faults that run in a northwest to southeast orientation. Therefore this setting for the azimuth should reveal the major faulting through the area, but will nothing to help in distinguishing the smaller faults that radiate around the salt domes. The altitude of 45° was determined due to the typical length of the faults in the area, along with the typical relief that is found from these faults. If the relief from the faults was much greater and the straightness of the surface faults was much greater, then a higher altitude could be used than 45°. The same is true in the other direction. For this reason an altitude of 45° degrees is a fair comprise between the two extremes of 0 and 90 degrees.

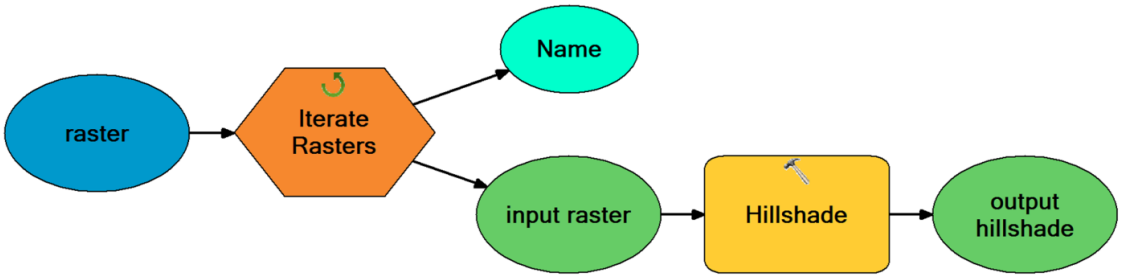

Figure 3-5: ArcGIS model builder model which takes the DEMs produced from the previous models and interprets hillshade images.

By creating a hillshade of the entire Fort Bend County it allowed the fault scarps to be more distinguishable than that of just the DEM, but not at the Fort Bend County scale. This can be seen in Figure 3-6. Looking at this figure you can see that there were

some technical problems that were encountered which created blank lines in the hillshade. Many different attempts were made to lessen the extent of these flaws in the hillshade, but no solution was determined.

Overlaying the hillshade with thirty three percent transparency on the DEM makes for an interesting result of even more clarity, but once again not at the Fort Bend County scale. This can be seen in Figure 3-7.

For this reason it is necessary to create subsets of Fort Bend County in which these details can become clear. By mosaicing smaller sections of Fort Bend County, it allows for the colors in the DEM to be spread out over smaller amounts of elevation, and therefore enhances the ability to distinguish smaller amounts of elevation change. For this reason DEM subsets were made of the Needville, Arcola, Addicks, Long Point, Pleak, and Thompsons faults.

From the mosaiced subset of the Needville fault in Figure 3-8, it is easily seen that the northwest side is at a higher elevation that the southeast side.

From the mosaiced subset of the Arcola fault in Figure 3-9, it is easily seen that the northwest side is at a higher elevation that the southeast side.

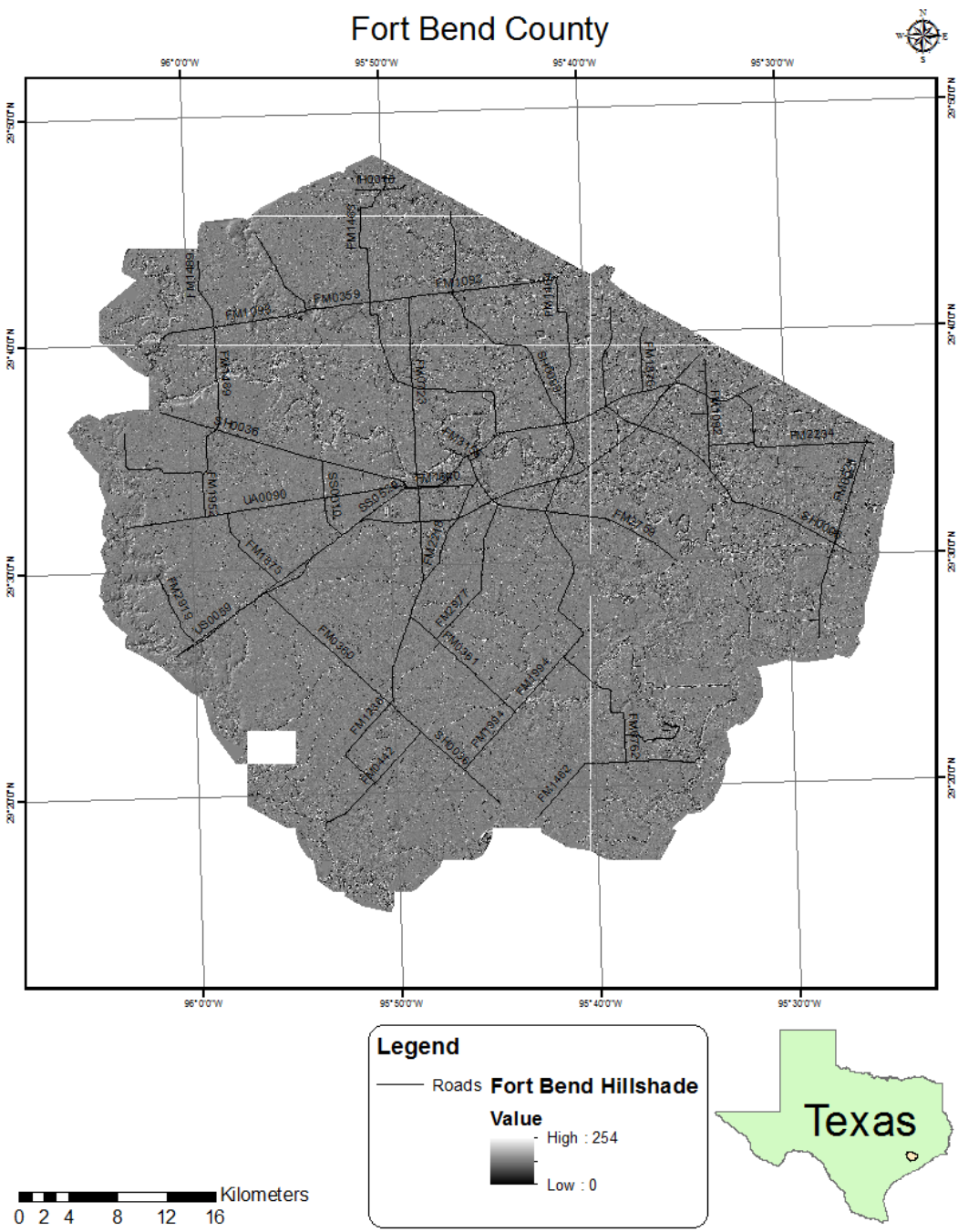

Figure 3-6: Fort Bend County Hillshade produced from the DEM that was produced from 2005 LiDAR data.

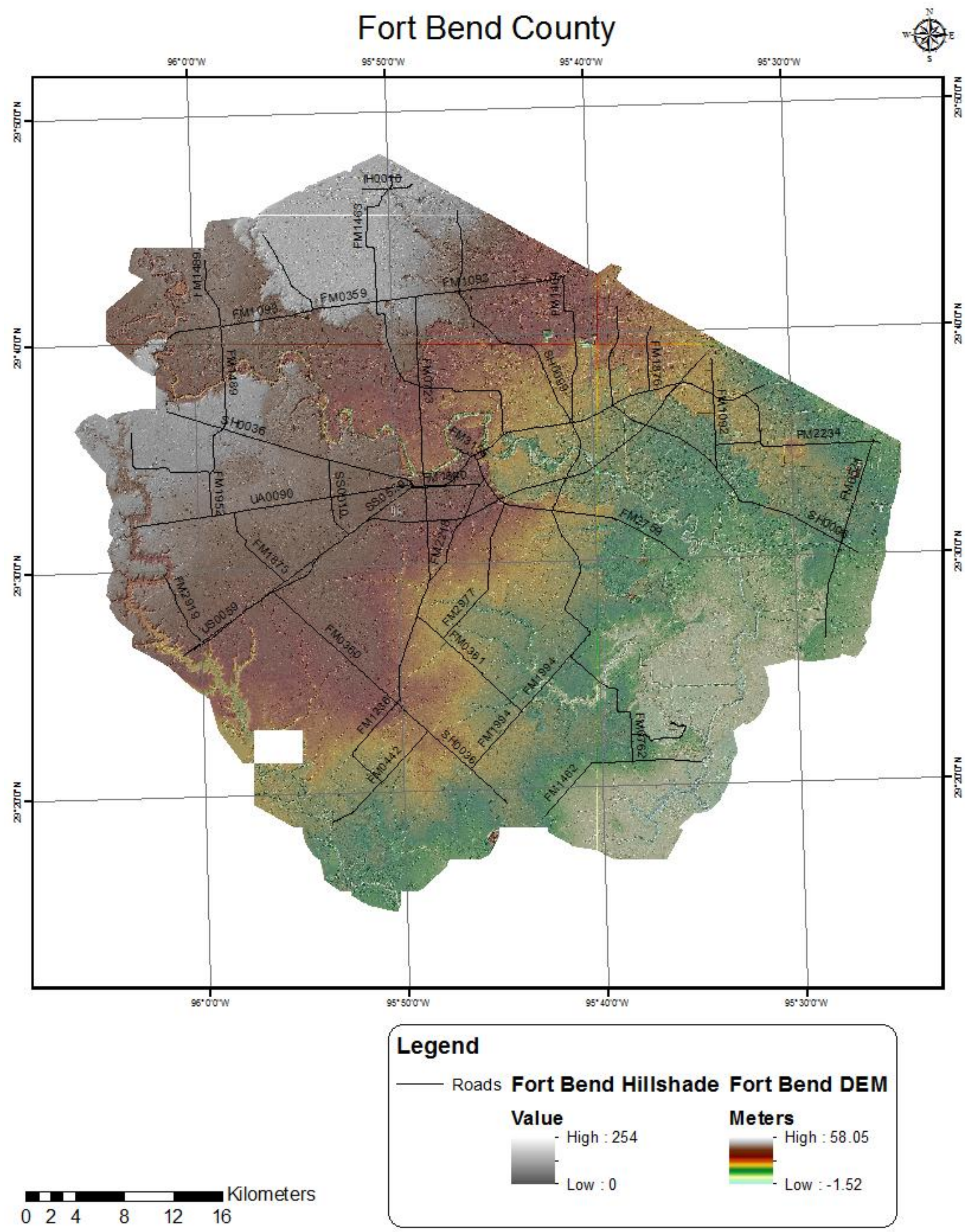

Figure 3-7: Fort Bend County with a hillshade overlaid on a DEM to better reveal areas of faulting.

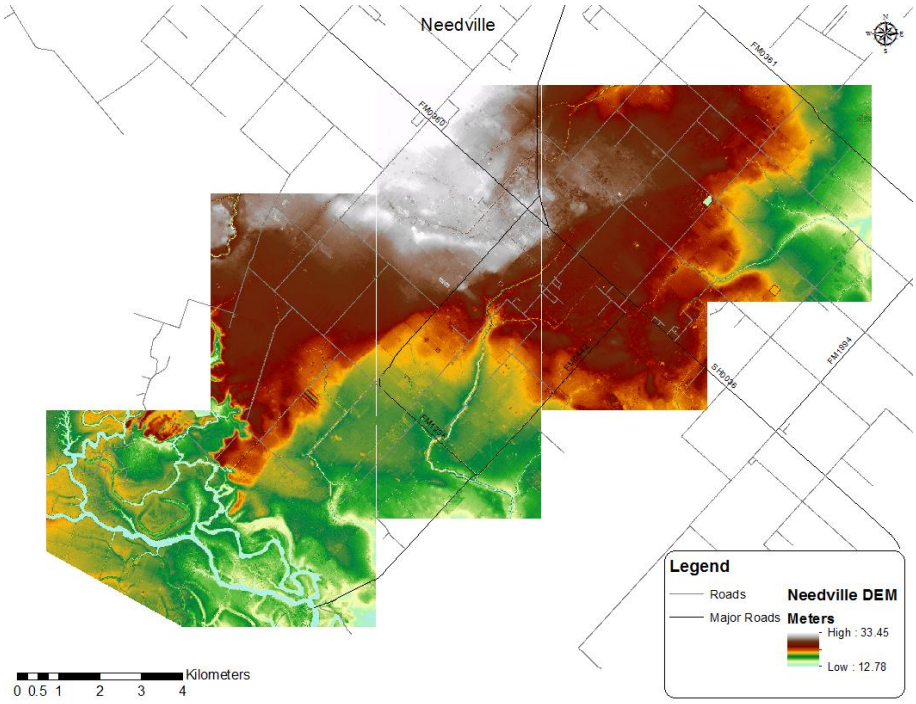

Figure 3-8: Needville DEM produced from 2005 LiDAR data.

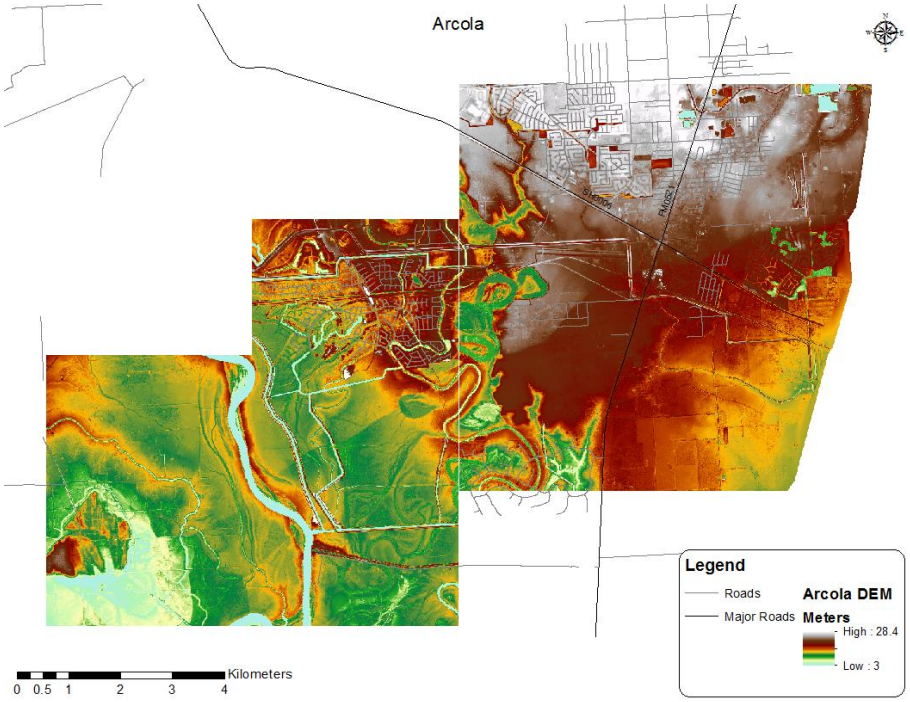

Figure 3-9: Arcola DEM produced from 2005 LiDAR data.

The Addicks fault is a little harder to see in Fort Bend County in this set of LiDAR than that of the Needville and Arcola faults, but it is still visible and clear that the northwest side is higher than the southeast side. This can be seen in Figure 3-10.

The Long Point fault is much like the Addicks fault in terms of visibility as seen in Figure 3-11, but the Northwest is still higher than the Southeast.

The Pleak faults as seen in Figure 3-12 is on a much smaller scale than that of the other faults and is in a far less developed area than the Addicks or Long Point fault. For these reasons the LiDAR displays these two faults very clearly and that on both of them the northwest side is higher than the southeast side. The Pleak faults were not able to be confirmed from aerial photography, or by field observation. As the Pleak faults were not a focus in this study no further attempts were made to confirm this fault.

Around Thompsons there are multiple faults. This is the effect of the Thompsons salt dome. For this reason the faulting in this area becomes very difficult to distinguish, because there is so much faulting occurring in all different directions with both normal and antithetic faulting outcropping at the surface as can be seen in Figure 3-13.

Also by creating the smaller subsets the hillshades become much more interesting as seen in Figure 3-14, Figure 3-15, Figure 3-16, Figure 3-17, Figure 3-18, and Figure 3-19.

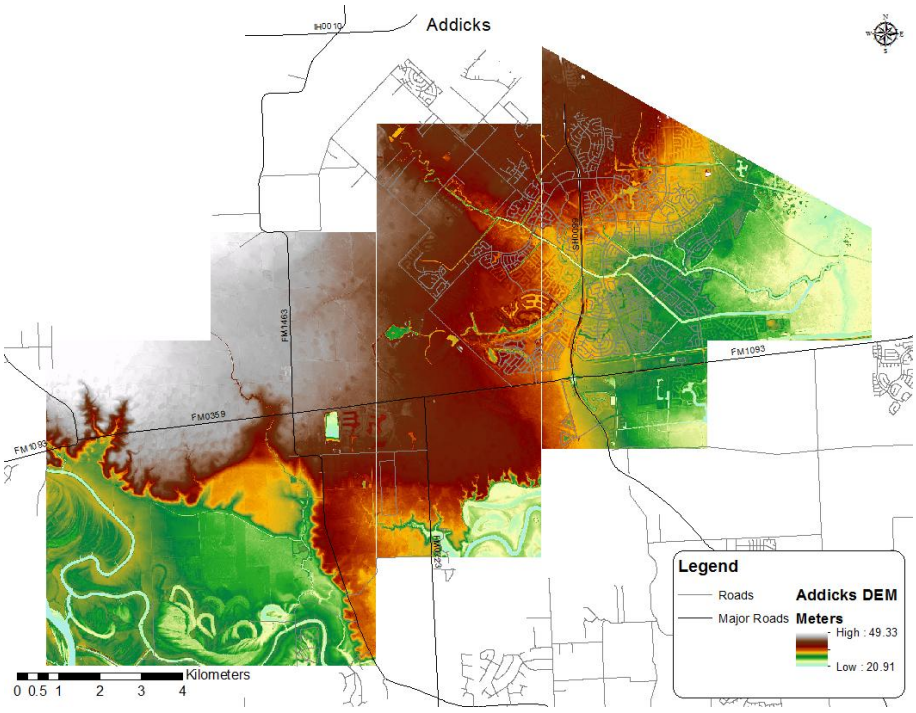

Figure 3-10: Addicks DEM produced from 2005 LiDAR data.

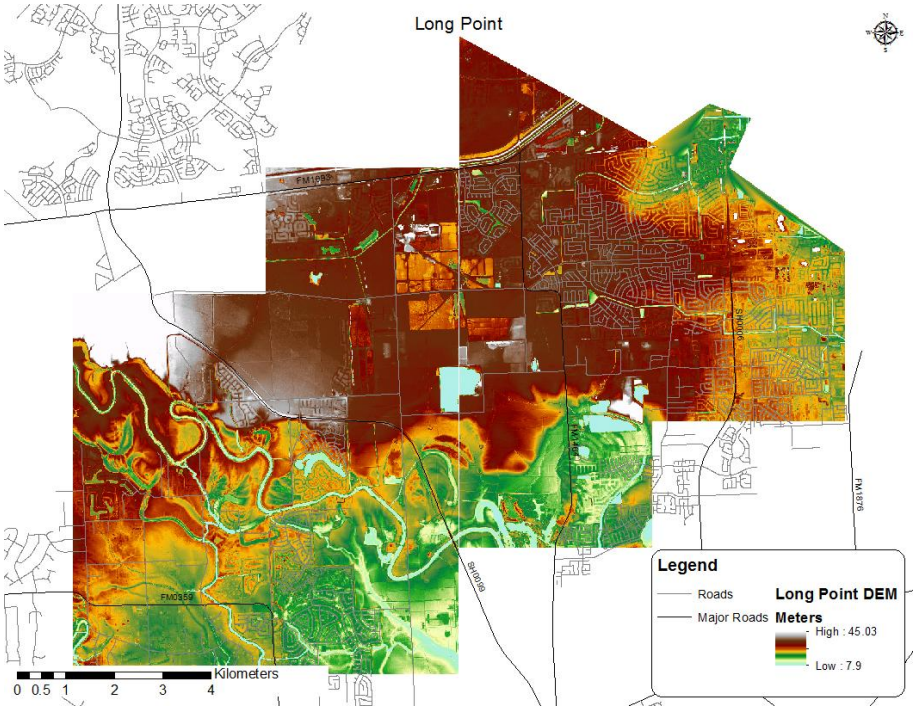

Figure 3-11: Long Point DEM produced from 2005 LiDAR data.

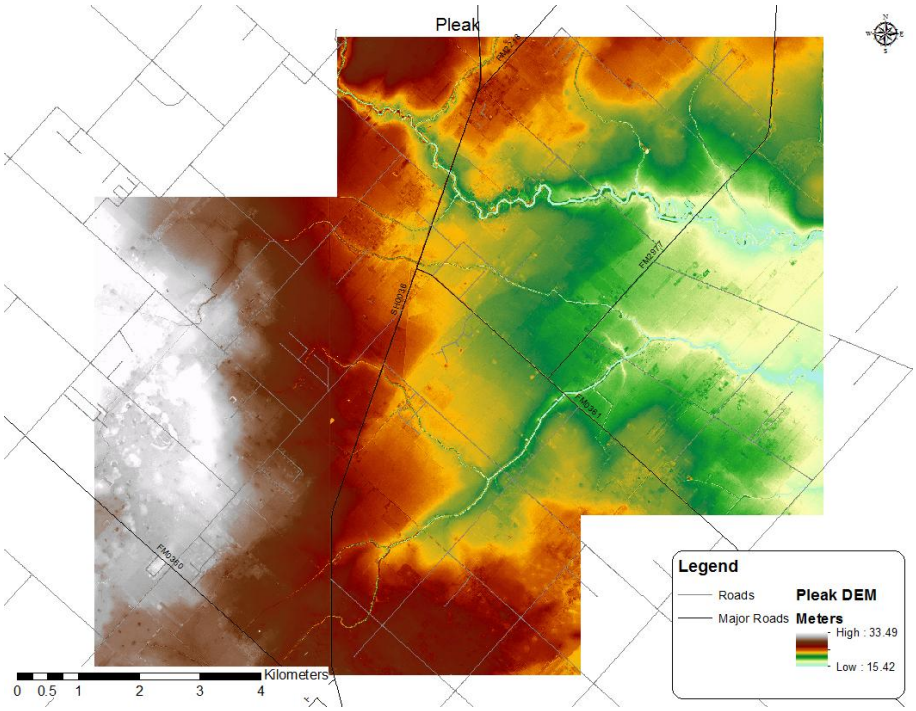

Figure 3-12: Pleak DEM produced from 2005 LiDAR data.

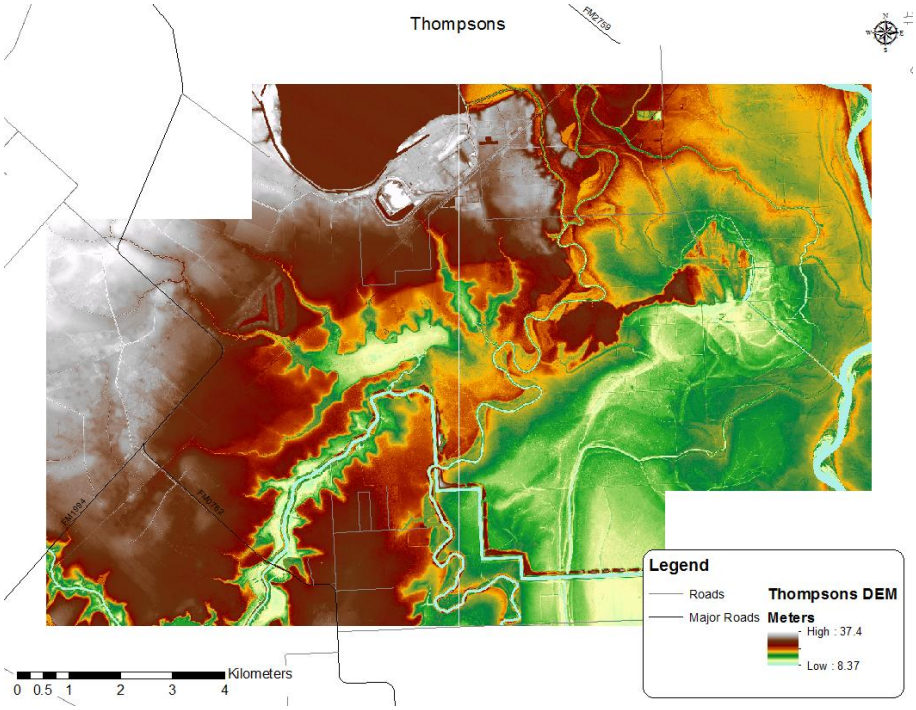

Figure 3-13: Thompsons DEM produced from 2005 LiDAR data.

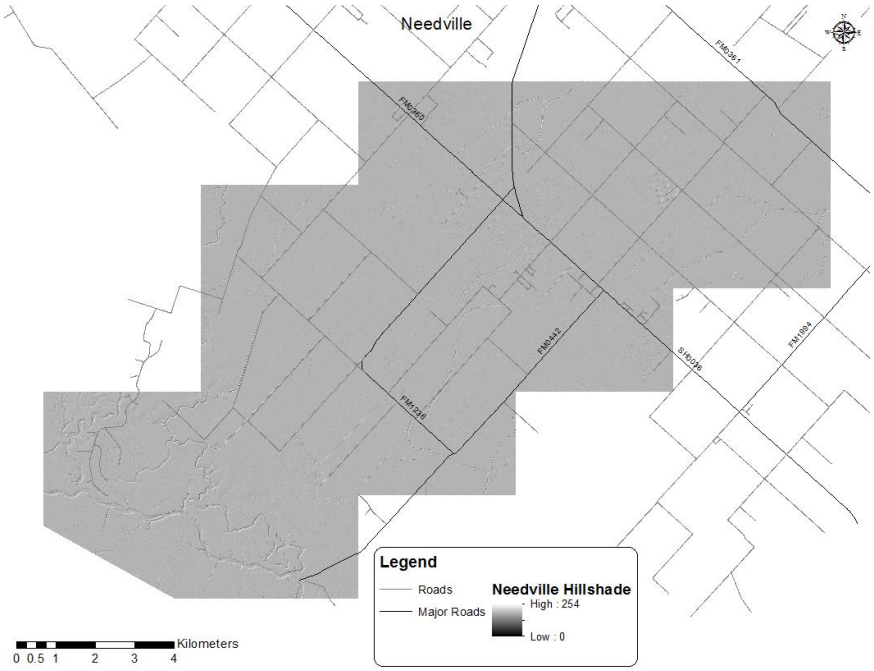

Figure 3-14: Needville hillshade produced from the DEM that was produced from 2005 LiDAR data.

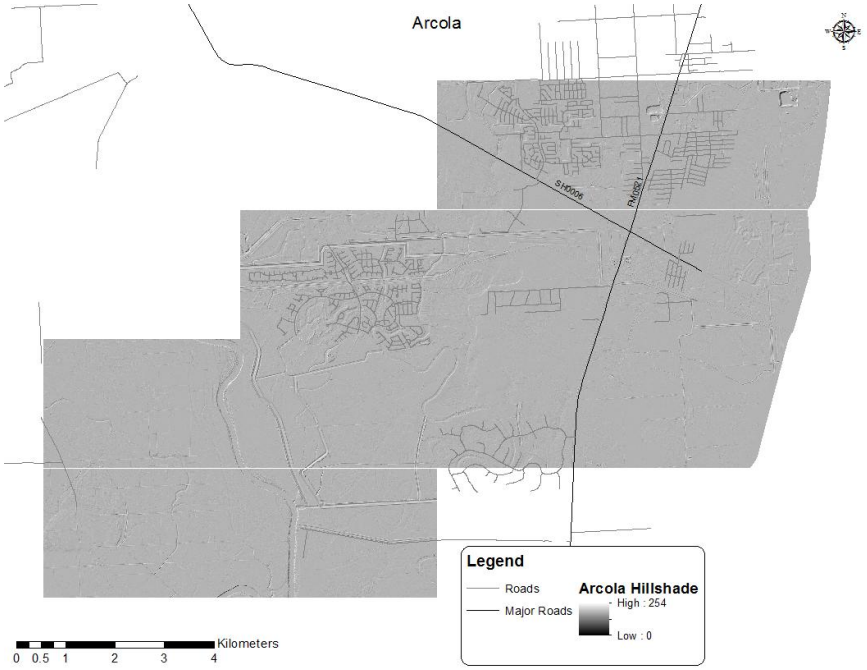

Figure 3-15: Arcola hillshade produced from the DEM that was produced from 2005 LiDAR data.

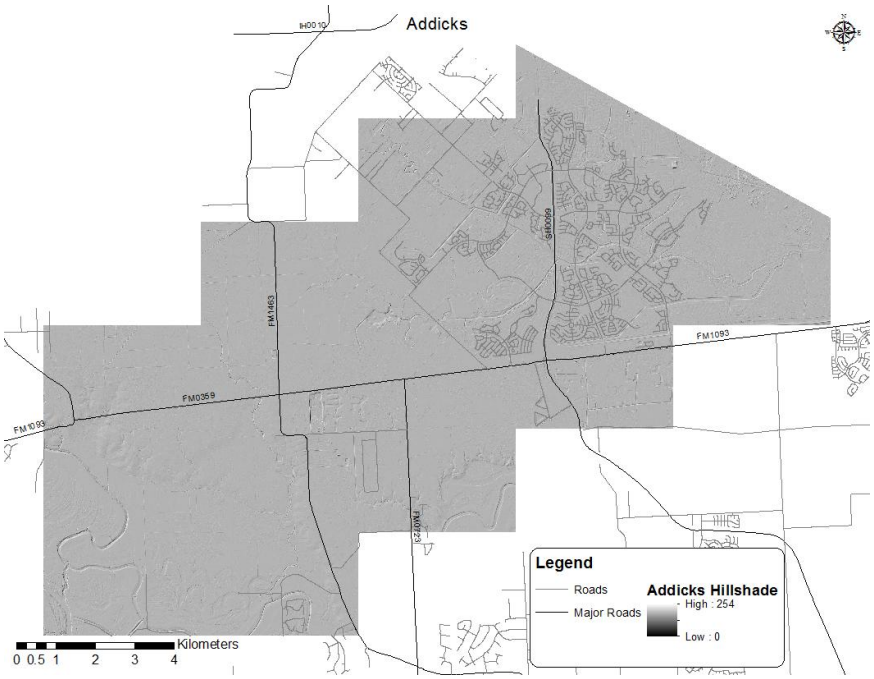

Figure 3-16: Addicks hillshade produced from the DEM that was produced from 2005 LiDAR data.

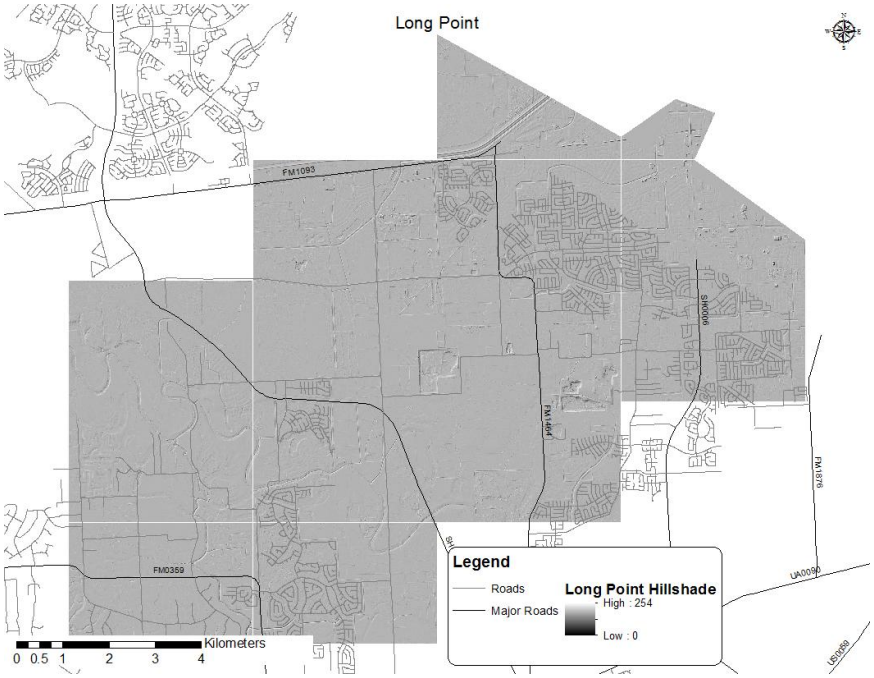

Figure 3-17: Long Point hillshade produced from the DEM that was produced from 2005 LiDAR data.

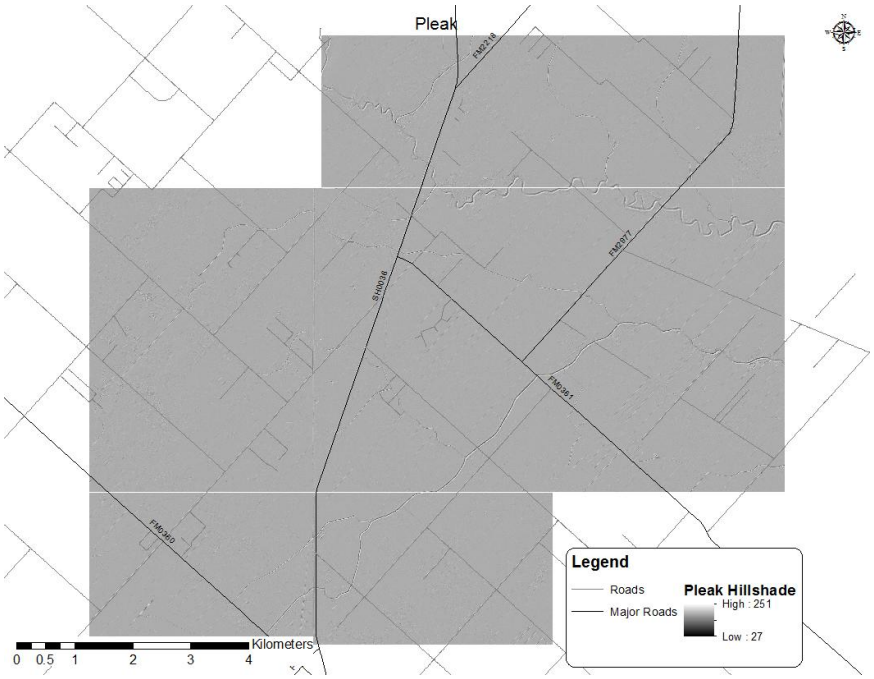

Figure 3-18: Pleak hillshade produced from the DEM that was produced from 2005 LiDAR data.

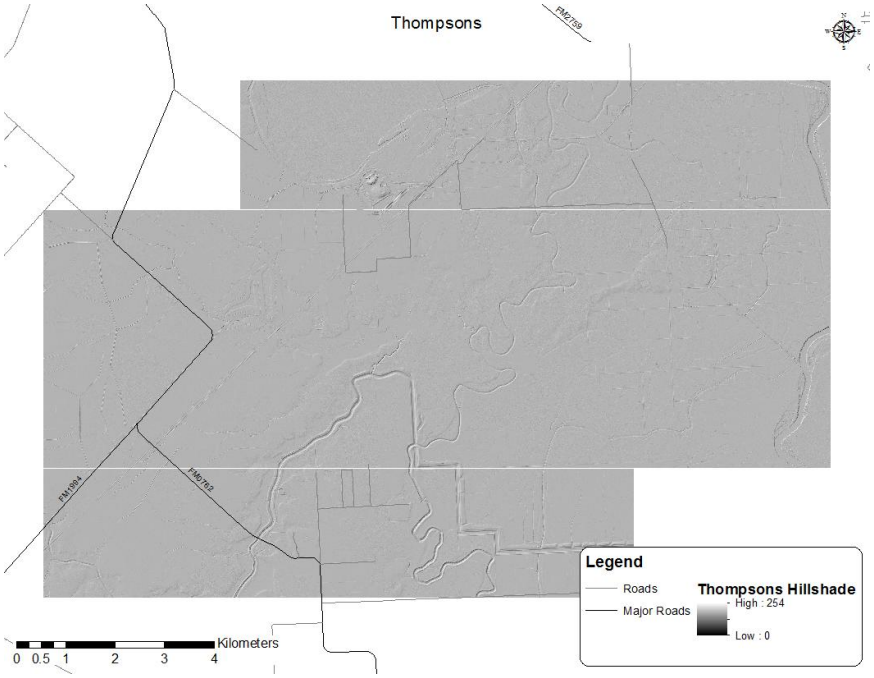

Figure 3-19: Thompsons hillshade produced from the DEM that was produced from 2005 LiDAR data.

The result of overlaying the hillshade with thirty three percent transparency on the DEM becomes even more interesting in the subsets as can be seen in Figure 3-20, Figure 3-21, Figure 3-22, Figure 3-23, Figure 3-24, and Figure 3-25.

Fort Bend County is the only place that LiDAR was used to produce the bare Earth DEM. For the rest of the Texas Gulf Coast a DEM was created from Texas Natural Resources Information System Stratmap Elevation Spots(TNRIS, 2012). These data are a lot less dense, and therefore produces a lower resolution DEM. The resolution of this DEM is approximately 3,000 meters, which is lower than that which is required to be able to interpret the low relief fault scarps that are present along the Texas Gulf Coast as can be seen in Figure 3-26.

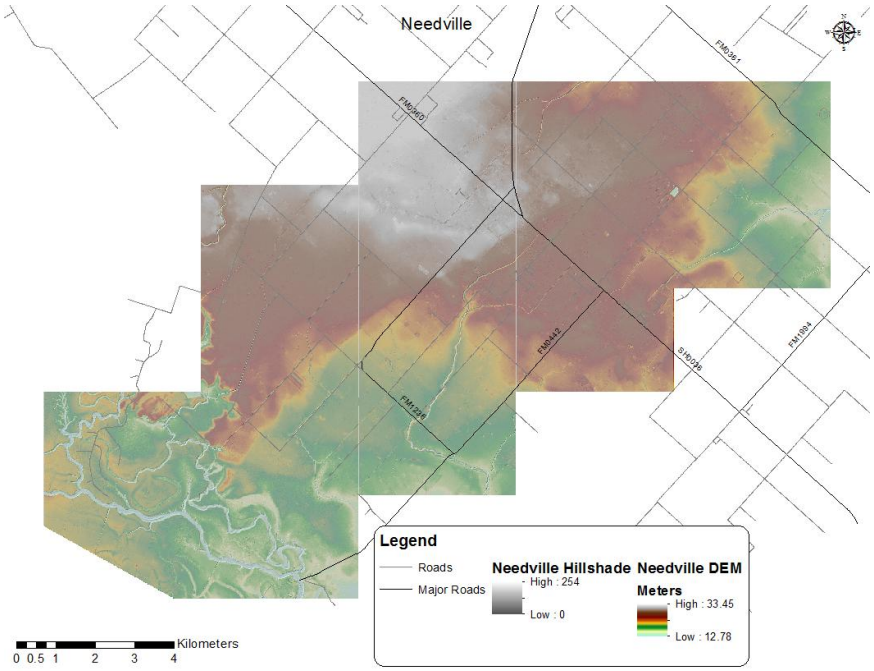

Figure 3-20: Needville with a hillshade overlaid on a DEM to better reveal areas of faulting.

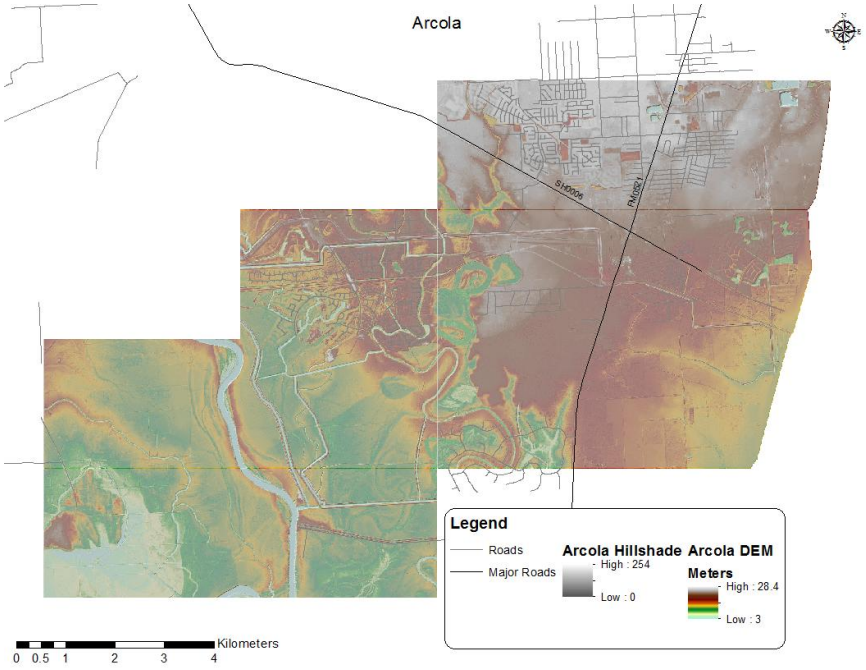

Figure 3-21: Arcola with a hillshade overlaid on a DEM to better reveal areas of faulting.

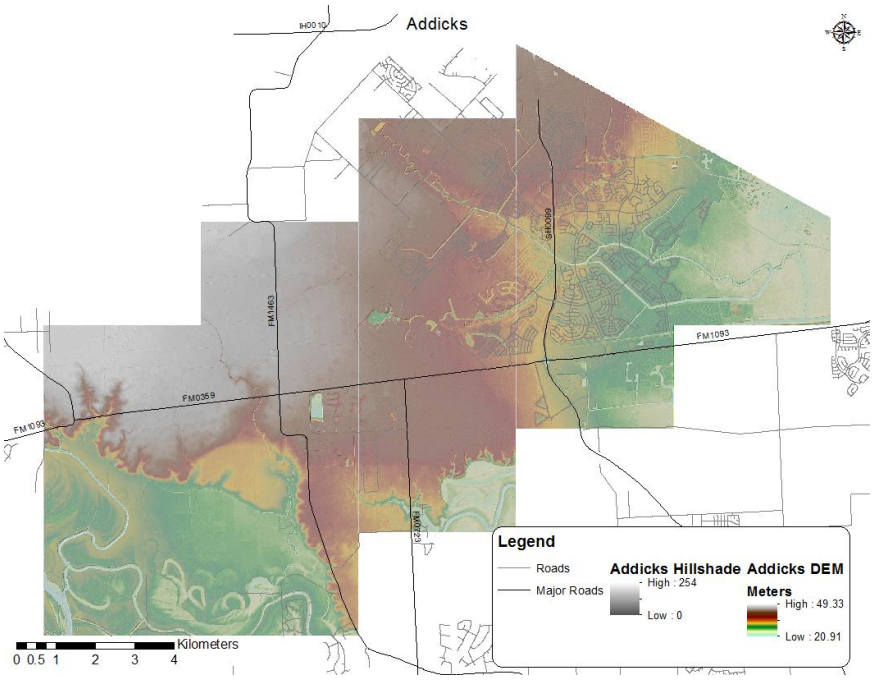

Figure 3-22: Addicks with a hillshade overlaid on a DEM to better reveal areas of faulting.

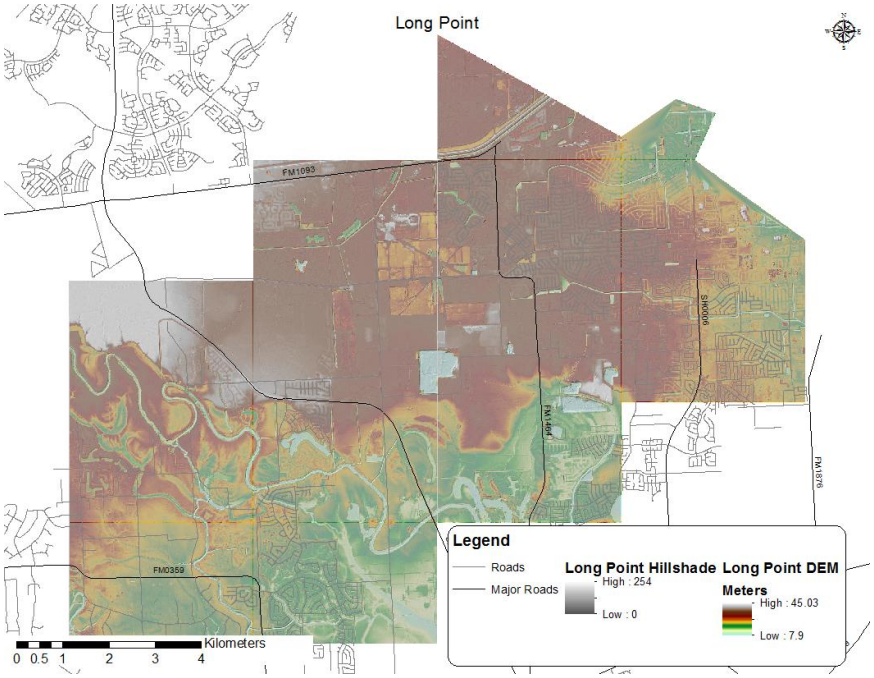

Figure 3-23: Long Point with a hillshade overlaid on a DEM to better reveal areas of faulting.

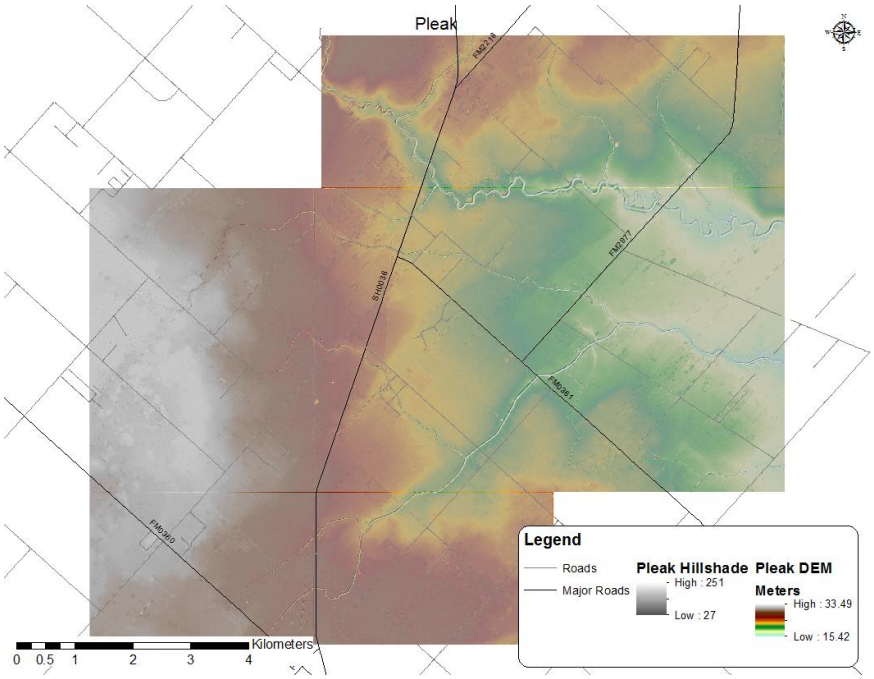

Figure 3-24: Pleak with a hillshade overlaid on a DEM to better reveal areas of faulting.

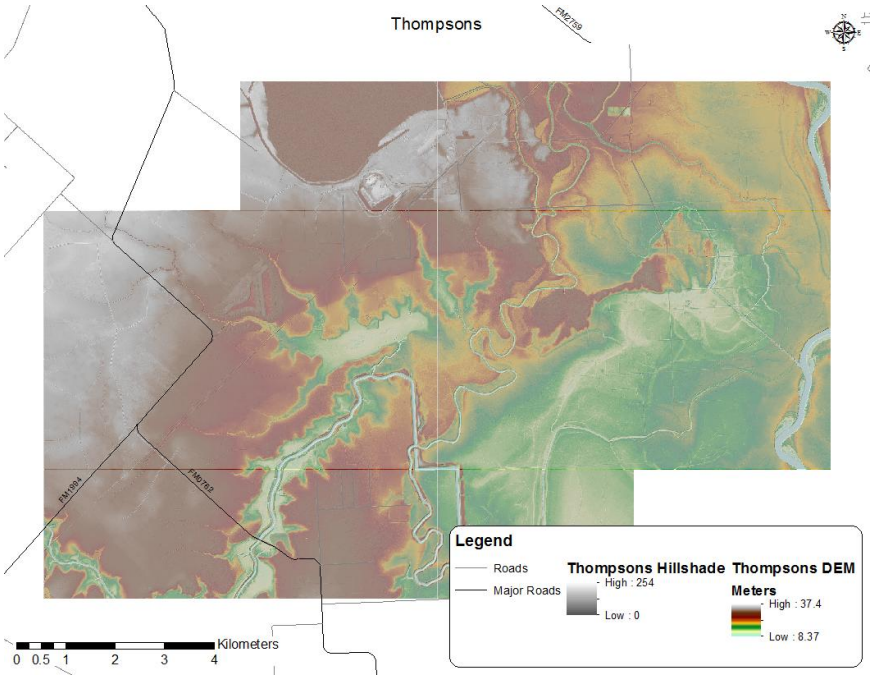

Figure 3-25: Thompsons with a hillshade overlaid on a DEM to better reveal areas of faulting.

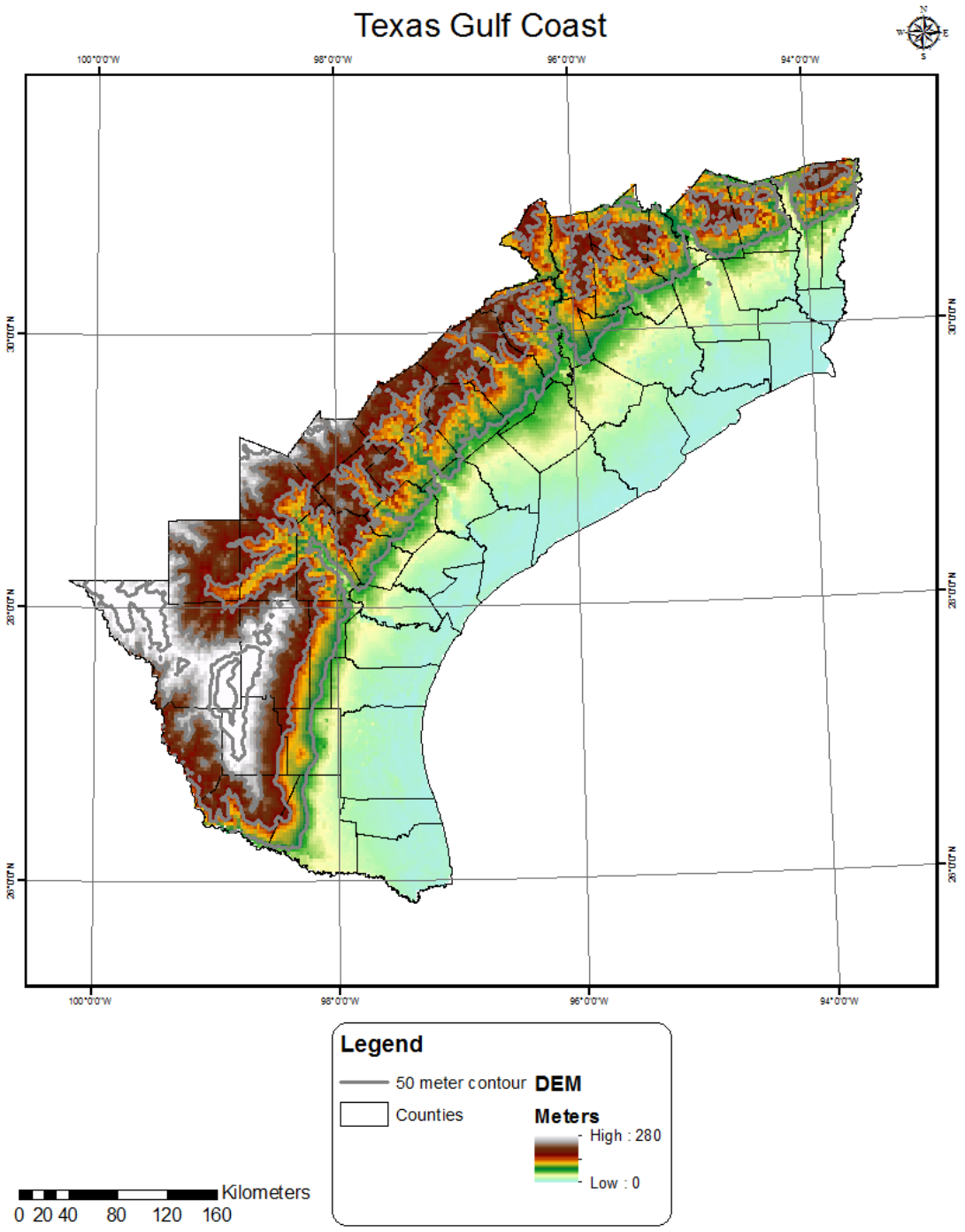

Figure 3-26: DEM of the Texas Gulf Coast which was produced from TNRIS Stratmap Elevation Spots.

3.1.3 GPR

Through the use of LiDAR and satellite imagery, locations were chosen that are ideal for conducting GPR surveys. These surveys must be conducted at a high angle to the fault strikes as are the seismic surveys. Also ideally the surveys were to be done on a smooth surface that has had little man made interference. For this reason a survey was conducted on an older road crossing the Needville fault at a very high angle to the strike. The GPR provides the link between the surface faulting revealed through LiDAR and the faulting that is revealed in the available seismic sections. For this reason the GPR was conducted at the same location in which seismic was collected. GSSI SIR 3000 GPR with 100 & 400 MHz shielded antenna systems were used. It is very important to use a shielded system at this location due to the presence of multiple power lines that run both parallel and perpendicular to the survey.

The 400 MHz shielded antenna system is able to penetrate a depth of up to four meters depending on the soil conditions (GSSI, 2012). It is important to note that with a 400 MHz frequency has a wavelength of 0.75 meters, and therefore the highest resolution possible would be approximately one fourth the wavelength which is 0.19 meters. This means that bedding lithologies of approximately 19 centimeters or greater in thickness can be determined in approximately the uppermost 4 meters. This is very useful since LiDAR cannot see below the surface, and seismic cannot easily determine any bedding at this shallow of depth. Therefore the GPR is able to produce a possible

link between the LiDAR and the seismic. With the survey being located in Fort Bend County with its moist clay soils it is also important to remember dielectric constant of water compared to other materials. This is important because moister essentially acts as a barrier in which GPR cannot penetrate. The below Table 3-2 of dielectric constants is modified from GSSI.

Material	**Dielectric Constant**		**Material**	**Dielectric Constant**
Air	1		Wet Sandstone	6
Snow Firm	1.5		Wet Granite	6.5
Dry Loamy/Clayey Soils	2.5		Travertine	8
Dry Clay	4		Wet Limestone	8
Dry Sands	4		Wet Basalt	8.5
Ice	4		Tills	11
Coal	4.5		Wet Concrete	12.5
Asphalt	5		Volcanic Ash	13
Dry Granite	5		Wet Sands	15
Frozen Sand & Gravel	5		Wet Sandy Soils	23.5
Dry Concrete	5.5		Dry Bauxite	25
Dry Limestone	5.5		Saturated Sands	25
Dry Sand & Gravel	5.5		Wet Clay	27
Potash Ore	5.5		Peats	61.5
Dry Mineral/Sandy Soils	6		Organic Soils	64
Dry Salt	6		Sea Water	81
Frozen Soil/Permafrost	6		Water	81
Syenite Porphyry	6			

Table 3-2: Common dielectric constants modified from GSSI (GSSI, 2012).

The 2-D GPR surveyed line stretched from the 500 meter mark to the 610 meter mark of the seismic line as can be seen in Figure 3-27. Unfortunately the GPR survey was not conducted across the main location of the fault. The recorded data from the GPR survey was processed with the use of RADAN 7.0. Processing steps included position correction, range gain, IIR filter, spatial F-K Filter, deconvolution, and migration. The

detailed processing for both the 100MHz and 400MHz can be seen in the below Table 3-3.

Function	Purpose	100MHz	400MHz
Position Correction	Removes air wave, correcting first reflection to time zero	Corrected the first peak to time zero	Corrected the first peak to time zero
IIR Filter (Bandpass)	Removes data with frequencies higher and lower than entered range	High pass: 25 MHz Low pass: 100 MHz	High pass: 100 MHz Low pass: 400 MHz
Deconvolution	Removes multiples	Operator length: 31 Range Gain: 3 Prediction lag: 5	Operator length: 31 Ranger Gain: 4 Prediction lag: 5
Migration	Removes diffractions	Type: Kirchoff Width: 63 Velocity: auto-pick Range Gain: 4	N/A

Table 3-3: Steps that were taken to process the 100MHz and 400MHz GPR data that was collected along Bushnell Rd.

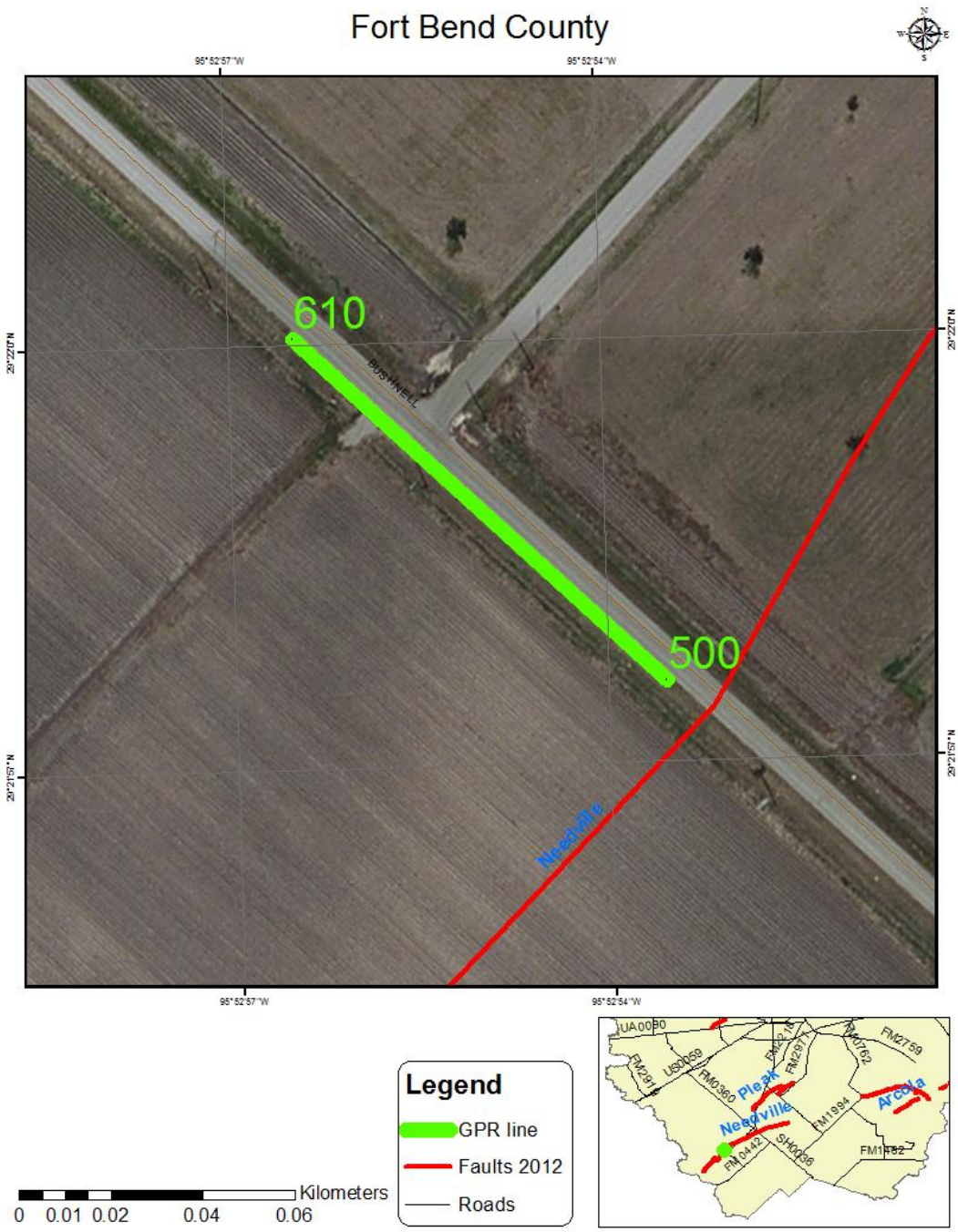

Figure 3-27: The green line represents the locations of the GPR sections along Bushnell road, while the red line represents the interpreted location of the Needville fault as it appears from the result of the LiDAR interpretation.

3.1.4 Seismic

No professional seismic sections are shown in this report due to legal reasons; however I was allowed to view a few seismic sections acquired by Seitel. From these sections I was able to confirm that the faulting is present along the eastern end of the Needville Fault.

Many aspects were considered for selecting the ideal location to shoot a seismic line. These include location and orientation of the fault, identifying locations where a survey is possible, and accessibility to the location.

The target for this research was anywhere from the far southwest end of the Needville fault to the furthest northeast end of the Arcola fault. Since both of these faults trend in a southwest to northeast orientation the best direction for the seismic line was considered to be oriented in a northwest to southeast direction, perpendicular to strike, to see the dip of the fault more clearly.

Available seismic equipment allowed max one kilometer length for the seismic line. The vibroseis truck weighs approximately 12,000 kg, and the truck's sweep can be felt around 100 meters away. This eliminates the possibility of conducting the survey within 100 meters of any housing or commercial buildings in order to ensure no damage is done. Also the vibroseis cannot be used on top of any pipelines for safety reasons.

Landowners were identified throughout the area through the use of the Fort Bend County Appraisal District website. Many land owners were contacted, and several declined to allow us on their property. However several were very interested, and provided permission. These include the George Ranch Foundation, Fort Bend County right of ways, and a few local property owners. The location that was chosen for the above reasons is along the southwest side of Bushnell road that is a few kilometers west of Needville. The location which can be seen in Figure 3-28 met all of our requirements for the survey. However this location does still have certain dangers that needed to be addressed. The road has multiple pipelines that cross under it as can be seen in Figure 3-29. The road also has a load limit wood bridge at the end of it that is restricted to 10,000 lbs, or approximately 4,536 kg.

The survey was conducted by laying out a 960 meter 2-D seismic line. The seismic line consisted of vertical geophones planted at 5 meter intervals for 955 meters for a total of 192 receivers. Every 24 geophones are connected to a geode through the use of a geophone cable. Then every geode is connected to the previous geode until it reaches back to the first geode which is connected back to the computer. A schematic of the seismic line layout can be seen in Figure 3-30.

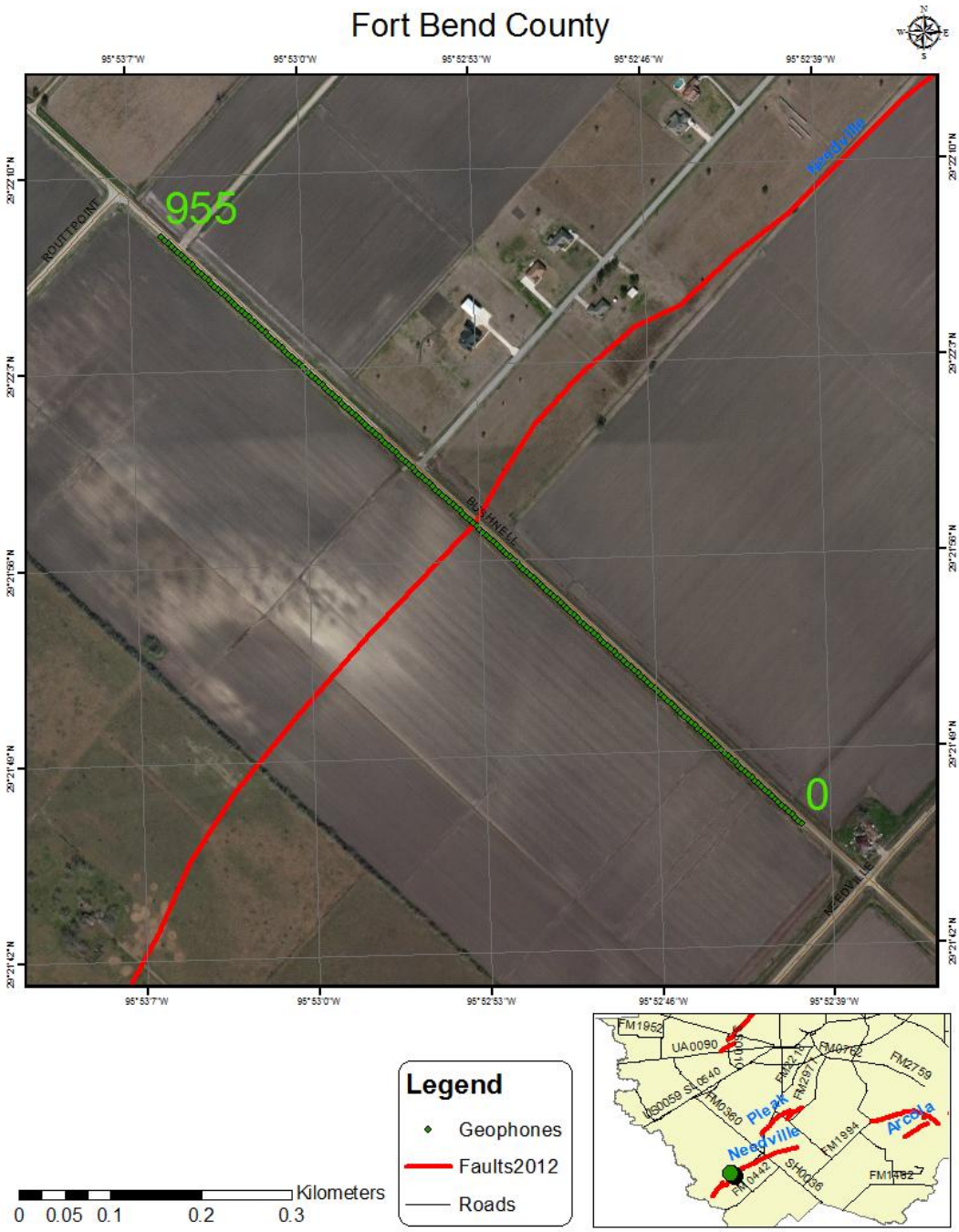

Figure 3-28: Green dots represent locations of geophones along Bushnell road, while the red line represents the interpreted location of the Needville fault as it appears from the result of the LiDAR interpretation.

Figure 3-29: Photo of 2D seismic survey being conducted on Bushnell Rd. with pipelines illustrated in red further down the road in front of the vibroseis truck.

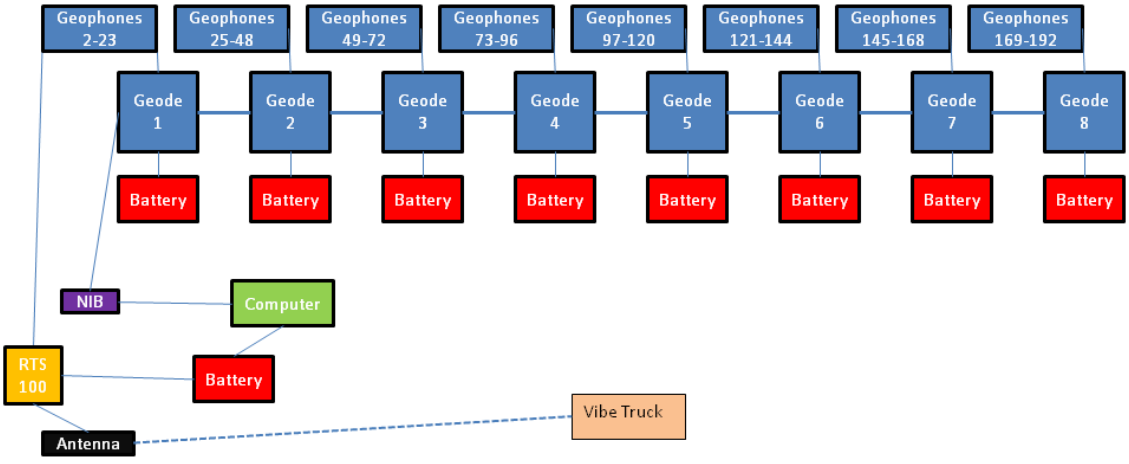

Figure 3-30: Schematic of the layout of the 2D shallow seismic survey conducted along Bushnell road.

The vibroseis truck ran a 12 second linear sweep of 10Hz to 150Hz. The shot interval from the vibroseis truck consisted of both 5 meter and 10 meter intervals. The reasoning for this is that due to time constraints due to weather about a third of the way through the survey the shot interval had to be changed from 5 meter to 10 meter in order to complete the survey in a shorter time span. The recording was done with a sampling rate of 1 milisecond for a record length of 4 seconds.

Once the data were collected, they then had to be processed before any interpretation could be conducted. The seismic was processed with the use of Vista Seismic Processing Software. The processing was conducted multiple times in order to determine the best processing steps and parameters to be used in order to reduce the noise and thus reveal the geologic structure. The processing steps can be seen in Table 3-4.

Unfortunately I was not able to obtain enough well log data close enough to our seismic section to perform a seismic to well log correlation. Only SP logs were obtained that were close enough, and therefore I was not able to correlate to the seismic. This correlation would have been very useful in being able to convert the time seismic to depth seismic and also to create meaningful lithology horizons on the seismic. Since this was not possible an assumption was made based on the average velocities of the area that every 1ms of time is equal to 1 meter of depth, and random horizons were picked.

Process	Description	Parameters
Load Data	Load data into Vista	
Compute Geometry	Geometry description for receivers, shots	
Trace Statistics	Eliminate traces that are bad	
Input Data		
Scaling	Exponential Time Power	• Exp.: 1.000000
Scaling	Data Scaling	• Scale: 1.000 Mean Scale • Input Time Gate File
Deconvolution	Surface Consistent Deconvolution Apply	• Type: Spiking Decon • Operator Length: 60.000 • Pre-Whitening: 1.000 • Components to Apply: • 1 - Line Component • 1 - SHOT_SEQUENCE_NUMBER : 4 COMP • 2 - RECV_SEQUENCE_NUMBER : 4 COMP
Scaling	Data Scaling	• Scale: 1.000 Mean Scale • Input Time Gate File
Output Data		
Input Data		
2D Transforms	Apply F-K Designed Filter File	• F-K File • Power: 1.00 TrcSmooth: 7 FreqSmooth: 5 • F-K Filter Operation: REJECT • Apply removable Agc 250.00 ms
Scaling	Data Scaling	• Scale: 1.000 Mean Scale • Input Time Gate File
Deconvolution	Time-Variant Spectrum Balancing	• BandWidth. 10.00 HZ Slope: 5.00 HZ • Start Frequency 0.00 HZ • Top Frequency to 120.00 HZ • Single Scalar AGC Window: 100.00 ms Scale: 1.0000 • AGC Start Gate File
Scaling	Data Scaling	• Scale: 1.000 Mean Scale • Input Time Gate File

Process	Description	Parameters
Trace Edit	Muting	• Interp, Offset[Trace] Dependent • Mute File • Taper Mute Zones by 4 Samples
Output Data		
Input Data		
True Surface Velocity	True Surface Normal Move-Out	• Velocity Referenced: True Surface • NMO File • Velocity Percent: 100.00 % • Stretch Mute: 30.00 Linear Ramp: 4 • Mute Velocity Inversions
Scaling	Automatic Gain Control (AGC)	• L1/L2 Norm Equalization • AGC Length: 100.00 Scale: 1.000 Norm Eq: L1 Ignore Hard-Zero • Apply Signal Bandpass Filter: 25.00/35.00 120.00/150.00 Hz
Stack	Common Mid-Points Stack	• Stack: 1 / (N + 1) • CMP Stack Geometry Header Update: OFF
Filtering	Ormsby Band-Pass	• 25.00/35.00-120.00/150.00 Hz • Domain Filter Application: Frequency
Scaling	Automatic Gain Control (AGC)	• L1/L2 Norm Equalization • AGC Length: 100.00 Scale: 1.000 Norm Eq: L1 Ignore Hard-Zero • Apply Signal Bandpass Filter: 25.00/35.00 120.00/150.00 Hz
Output Data		
Input Data		
Signal Enhancement	2D F-X Deconvolution	• FX Filter [Levinson-Durbin]: 3 Design: 100 End Freq: 100.0 Hz(Taper: 10.0 Hz] Power: 1.000000 factor: 1.000000 • Restore Trace Mutes
Scaling	Automatic Gain Control (AGC)	• L1/L2 Norm Equalization • AGC Length: 500.00 Scale: 1.000 Norm Eq: L1 Ignore Hard-Zero
Output Data		

Table 3-4: Above is a table of the steps that were taken to process the 2D seismic data that was collected along Bushnell Rd.

3.1.5 Well Logs

Well Logs were obtained from GeoMap, E P Energy, and the Texas Railroad Commission. In addition to acquiring well logs from GeoMap, I was also permitted to view the structure contour maps, but these GeoMap structure maps are not presented in this report for legal reasons. I obtained paper copies of well logs from GeoMap, while the logs obtained from E P Energy and the Texas Railroad Commission were received in Tiff format. In order for the well logs to be correlated and placed into a presentable format I requested assistance from Neuralog. Neuralog is a company that specializes in producing well log printers, scanners, and software. Neuralog assisted by providing me with the following software: NeuraMap, NeuraLog, NeuraSection, and NeuraScanner. Neuralog also provided me with a NeuraScanner in order to scan in all of the paper logs I retrieved from GeoMap.

Well logs were initially obtained in what were hoped to be near perpendicular lines to the surface faults that were found in the LiDAR. With these initial logs rough cross sections were made that confirmed that the faults found on the surface are also visible at depth.

With the knowledge of the faults seen in these initial well logs many more well logs were obtained from additional locations. Many reports were also located that have stratigraphic cross sections that were formed from the use of well logs and other data. The cross sections and well location overview maps from these reports can be seen in

the Appendix. From these reports the overview maps were georeferenced in ArcGIS in order to determine the location of the wells used to create the cross sections. Then by examining the well logs in the cross sections, stratigraphic tops were located and the well logs were then either brought into NeuraLog, or the statigraphic tops were brought directly into a shapefile in ArcGIS. The idea behind this is that if a high enough density of well logs could be obtained, then some rough structure maps of the Needville and Arcola areas could be formed. With these structural maps salt domes and faults were identified.

Although the primary focus is on the Needville and Arcola areas it was important to go beyond these areas with the well correlations. This is important in order to minimize the effects of individual well log interpretations on the regional structure. For example before the regional well log correlations were added there were a few well logs that were located near the edge of the extent of the core group of well logs in Fort Bend County that were over salt domes. These few wells cause the structure of the area to be unclear without wells that are further out to produce a regional structure for the area.

3.1.6 Gravity

Some gravity data was obtained through GeoNet, which is a gravity and magnetic database that is run by the University of Texas at El Paso (UTEP). Unfortunatly this gravity is too sparse in locations to be able to be useful in this study as can be seen in Figure 3-31. The majority of these data appears to have been collected along the

major roads, with lesser importance on the locations as the usage of the roads decreases. This was identified by the fact that Interstate 10 is very easily distinguished by the locations of the gravity readings, and then the rest of the readings to the south appear to be located mostly in a grid.

Attempts were made at trying to obtain higher density data through multiple organizations, but were found to be unsuccessful. Since for this study it would require a much higher resolution of data than what is obtainable in the public domain it became necessary for a gravity study to be conducted. For this reason gravity data were collected with a Scintrex CG-5 Autograv gravimeter along Bushnell road. This study was conducted by taking two measurements every twenty meters along the side of Bushnell road as can be seen in Figure 3-32, which is where the seismic and GPR surveys were also conducted.

There are several steps that are necessary when conducting a gravity survey. First the measurements must be made, and the location of the measurement in latitude, longitude, and elevation must be recorded. Then the raw gravity data must have several corrections applied in order to have data that means anything. These steps include the Tidal, Drift, Latitude, Free Air, Bouguer, and Terrain corrections. The result of these corrections is the relative Bouguer Anomaly. In order for this to be an absolute Bouguer Anomaly an additional step of calibrating the Scintrex CG-5 Autograv with a known

gravity reference point would be required. For this survey it is not necessary to have an absolute Bouguer Anomaly, and therefore this calibration was not conducted.

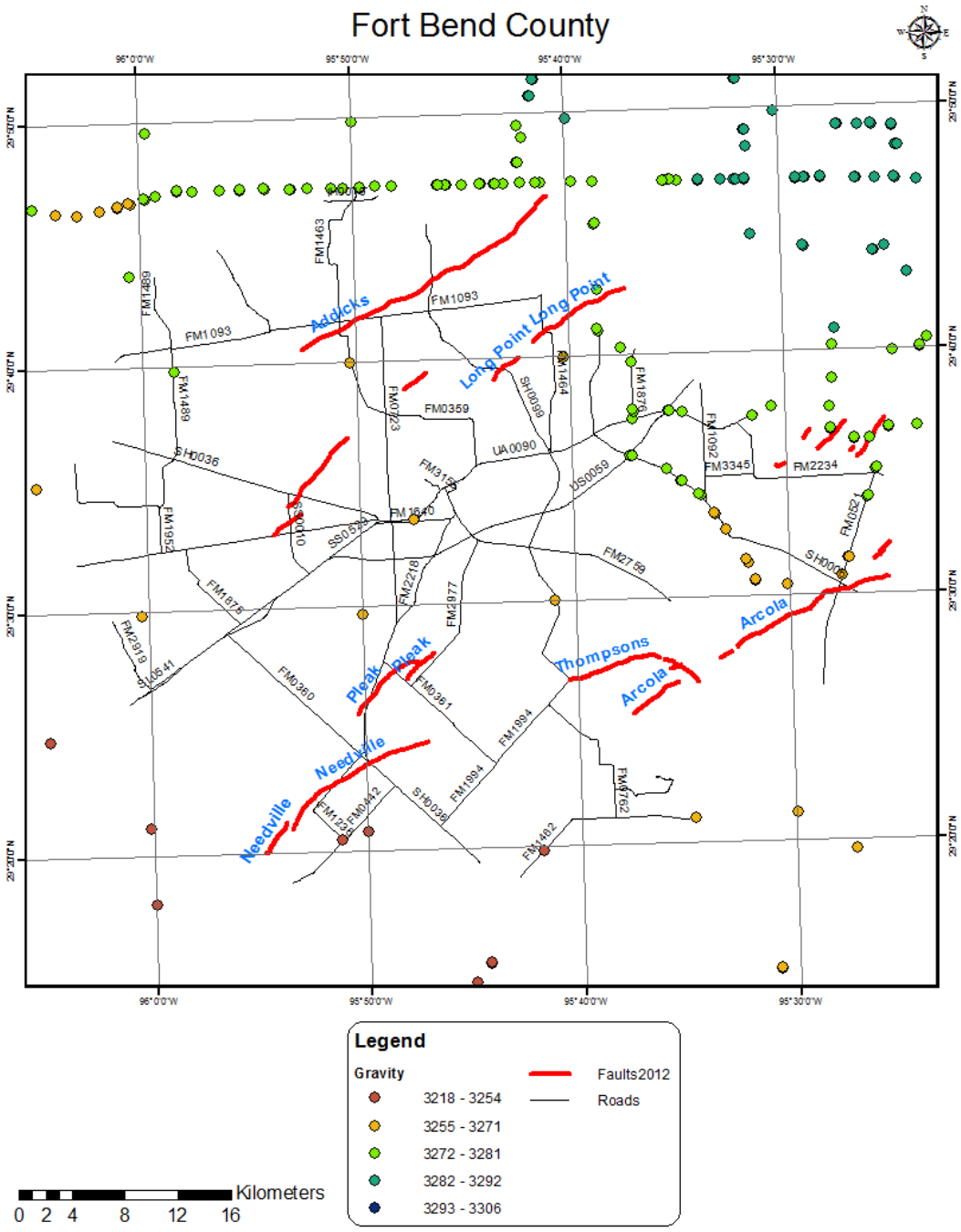

Figure 3-31: Locations of gravity measurements displayed in ArcGIS as downloaded through GeoNet by the United States Geological Survey (USGS) through the University of Texas Elpaso (UTEP)

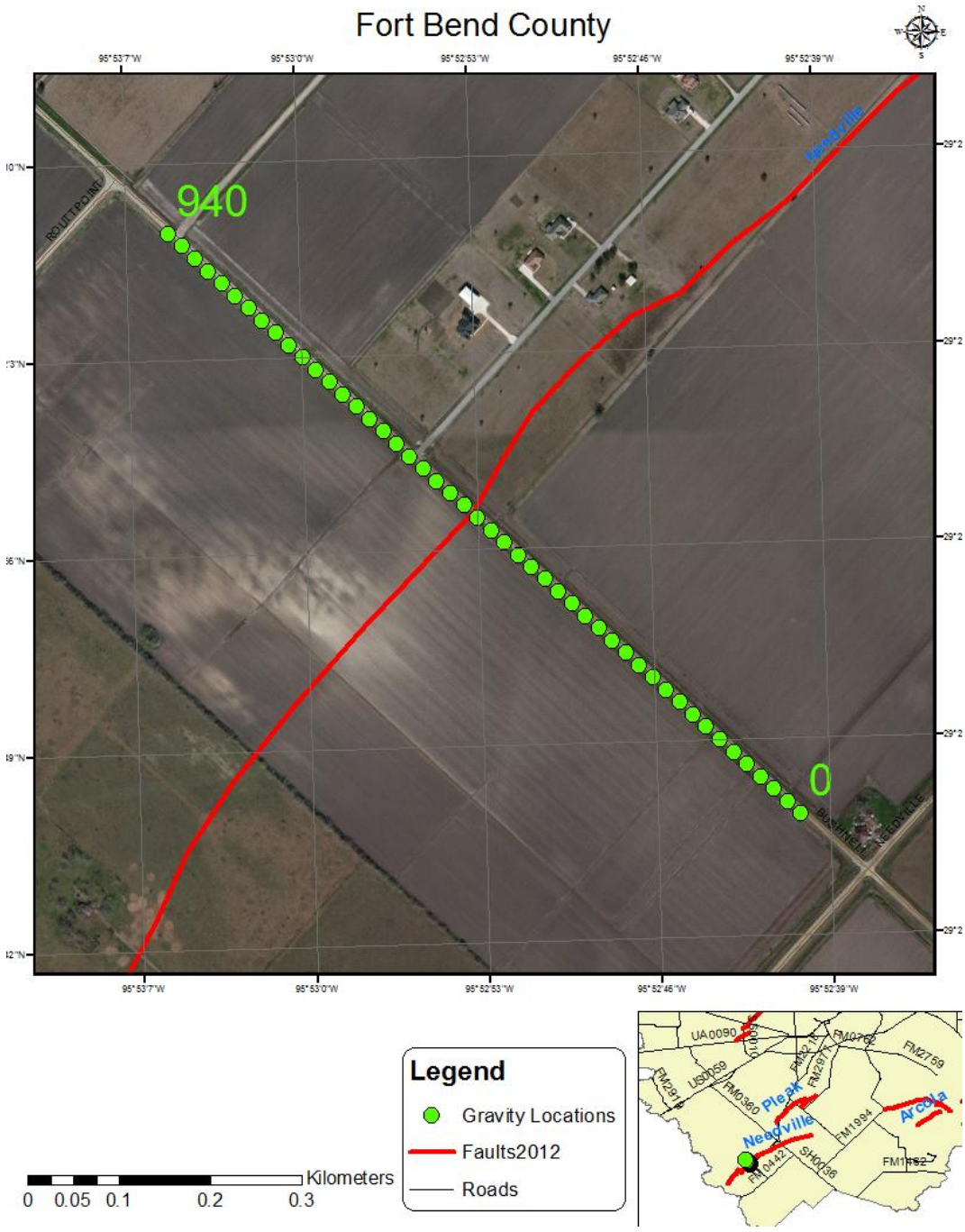

Figure 3-32: Green dots represent locations where gravity measurements were taken along Bushnell road, while the red line represents the interpreted location of the Needville fault as it appears from the result of the LiDAR interpretation.

Chapter 4

4.1 Results

4.1.1 GPS

There are enough GPS data available in Fort Bend County to be able to draw a conclusion about the Arcola fault as can be seen in Figure 4-1. Unfortunately for the Needville and Thompsons faults GPS stations are available only on the north side of the two faults. For Arcola GPS station PAM 40 is approximately one kilometer south of the fault, and GPS station PAM 16 is approximately seven kilometers north of the fault. GPS station PAM 14 is located north of the Thompsons fault and could also be associated with being on the north side of the Arcola fault. This amount of GPS data does not provide multiple GPS stations on each side of the fault in order to make sure that these GPS stations are reliable.

For the Arcola fault it can be seen in Figure 4-1 that PAM 40 south of the fault has decreased in elevation from 1997-2011 by approximately 18 centimeters. During the same time span PAM 16 north of the fault only decreased in elevation by approximately 13 centimeters. Also PAM 14 during the same time span decreased in elevation by approximately 9 centimeters. These three decreases in elevation all agree with the idea that the south side of the Arcola fault is decreasing in elevation more than the north side of the fault.

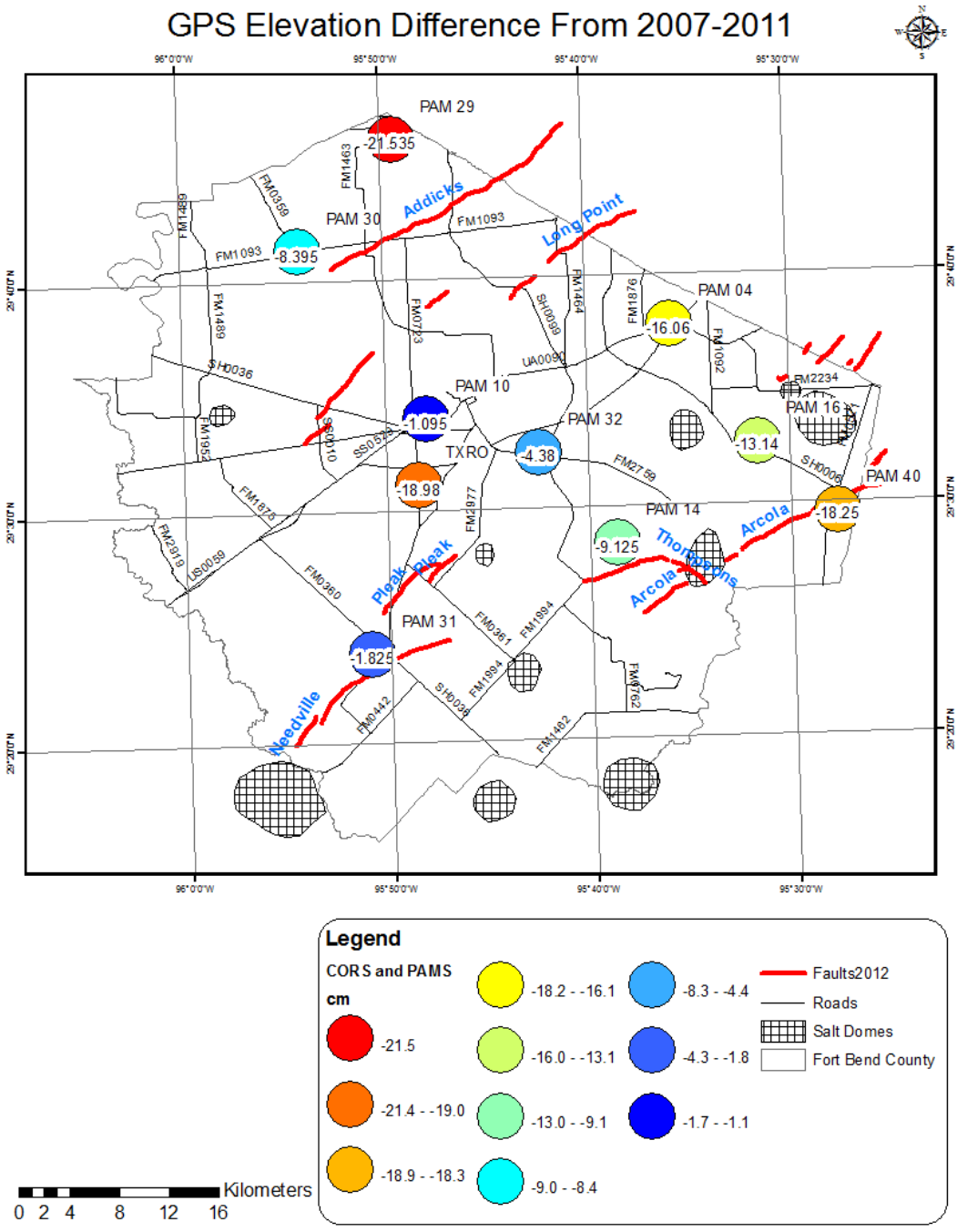

Figure 4-1: CORS and PAMS GPS elevation differences from 2007 to 2011.

In addition to the amount of deformation another analysis was conducted based on the rate of deformation. This was done by using the past elevation reading from the PAM and COR GPS stations on a varying span of three to fifteen years depending on the amount of data available for each location. The result of this can be seen in Figure 4-2. From rate of deformation it can be seen that PAM 40 south of the Arcola fault has been decreasing in elevation by approximately 18 millimeters per year from 2007-2010. The rate of deformation for PAM 16 is a decrease in elevation by approximately 12 millimeters per year from 2001-2010. Then for PAM 14 which is north or the Thompsons fault has a decrease in elevation of approximately 9 millimeters per year from 2001-2010. These rates of deformation confirm that the south side of the Arcola fault is decreasing in elevation at a greater rate than that of the north side of the fault.

4.1.2 LiDAR

The LiDAR proved to be very effective in the mapping of the faults on the surface. Many of the faults that were found using LiDAR were also confirmed by trips to the field. In the DEM overview map in Figure 4-3, it can be seen that multiple faults are present in Fort Bend County. These faults are the Needville, Arcola, Addicks, and Long Point faults as they are identified in Figure 4-2. However at this scale it is impossible to see the full extent of the faults and the many other relatively smaller faults that appear in the Fort Bend.

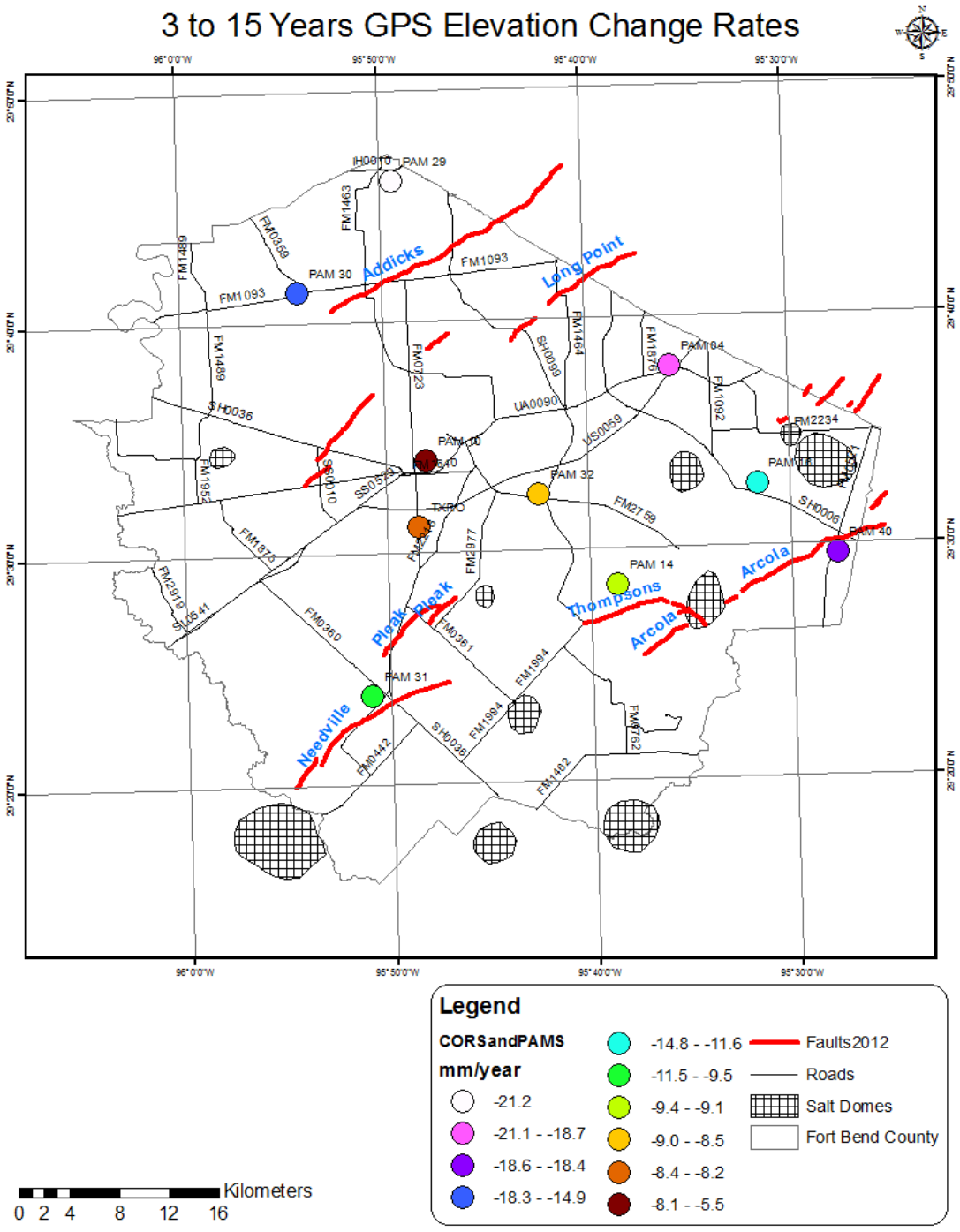

Figure 4-2: CORS and PAMS three to fifteen year GPS elevation change rates.

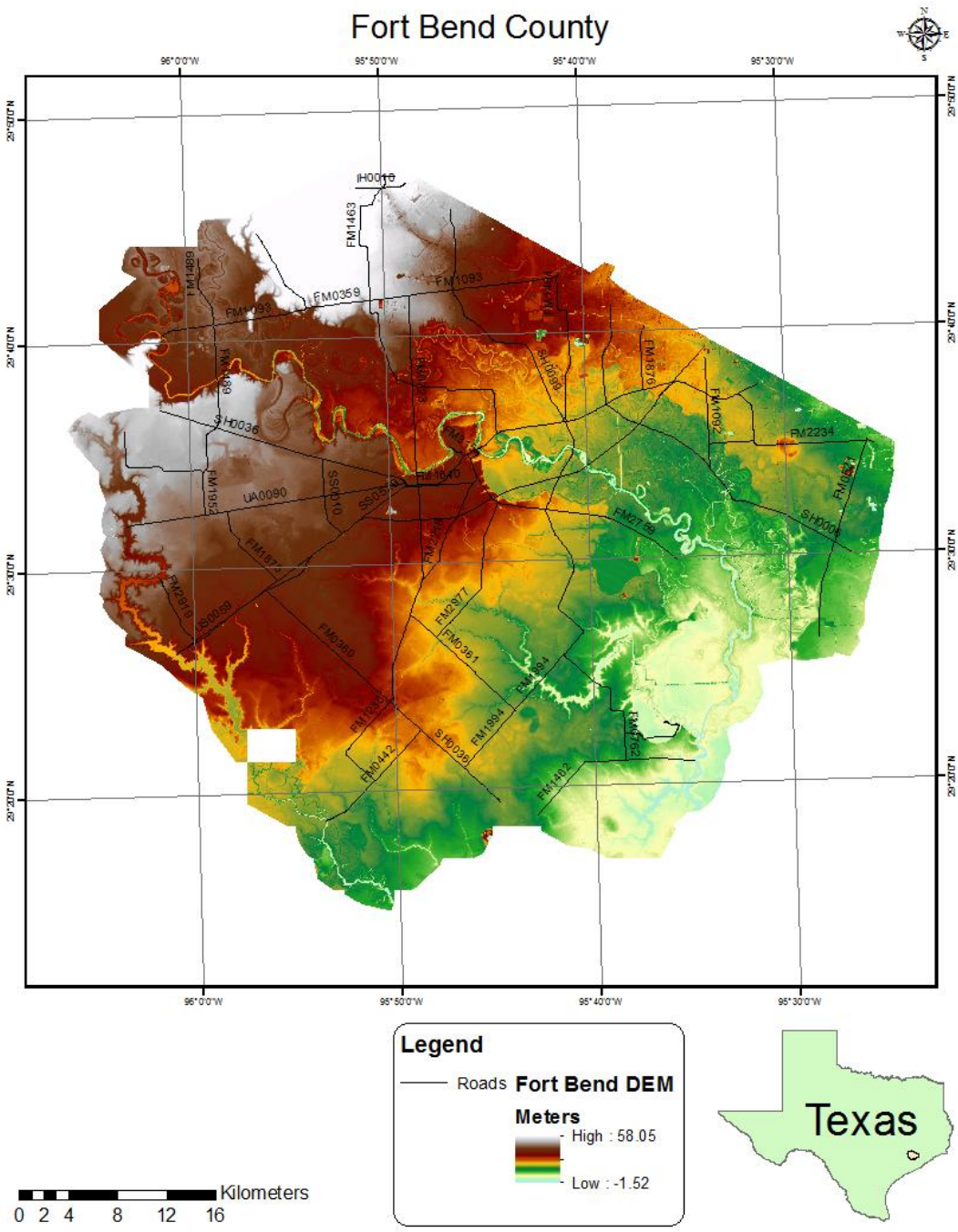

Figure 4-3: Fort Bend County DEM produced from 2005 LiDAR data.

By examining the previous figures along with a more in depth analysis of each area, surface fault picks were chosen as can be seen in Figure 4-4 to Figure 4-9.

From these surface fault picks, several profiles were produced for the Needville and Arcola Faults. These profiles can be seen in Figure 4-10 to Figure 4-31.

By combining all of these fault picks along with others not displayed above, the fault map in Figure 4-32 was created. This is the first geologic fault map of Fort Bend County that is created from the use of LiDAR. One of the hypotheis to be tested in this study included that is it possible that the Needville fault and Arcola fault are in fact the same fault. This connection had never been made between the two faults because of the extent of the Brazos River meandering plan has eroded away any possible correlation between the faults. However after creating the Fort Bend fault map from the LiDAR data it has become clear that these are probably two separate and distinct faults. This is apparent by the way that both the Needville fault and Arcola fault curve toward the south on their east and west ends respectively. The argument could be made that this curve is caused by the lower elevations at the two respective ends from erosion caused by the meandering of the Brazos River. This would mean that if the elevation remained constant then the faults would possibly not have this curve and that the curve is probably just an illusion due to not looking at the true strike and dip of the faults. Another possibility could be that if you were to create a trend line of the surface faulting with a one degree polynomial fit with each of the two faults, the resulting two lines do

not line up. This does not mean that these two faults are two separate faults, but I am unable to produce any evidence that they are the same fault. To do this would probably require a paleo-flow history of the meandering of the Brazos River, along with several northwest to southeast oriented seismic lines, and many well logs throughout the Brazos Rivers meandering plane. It is also still a possibility that the Brazos River lies on a strike slip fault zone between the Needville and Arcola faults.

While this shows that faulting is present in Fort Bend County, it does not show all of the faults that are present, and most likely does not even show the entire surface faulting that is present. However from this map there is enough faults found that show that the faulting in Fort Bend County not only is highly influenced with the regional scale faulting along the Texas Gulf Coast, but also that more local events are occurring that are driving mechanisms for the faulting. For example, the influence of local geologic events is evident by looking at the impact that the Thompson Salt Dome has on the area. As the Arcola Fault approaches the Thompson Salt Dome from both sides, the fault begins to fade out, while the formation of several other faults begin to appear. This produces a radiating effect of faulting emerging around the Thompson salt dome. This can be seen in Figure 4-32.

Through the use of ArcScene a 3D surface model has been created from the Digital Elevation Models. The 3D surface models have had elevation exaggeration done to them in an effort to make the faults very clear. Unfortunately the best way to

examine these models is to digitally fly through the model, and therefore it is not possible to provide a decent figure of this amazing model. However attached is a video of a fly through of the model is on the attached CD.

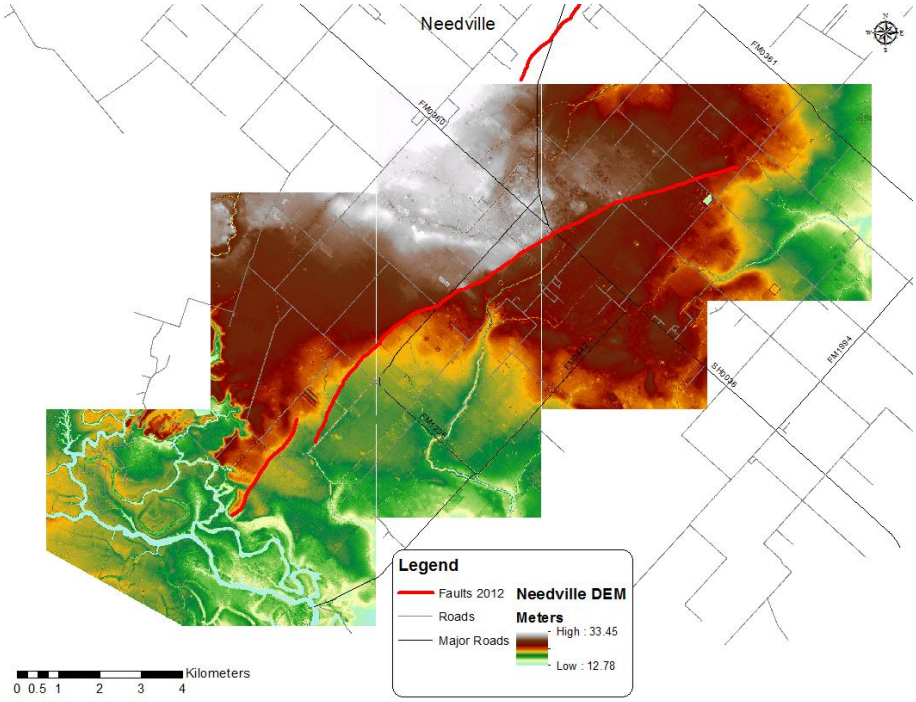

Figure 4-4: Needville Fault displayed in red that was interpreted from the DEM.

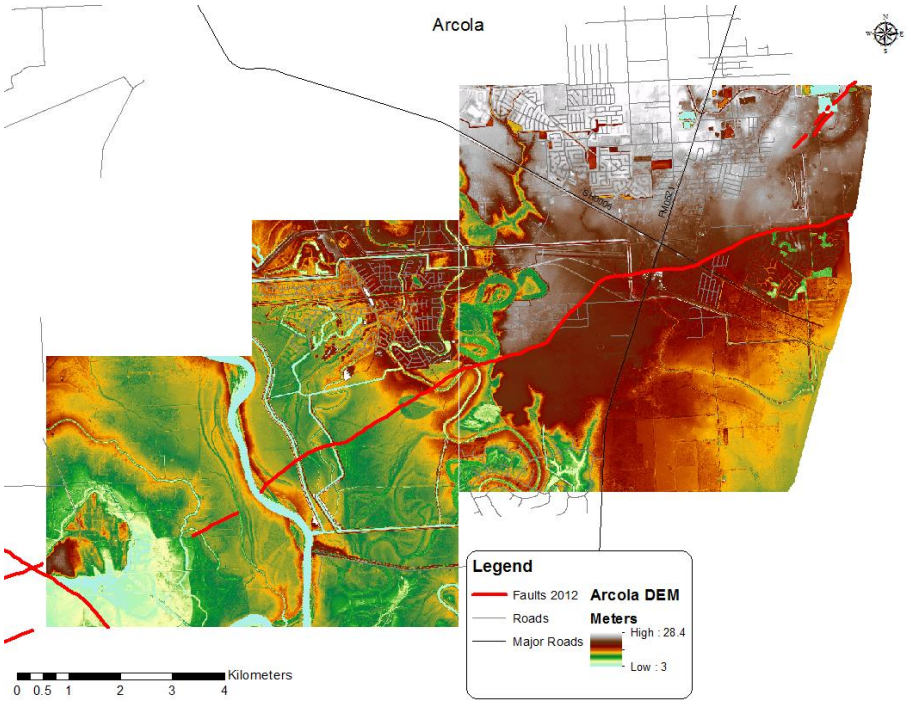

Figure 4-5: Arcola Fault displayed in red that was interpreted from the DEM.

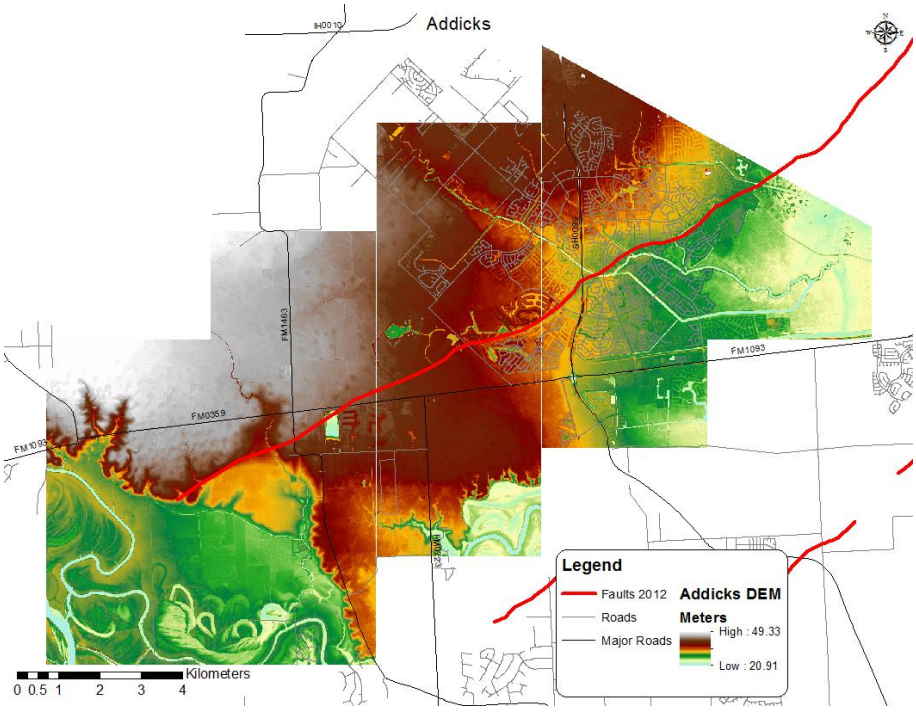

Figure 4-6: Addicks Fault displayed in red that was interpreted from the DEM.

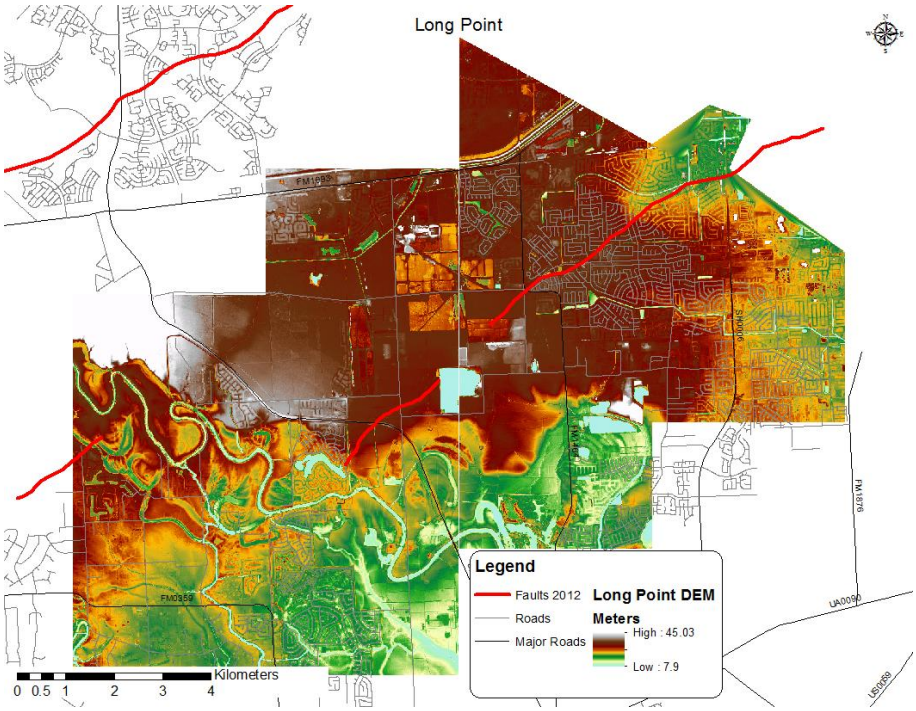

Figure 4-7: Long Point Fault displayed in red that was interpreted from the DEM.

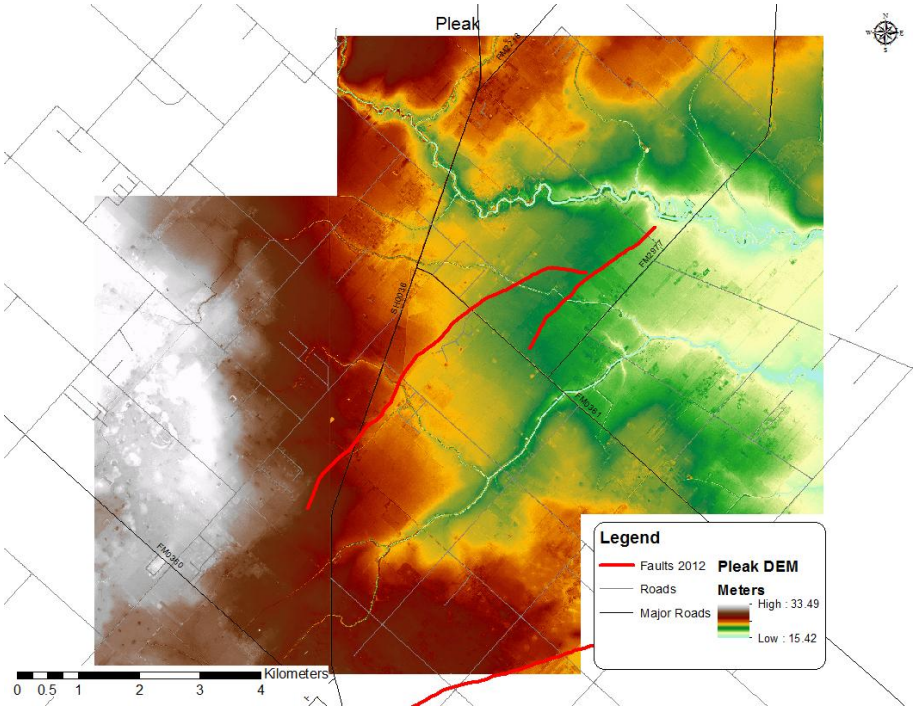

Figure 4-8: Pleak Fault displayed in red that was interpreted from the DEM.

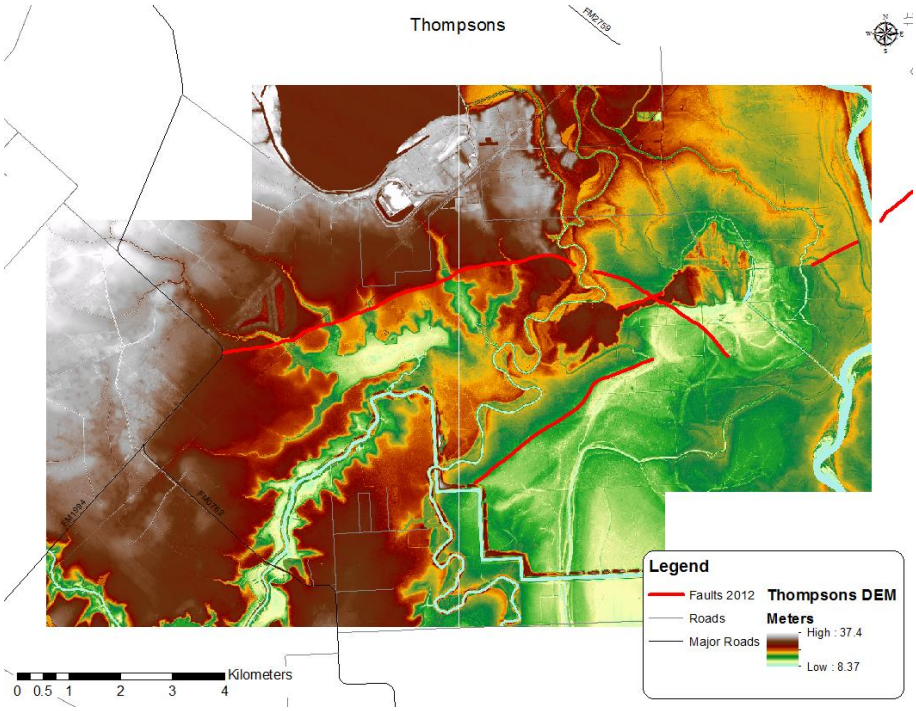

Figure 4-9: Thompsons Fault displayed in red that was interpreted from the DEM.

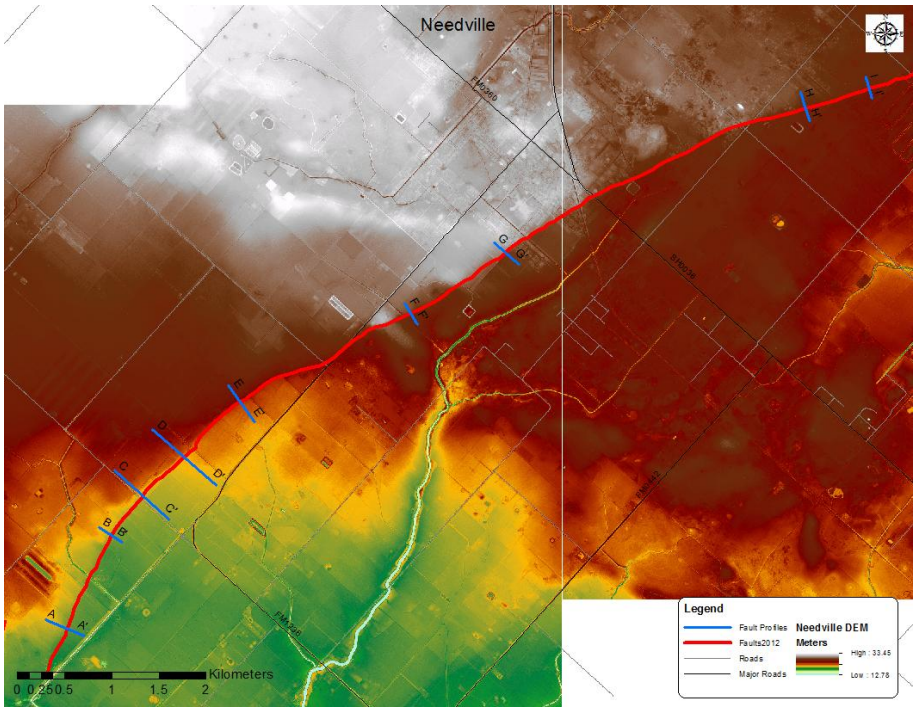

Figure 4-10: Needville Fault displayed in red that was interpreted from the DEM. Blue lines represent locations of elevation profiles.

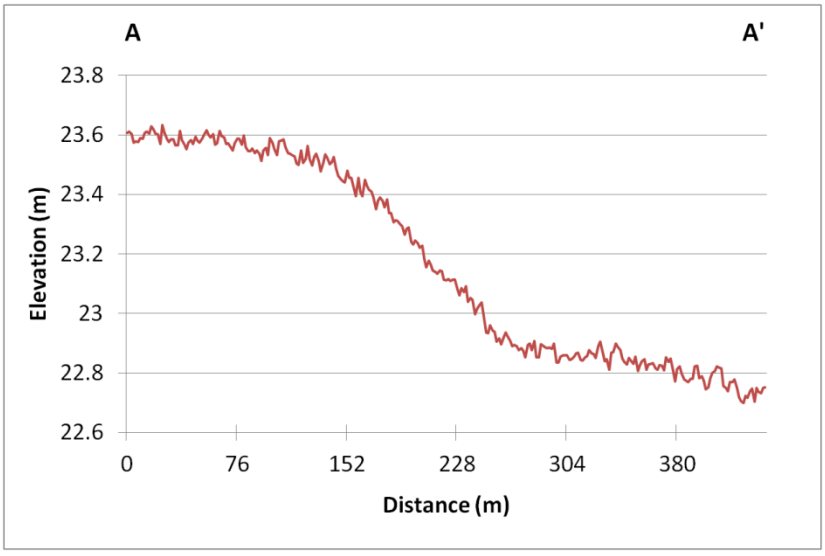

Figure 4-11: Elevation profile across Needville Fault which was interpreted from A to A' from a DEM created with 2005 LiDAR data.

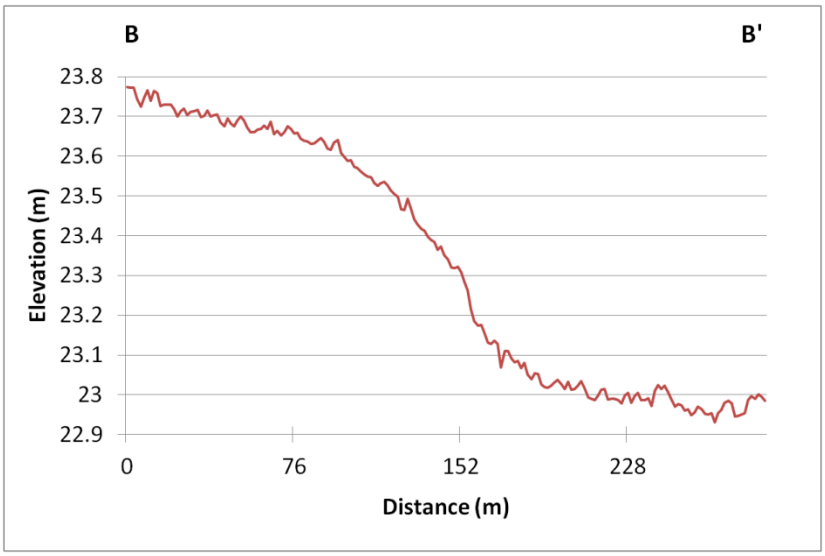

Figure 4-12: Elevation profile across Needville Fault which was interpreted from B to B' from a DEM created with 2005 LiDAR data.

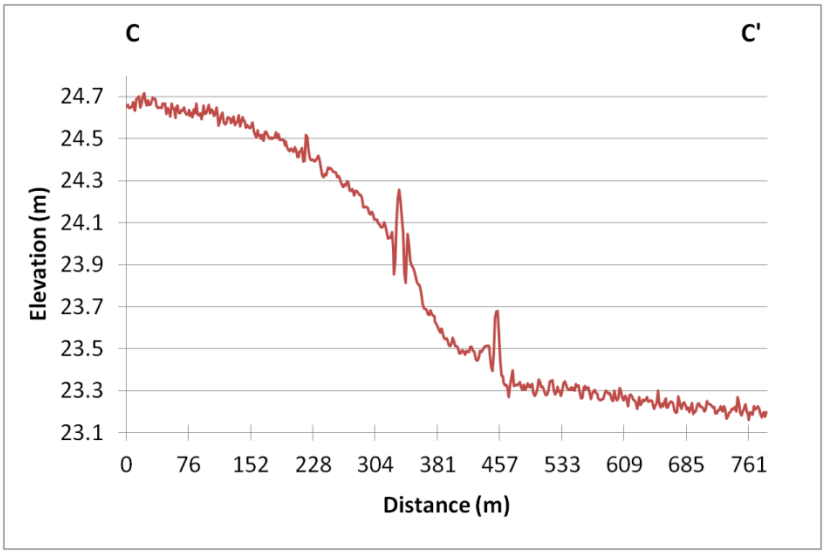

Figure 4-13: Elevation profile across Needville Fault which was interpreted from C to C' from a DEM created with 2005 LiDAR data.

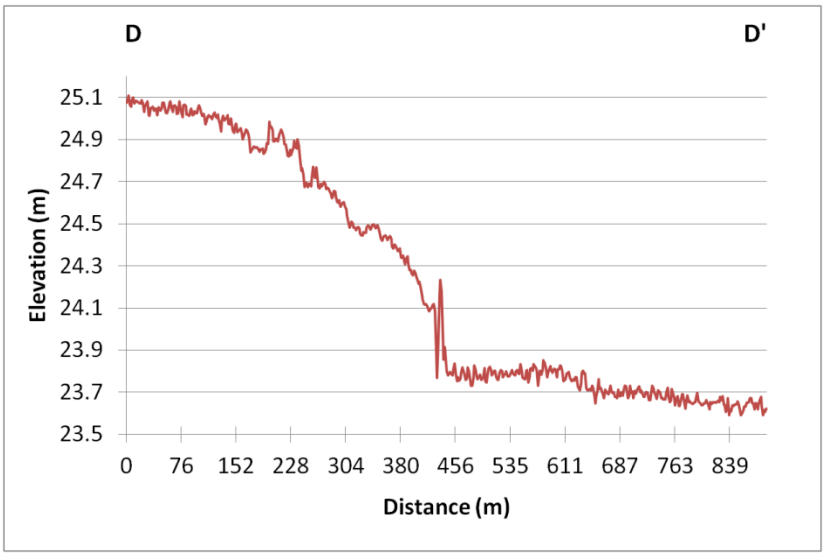

Figure 4-14: Elevation profile across Needville Fault which was interpreted from D to D' from a DEM created with 2005 LiDAR data.

Figure 4-15: Elevation profile across Needville Fault which was interpreted from E to E' from a DEM created with 2005 LiDAR data.

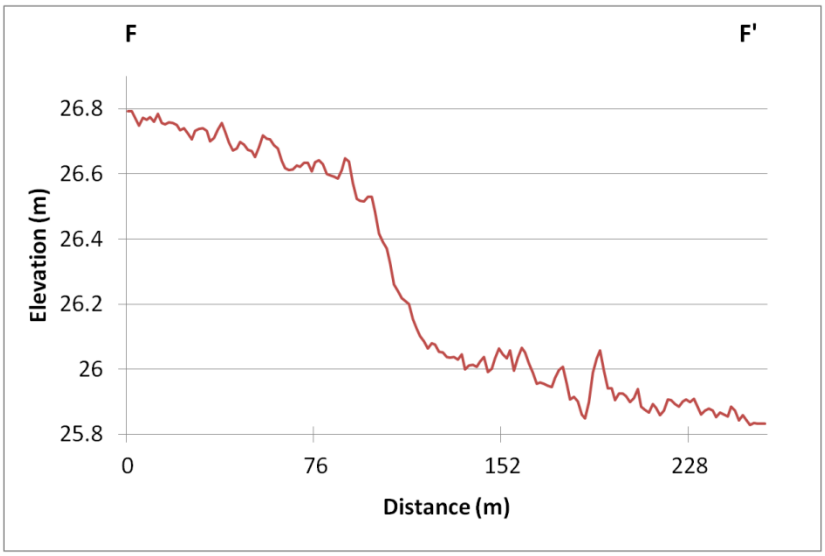

Figure 4-16: Elevation profile across Needville Fault which was interpreted from F to F' from a DEM created with 2005 LiDAR data.

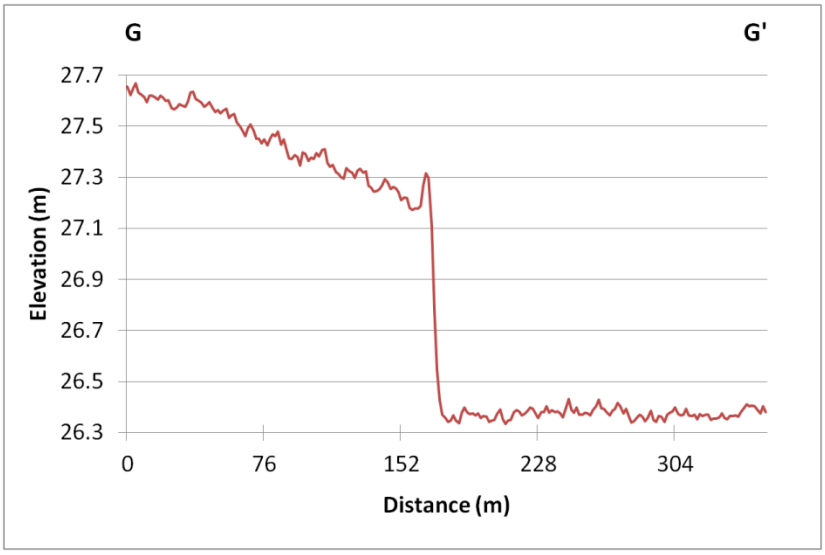

Figure 4-17: Elevation profile across Needville Fault which was interpreted from G to G' from a DEM created with 2005 LiDAR data.

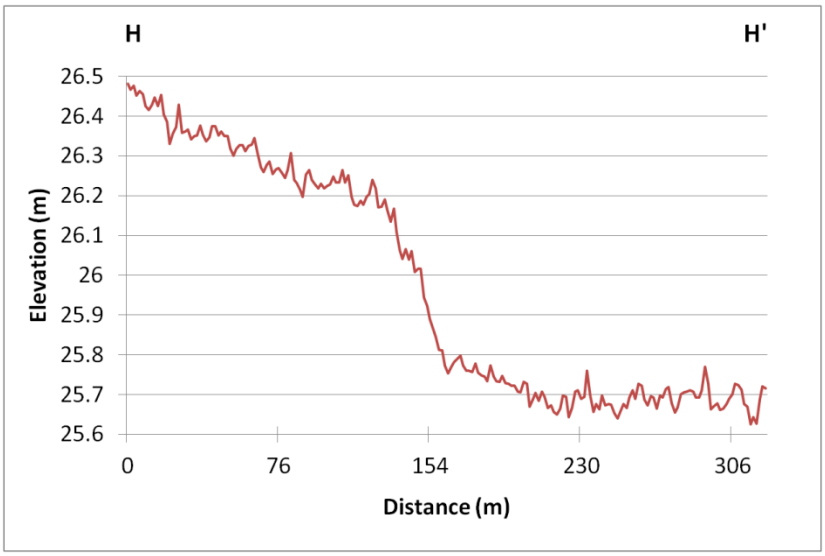

Figure 4-18: Elevation profile across Needville Fault which was interpreted from H to H' from a DEM created with 2005 LiDAR data.

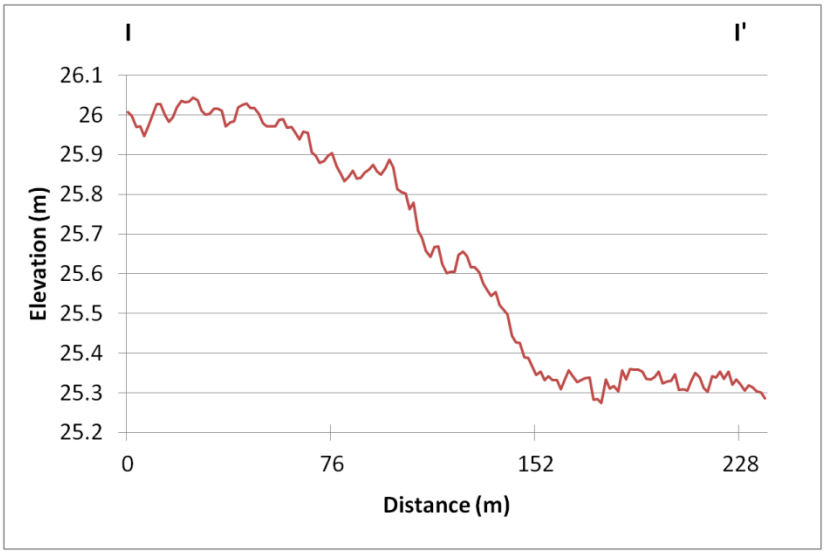

Figure 4-19: Elevation profile across Needville Fault which was interpreted from I to I' from a DEM created with 2005 LiDAR data.

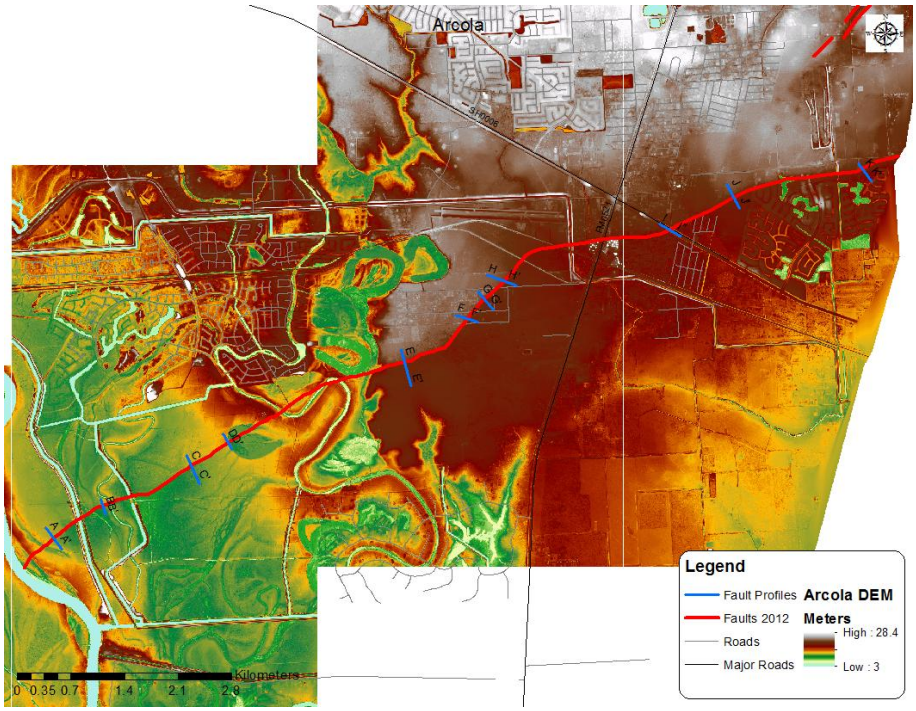

Figure 4-20: Arcola Fault displayed in red that was interpreted from the DEM. Blue lines represent locations of elevation profiles.

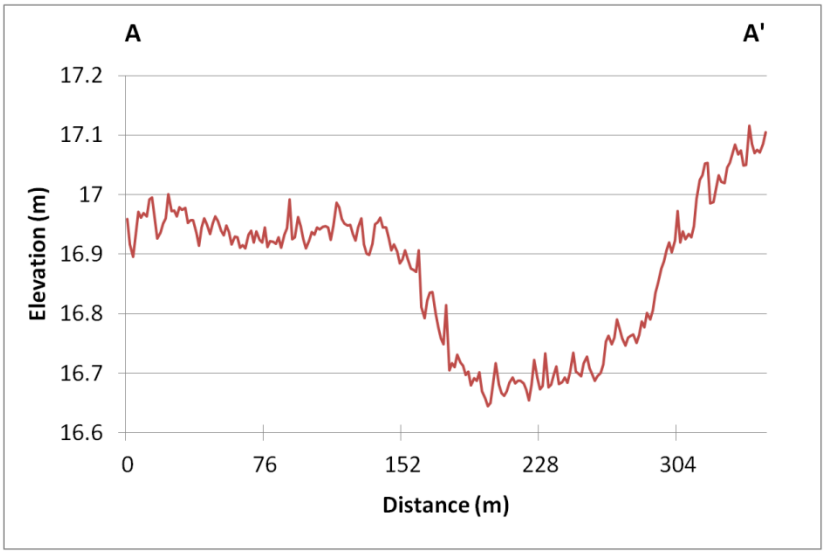

Figure 4-21: Elevation profile across Arcola Fault which was interpreted from A to A' from a DEM created with 2005 LiDAR data.

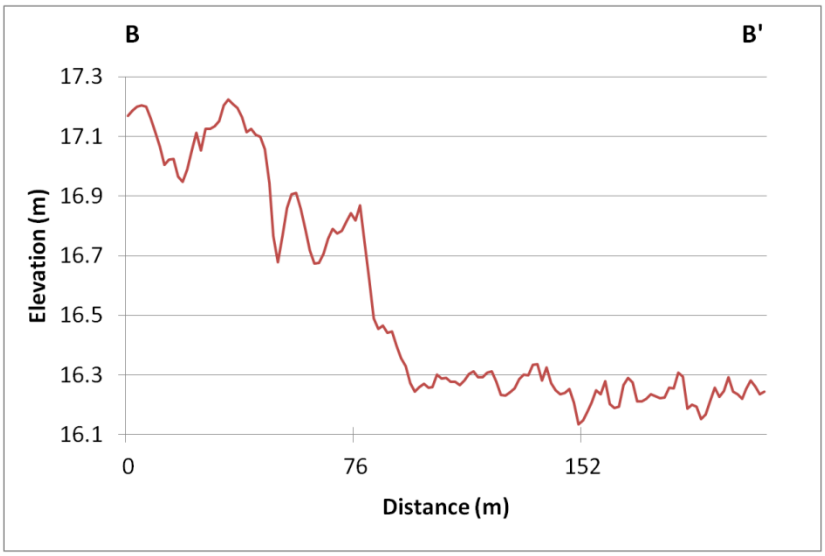

Figure 4-22: Elevation profile across Arcola Fault which was interpreted from B to B' from a DEM created with 2005 LiDAR data.

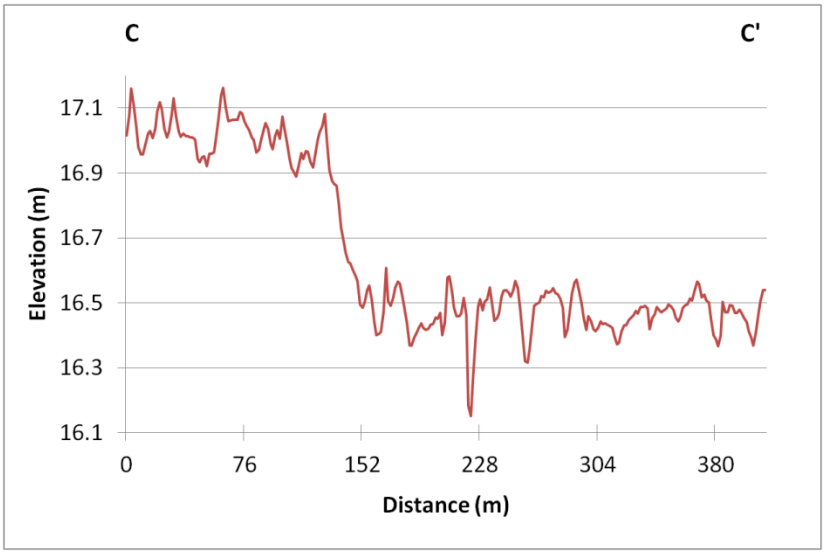

Figure 4-23: Elevation profile across Arcola Fault which was interpreted from C to C' from a DEM created with 2005 LiDAR data.

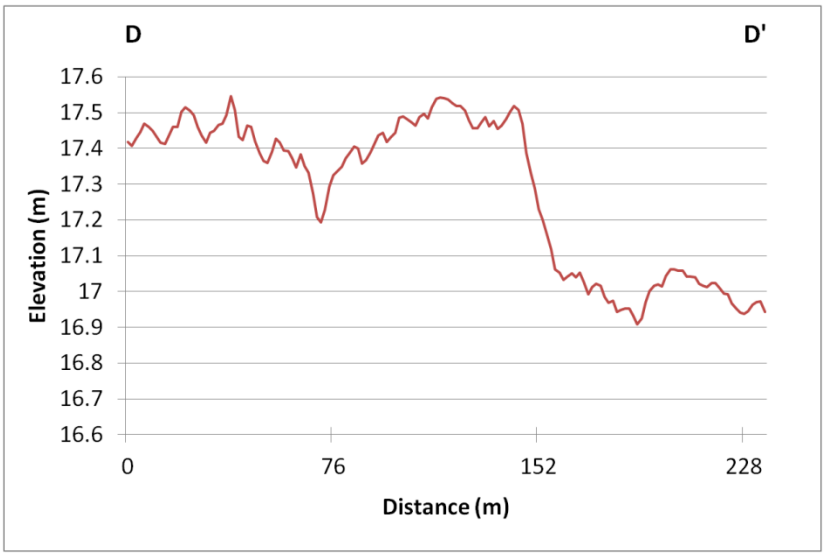

Figure 4-24: Elevation profile across Arcola Fault which was interpreted from D to D' from a DEM created with 2005 LiDAR data.

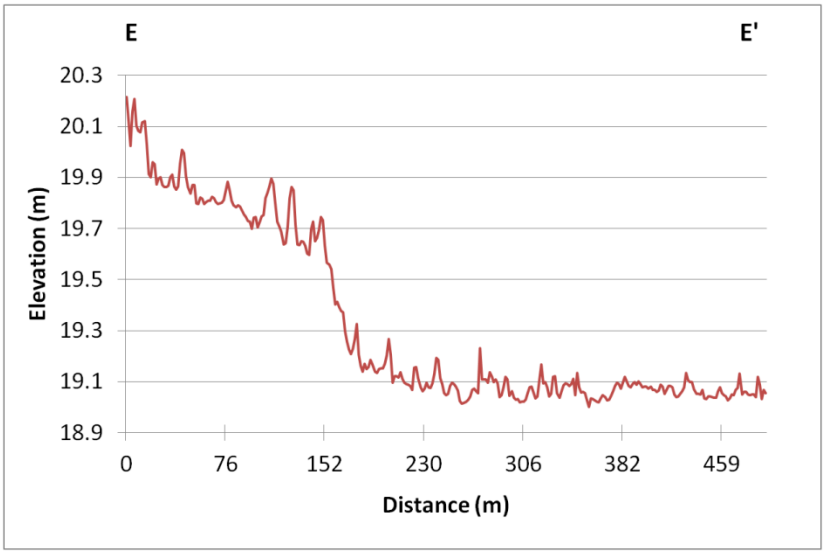

Figure 4-25: Elevation profile across Arcola Fault which was interpreted from E to E' from a DEM created with 2005 LiDAR data.

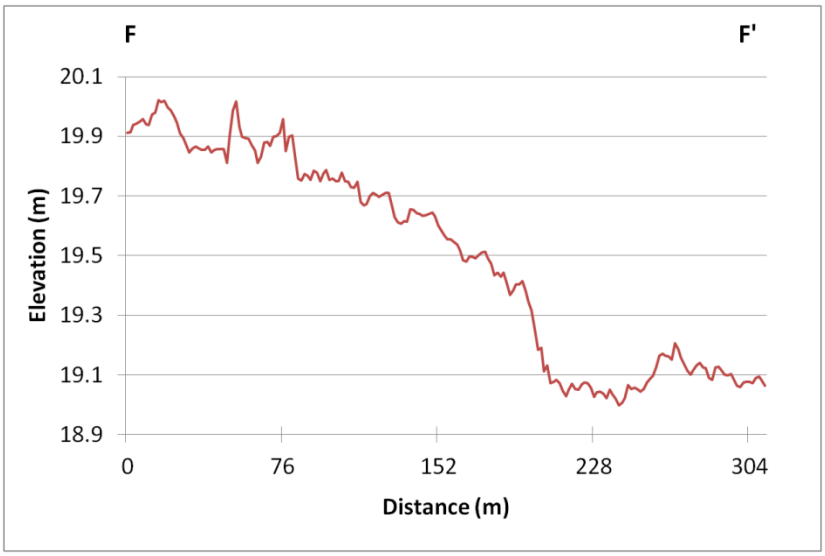

Figure 4-26: Elevation profile across Arcola Fault which was interpreted from F to F' from a DEM created with 2005 LiDAR data.

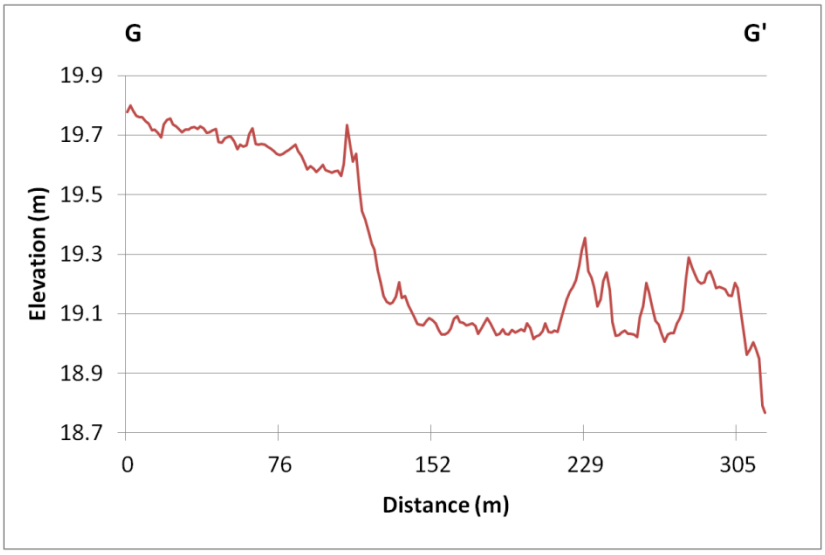

Figure 4-27: Elevation profile across Arcola Fault which was interpreted from G to G' from a DEM created with 2005 LiDAR data.

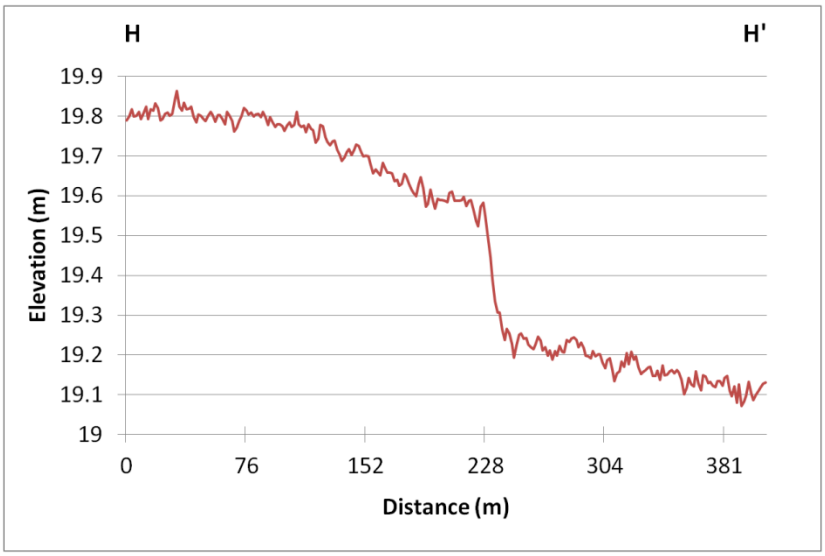

Figure 4-28: Elevation profile across Arcola Fault which was interpreted from H to H' from a DEM created with 2005 LiDAR data.

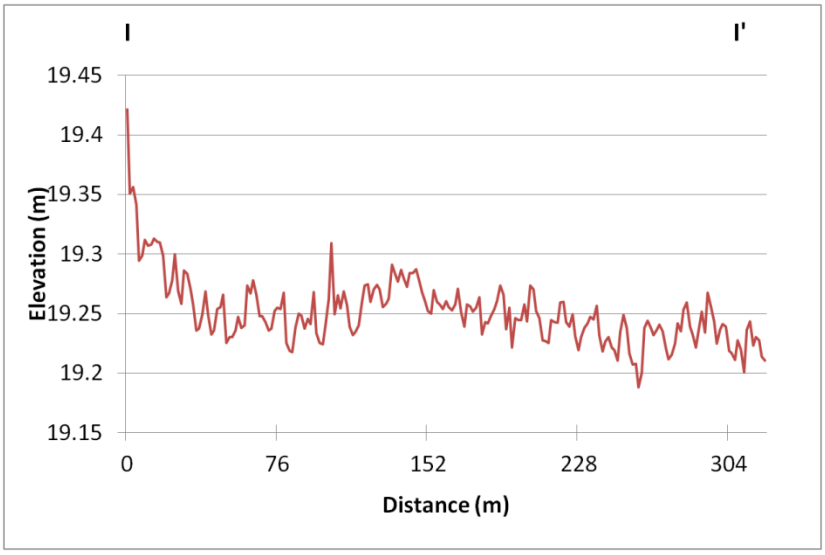

Figure 4-29: Elevation profile across Arcola Fault which was interpreted from I to I' from a DEM created with 2005 LiDAR data.

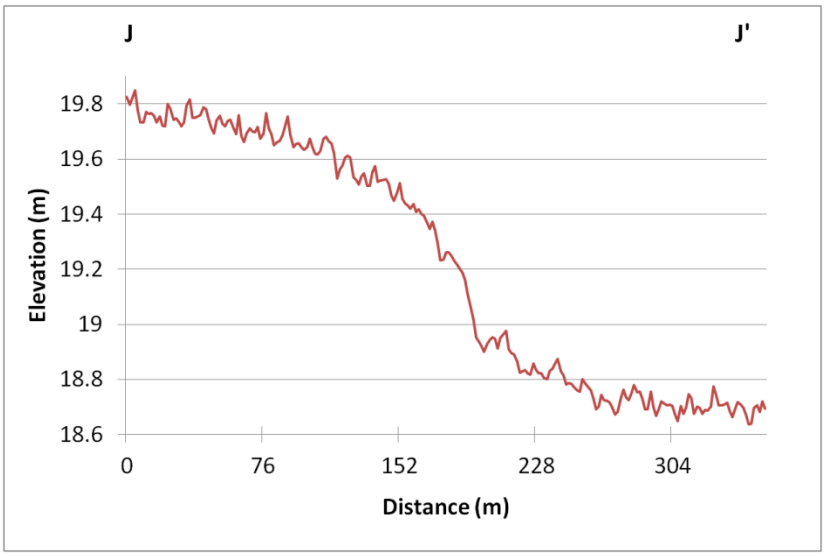

Figure 4-30: Elevation profile across Arcola Fault which was interpreted from J to J' from a DEM created with 2005 LiDAR data.

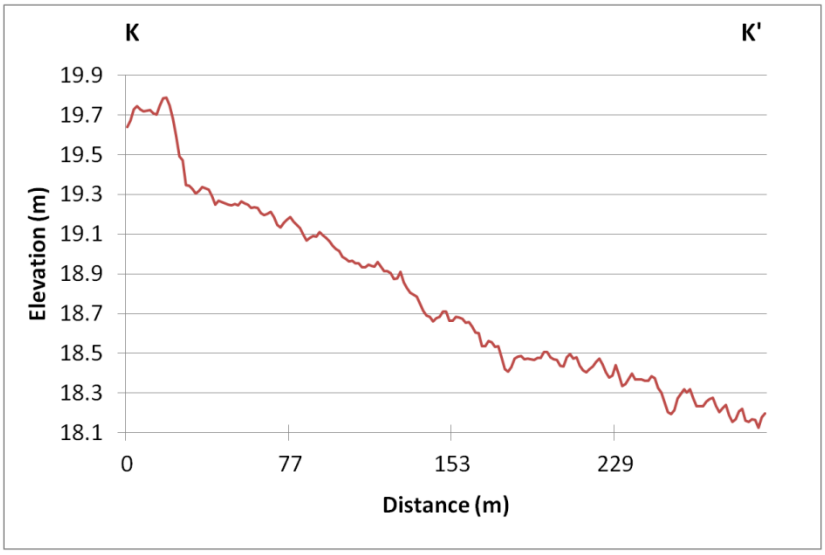

Figure 4-31: Elevation profile across Arcola Fault which was interpreted from K to K' from a DEM created with 2005 LiDAR data.

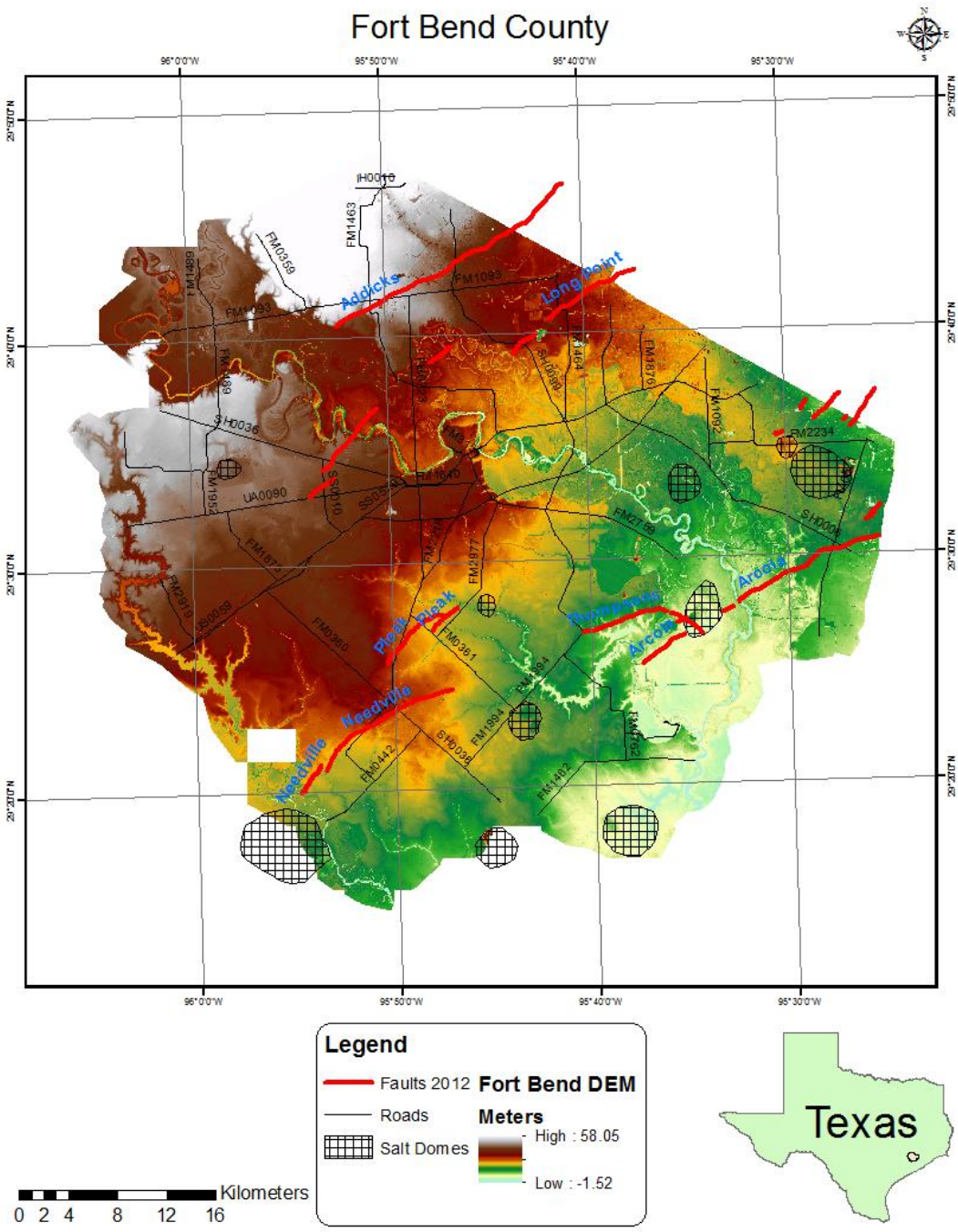

Figure 4-32: Fort Bend County faults displayed in red and salt domes in black both overlaid on the DEM produced from 2005 LiDAR.

4.1.3 GPR

GPR data were collected on a section of the seismic line that was believed to be correlative to the location of the fault using both the 100 MHz and 400 MHz antennas. This exact location along the line for the GPR survey is from flag number 201 to 223. The 100 MHz results did not produce any valuable information that was not present in the 400 MHz and therefore was left out of the final results. The 400 MHz produced very clear images for the top couple meters, but show very little disturbance in the layering of the sediments as can be seen in Figure 4-33. There is a small deformation that appears to coincide with the dip direction of the Needville fault around the 65 meter mark as can be seen in the non-interpreted Figure 4-34 and the interpreted Figure 4-35. This small amount of deformation was very disappointing until it was realized that the GPR section was not located over the main fault location. This was identified when creating a 3D visualization of the area through the use of ARCScene. With the proper location of the main part of the fault identified as being off the end of the GPR section the GPR results became very satisfactory. This GPR section confirms that there is consistent relatively non-deformed sediment near the fault with the only disturbance being a possible very small fault that is part of the Needville fault system. It is unfortunate that when this error was realized that there was not enough time to perform another GPR survey. Since GPR provides a link between the LiDAR and the seismic a full image of the fault is therefore no longer possible to produce.

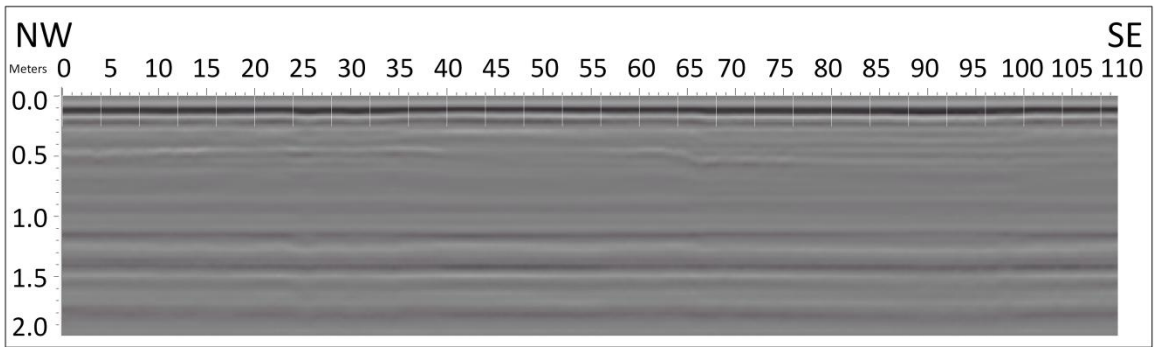

Figure 4-33: Ground Penetrating Radar (GPR) cross section across Needville fault which was collected along Bushnell road in Needville, Texas.

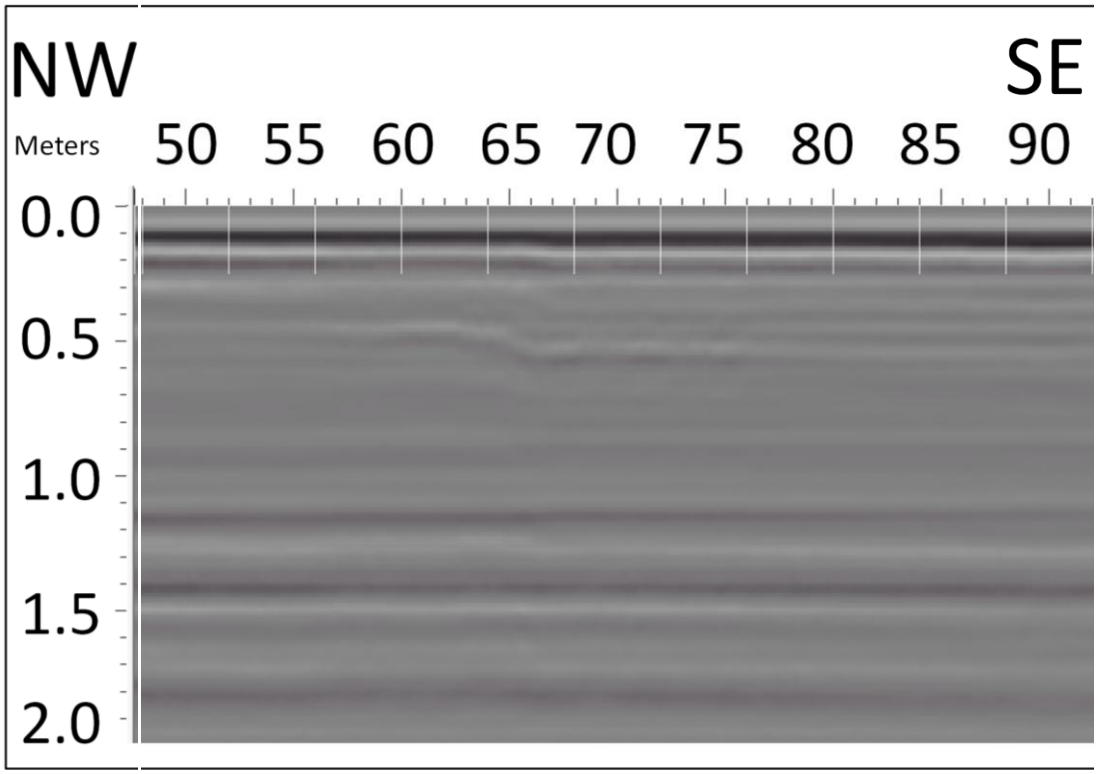

Figure 4-34: Ground Penetrating Radar (GPR) cross section across Needville fault which was collected along Bushnell road in Needville, Texas. This GPR section is focused in on an area of disturbance.

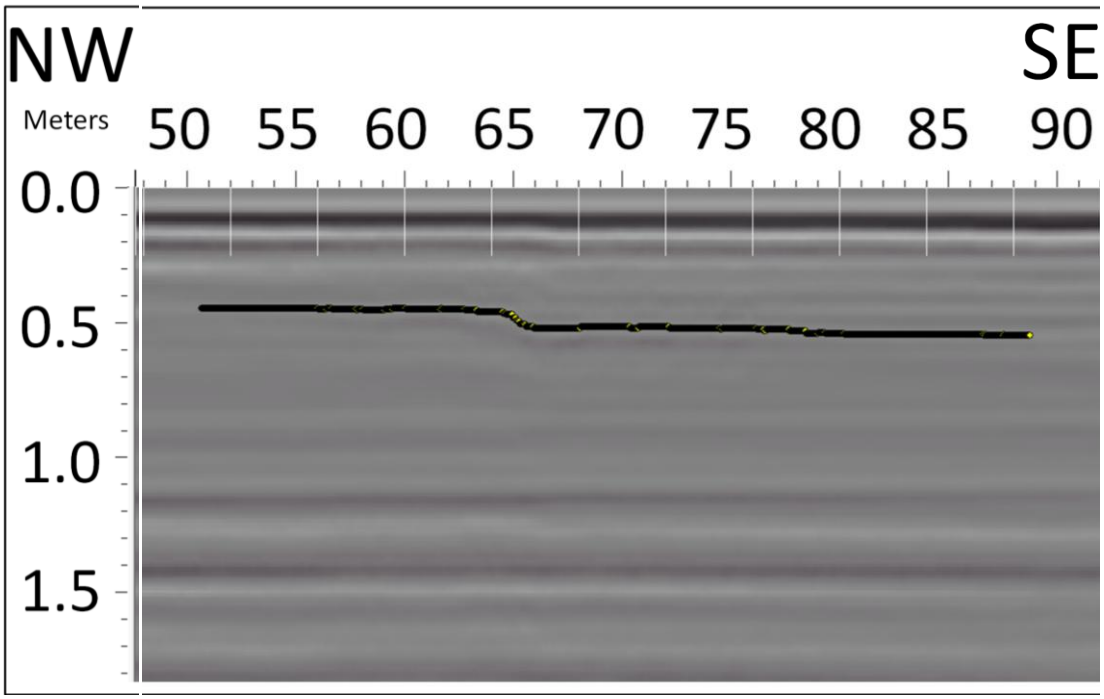

Figure 4-35: Ground Penetrating Radar (GPR) cross section across Needville fault which was collected along Bushnell road in Needville, Texas. This GPR section is focused in on an area of disturbance as can be seen by the picked horizon.

4.1.4 Seismic

The 2D seismic line proved to be successful in revealing the complexity of the faulting near Needville as can be seen in Figure 4-36, and with horizons picked in Figure 4-37. As you can see there is not really a sharp and distinct fault, but rather a faulting zone that starts at the surface around the 550 meter mark, and can be followed relatively easily to time of 800ms at the 300 meter mark. Not only do the seismic reflections reveal the fault, but also the fault can be seen in the velocity data as a low velocity zone as is seen in Figure 4-38. Adjusting the aspect ratio on the seismic line to where the y-axis is 1000ms another feature displays clearer as can be seen in Figure

4-39 and Figure 4-40. This might be an antithetic fault that seems to start at around 450ms at about the 425 meter mark, and is still visible until about time of 850ms at the 625 meter mark.

From these observations the Needville Fault was interpreted along with a possible second fault. This interpretation can be seen in Figure 4-41 with no horizons, and in Figure 4-42 with the horizons. The yellow line identifies the Needville Fault, and the red line identifies what may be an antithetic fault.

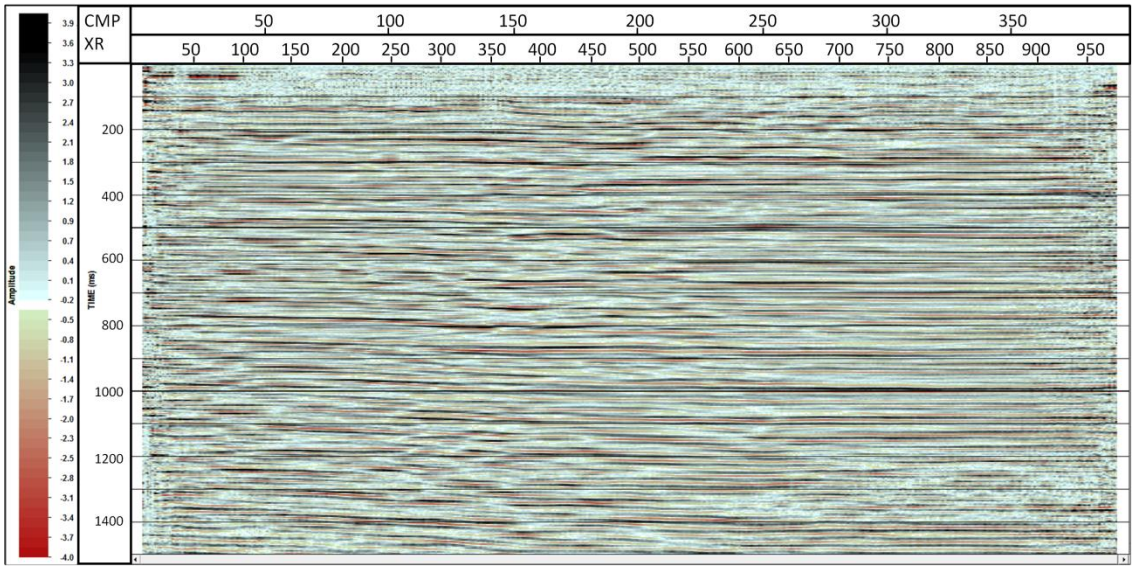

Figure 4-36: Seismic reflections section along Bushnell Rd. in Needville, Texas.

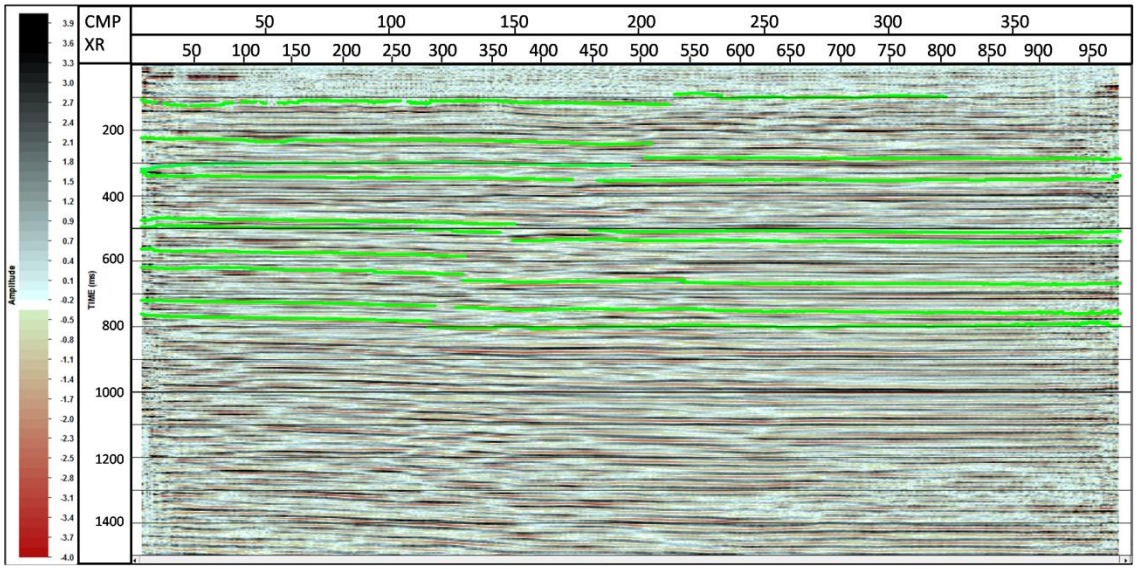

Figure 4-37: Seismic reflections section with horizons picked along Bushnell Rd. in Needville, Texas.

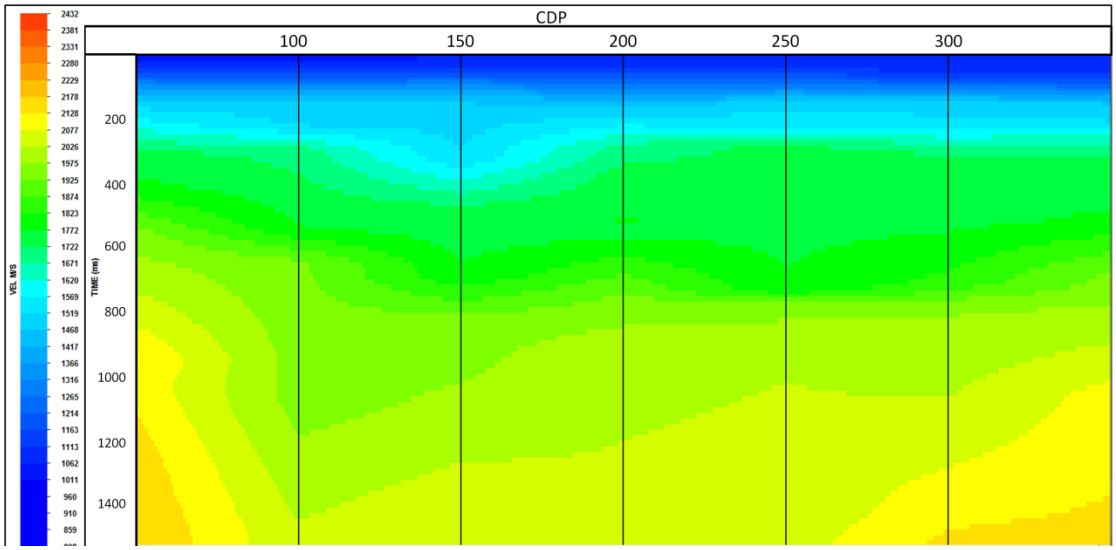

Figure 4-38: Velocity model derived from seismic section acquired along Bushnell Rd. in Needville, Texas.

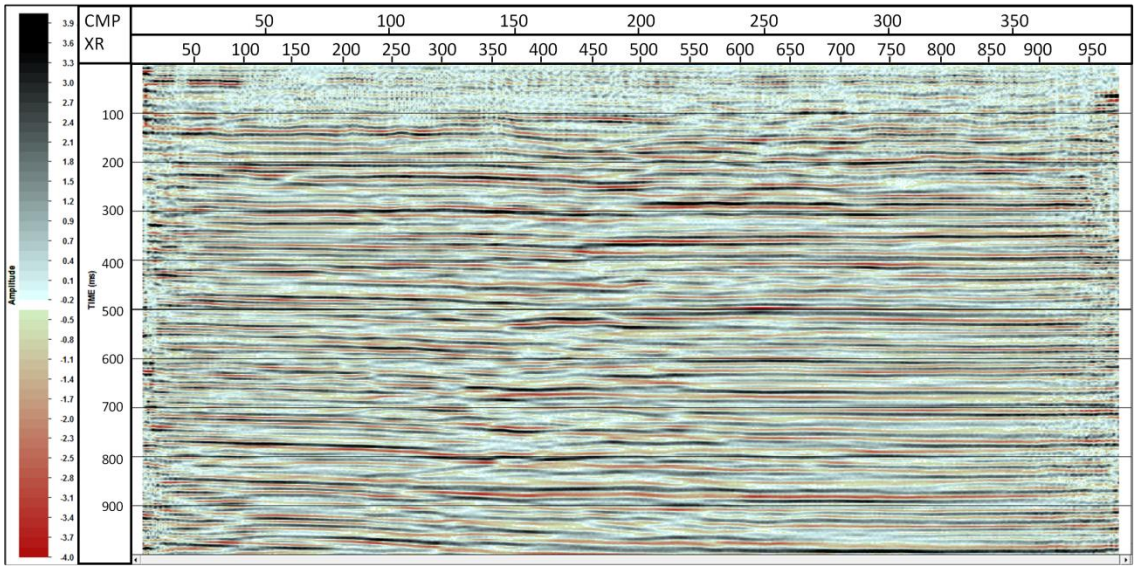

Figure 4-39: Seismic reflection section along Bushnell Rd. in Needville, Texas.

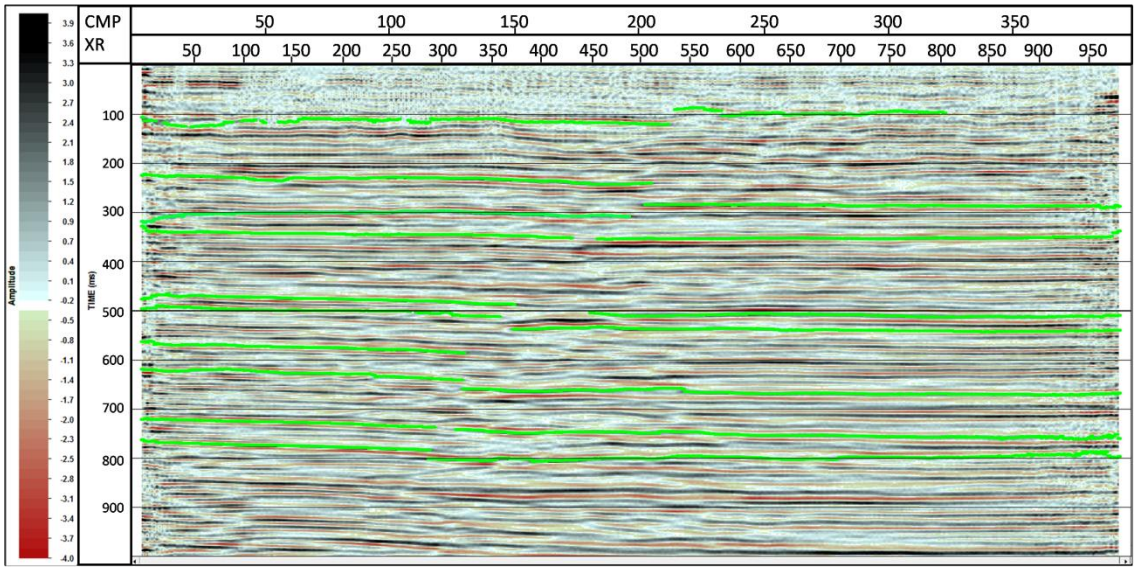

Figure 4-40: Seismic reflection section with horizons picked along Bushnell Rd. in Needville, Texas.

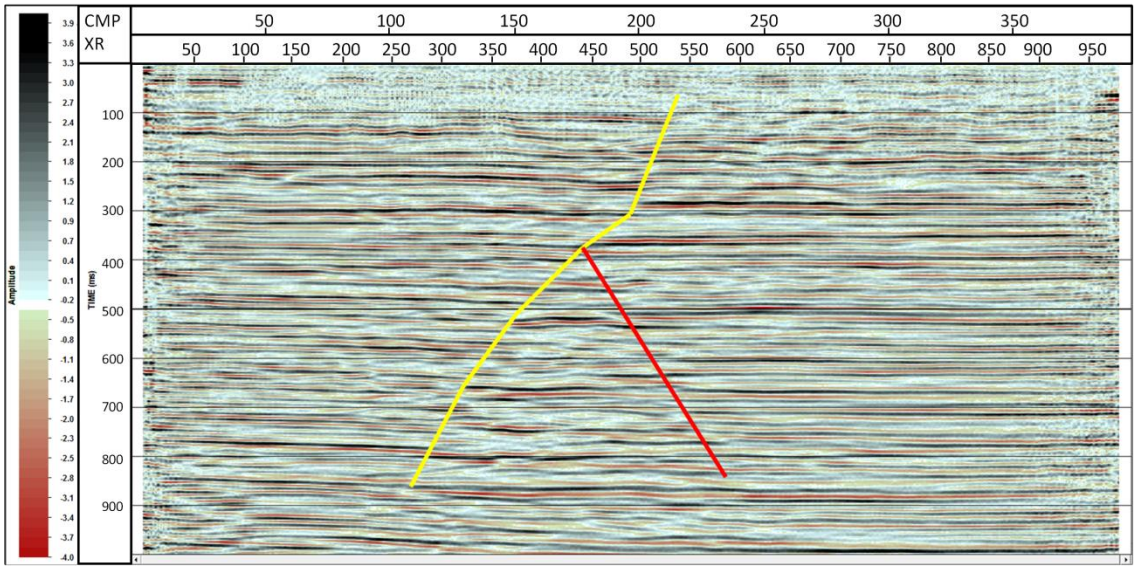

Figure 4-41: Seismic reflection section along Bushnell Rd. in Needville, Texas with Needville fault displayed in yellow, and a possible antithetic fault displayed in red.

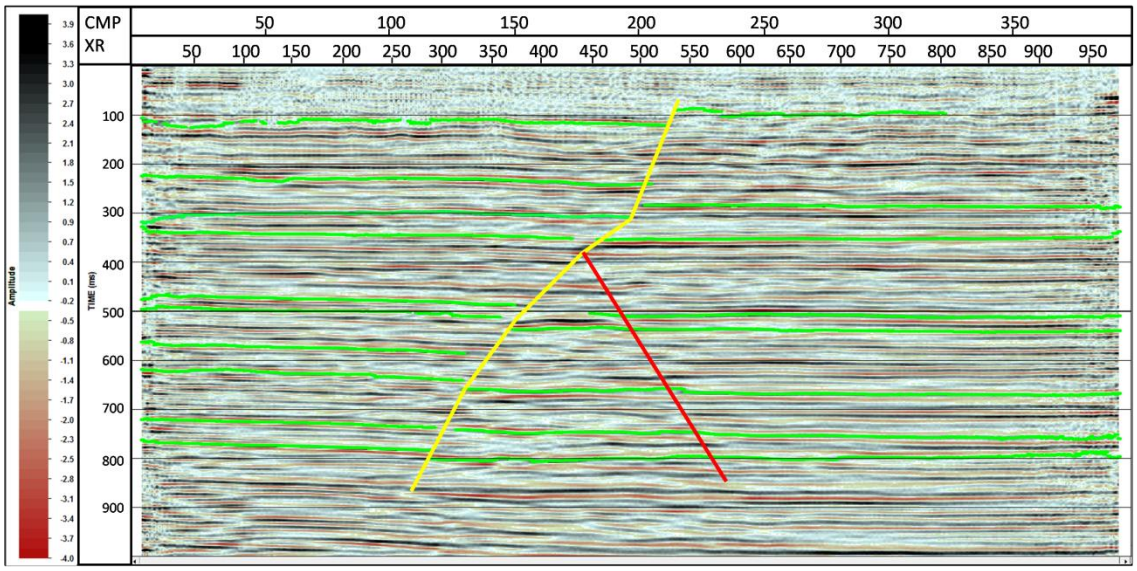

Figure 4-42: Seismic reflection section with horizons (in green) picked along Bushnell Rd. in Needville, Texas with Needville fault displayed in yellow, and a possible antithetic fault displayed in red.

4.1.5 Well Logs

The well logs provided results that were expected in that they confirmed the presence of both the Needville and Thompsons faults at the location of the cross sections as indicated in Figure 4-43 and Figure 4-45 respectively. The Needville and Thompsons cross sections can be seen in Figure 4-44 and Figure 4-46 respectively. Not enough well logs were able to be collected around the Arcola fault in order to conclude any presence of a fault or to even be able to produce a reliable cross section. This lack of well logs from the Arcola area is partially because of the greater number of salt domes in the area which caused many of the obtainable well logs to be affected by the presence of a salt dome. This salt dome presence enhances the difficulty in well log correlation from a well log near the salt dome to a well log unaffected by the salt dome.

The well logs from Needville clearly reveal a normal fault with approximately 75 meters of vertical offset that is dipping to the southeast, but also reveals a second fault that is slightly further to the southeast. I was unable to obtain enough well logs to be able to fully understand how this second fault is oriented. The well logs from Thompsons clearly show a fault that has approximately 75 meters of vertical displacement closer to the surface, and has closer to 69 meters of vertical displacement deeper, and is dipping to the southeast.

The ability to view the GeoMap structure maps proved to be very valuable in confirming that they were similar to the structure contour maps I produced from my

well correlations. However, they do not look the same since GeoMap has much more data, and therefore has a much higher density of which to form their contours. When picking correlation points for the well logs it was very clear that the most consistent formations across all the well logs from oldest to youngest were the Vicksburg (Figure 4-47), Frio (Figure 4-48), Anahuac (Figure 4-49), and R (Figure 4-50) Formations. The formation R is a mostly sand layer that is approximately 67 meters thick, and lies directly on top of the Anahuac Formation.

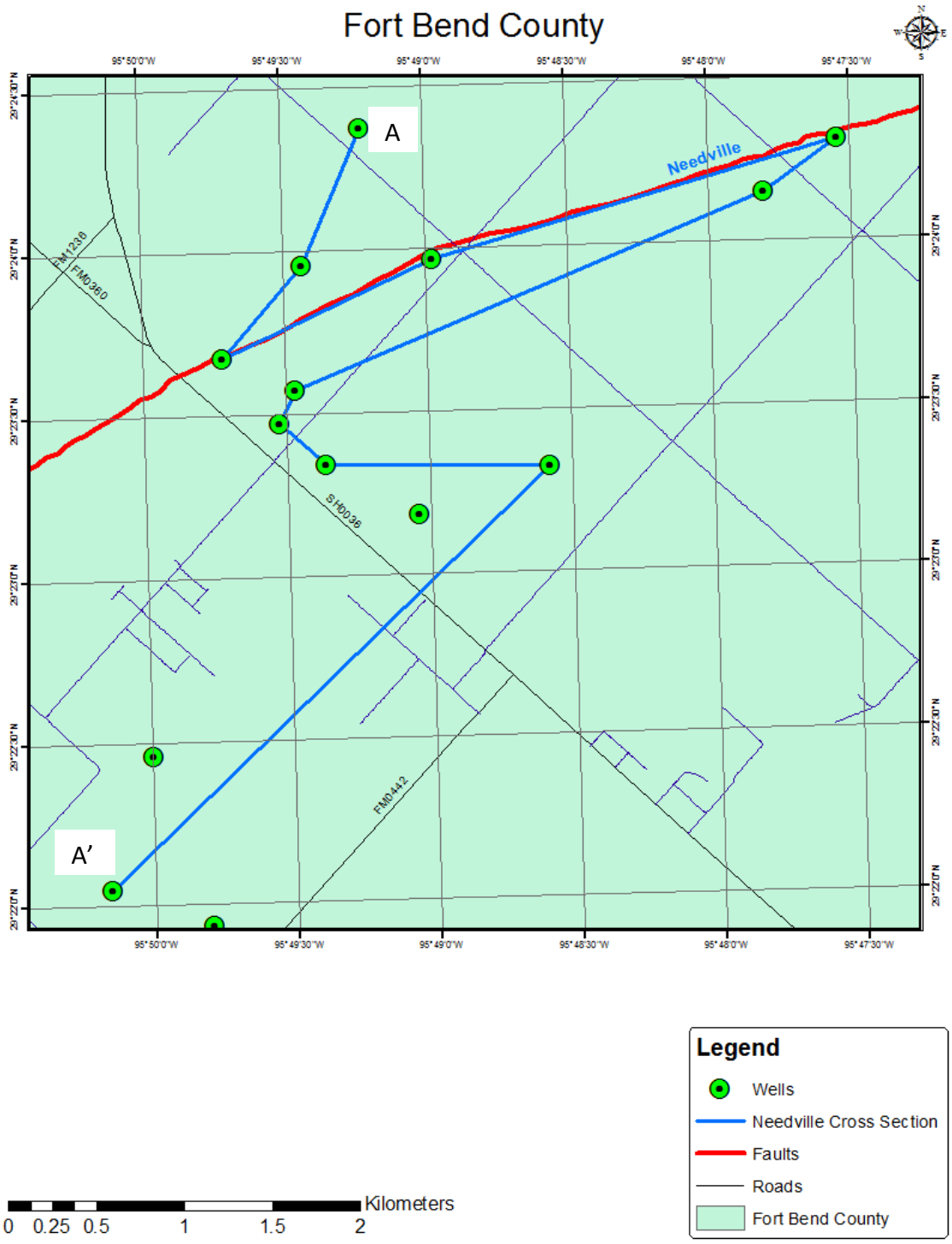

Figure 4-43: Location of Needville cross section produced from correlated well logs.

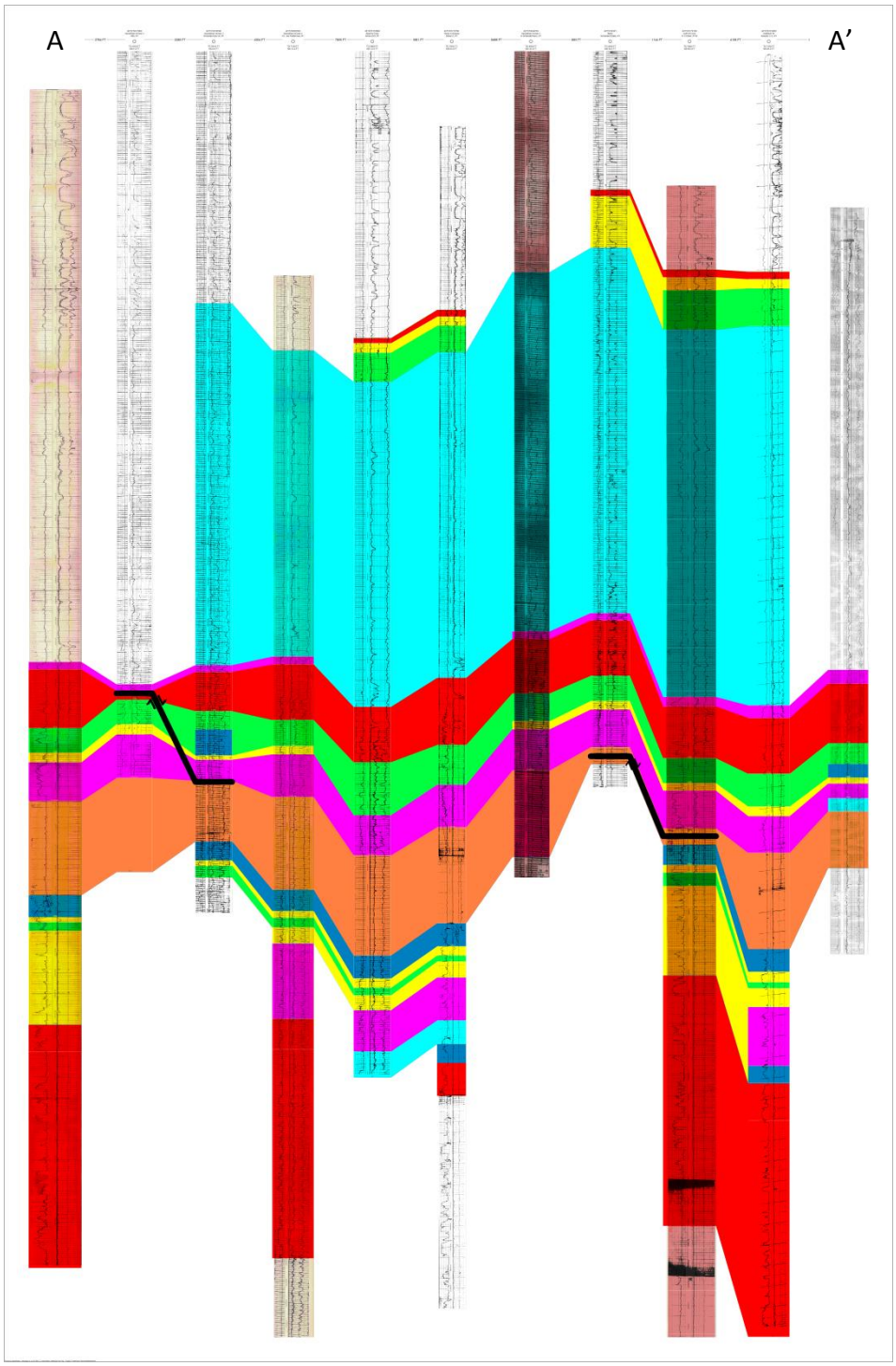

Figure 4-44: Needville cross section produced from correlated well logs.

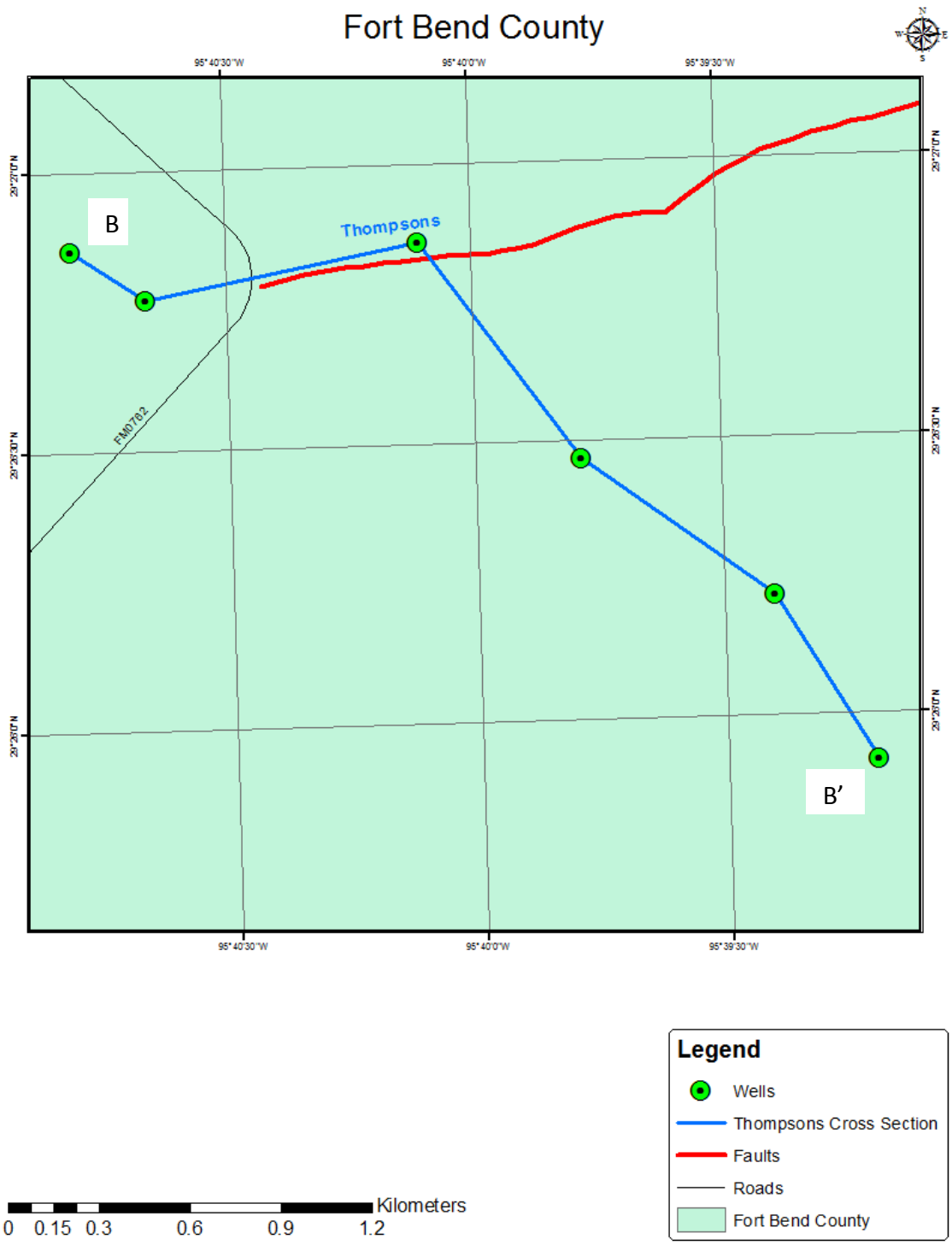

Figure 4-45: Location of Thompson cross section produced from correlated well logs.

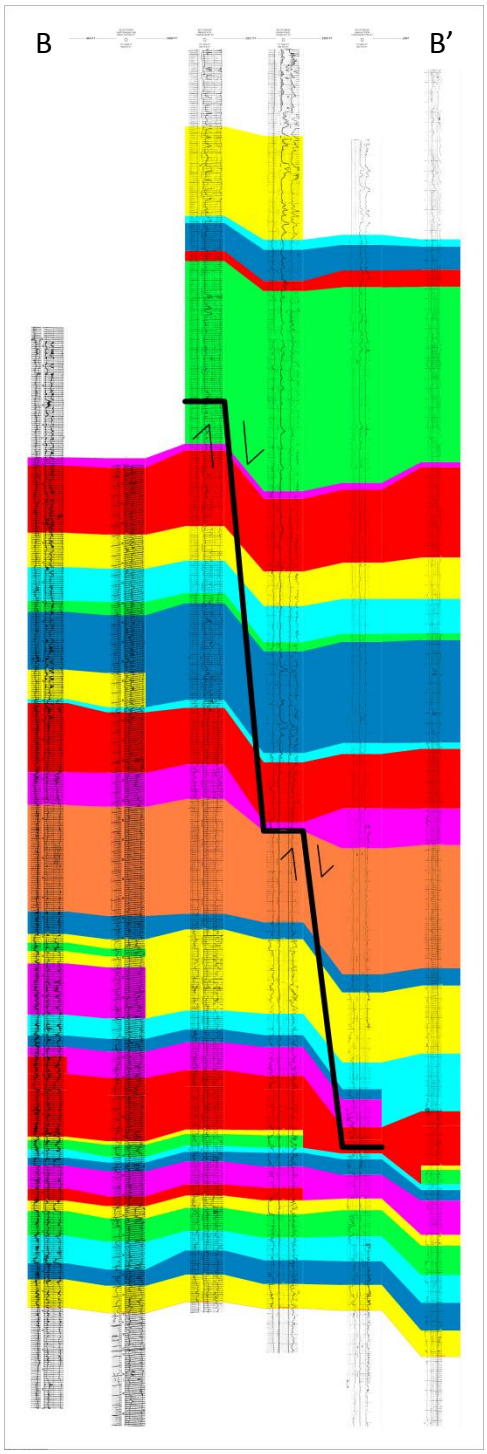

Figure 4-46: Thompsons cross section produced from correlated well logs.

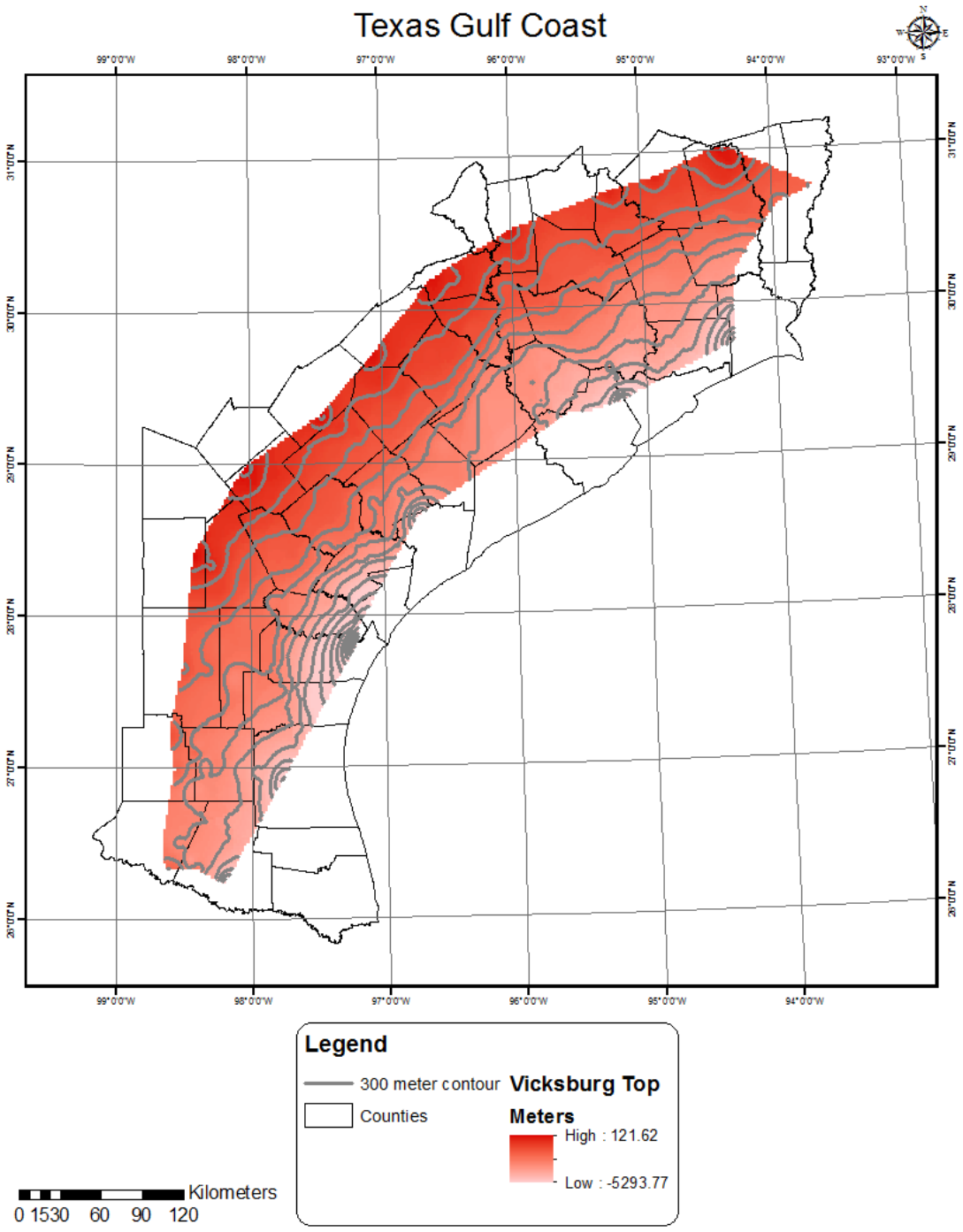

Figure 4-47: Structure contour map of the Vicksburg formation as picked from the collected well logs along the Texas Gulf Coast.

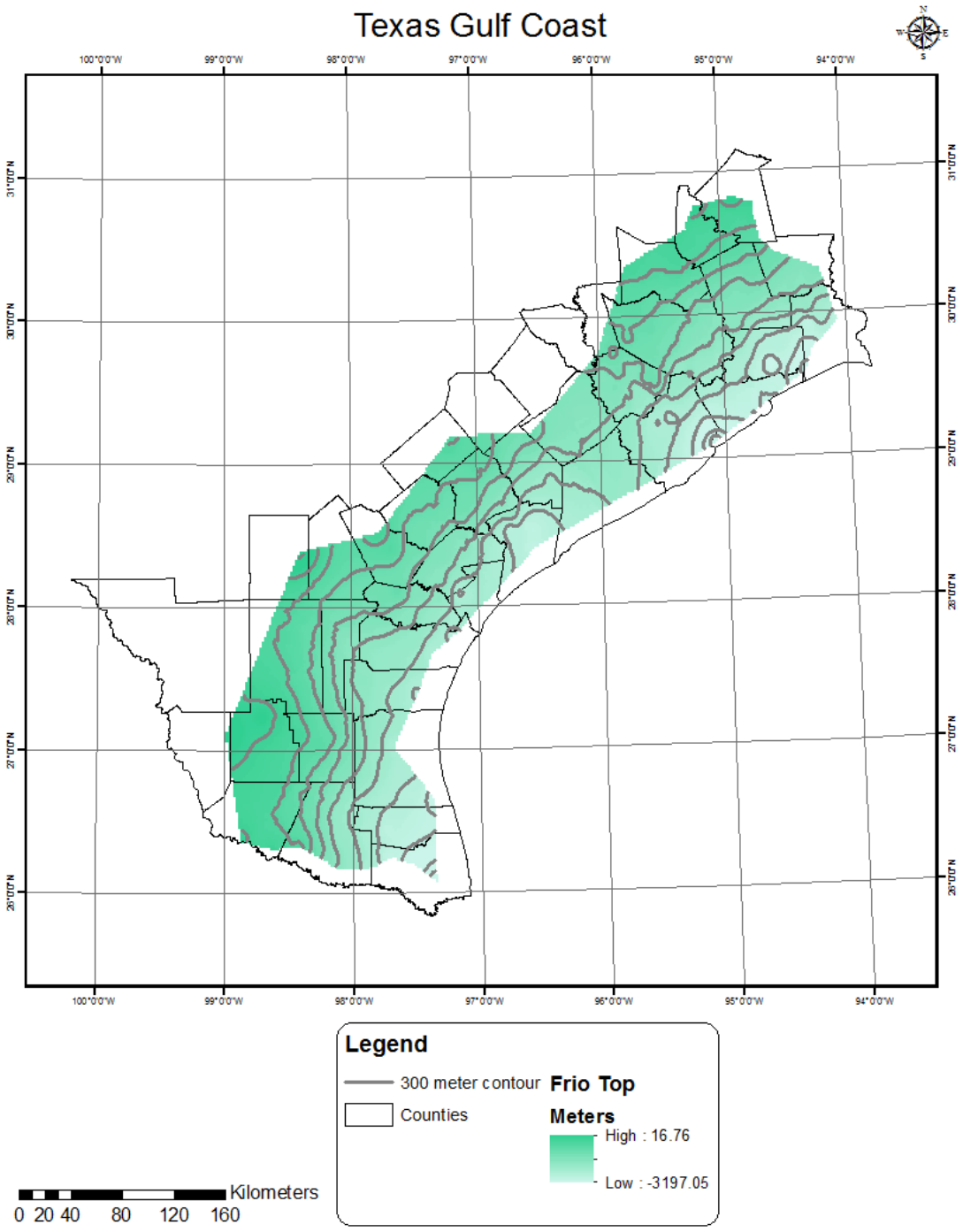

Figure 4-48: Structure contour map of the Frio formation as picked from the collected well logs along the Texas Gulf Coast.

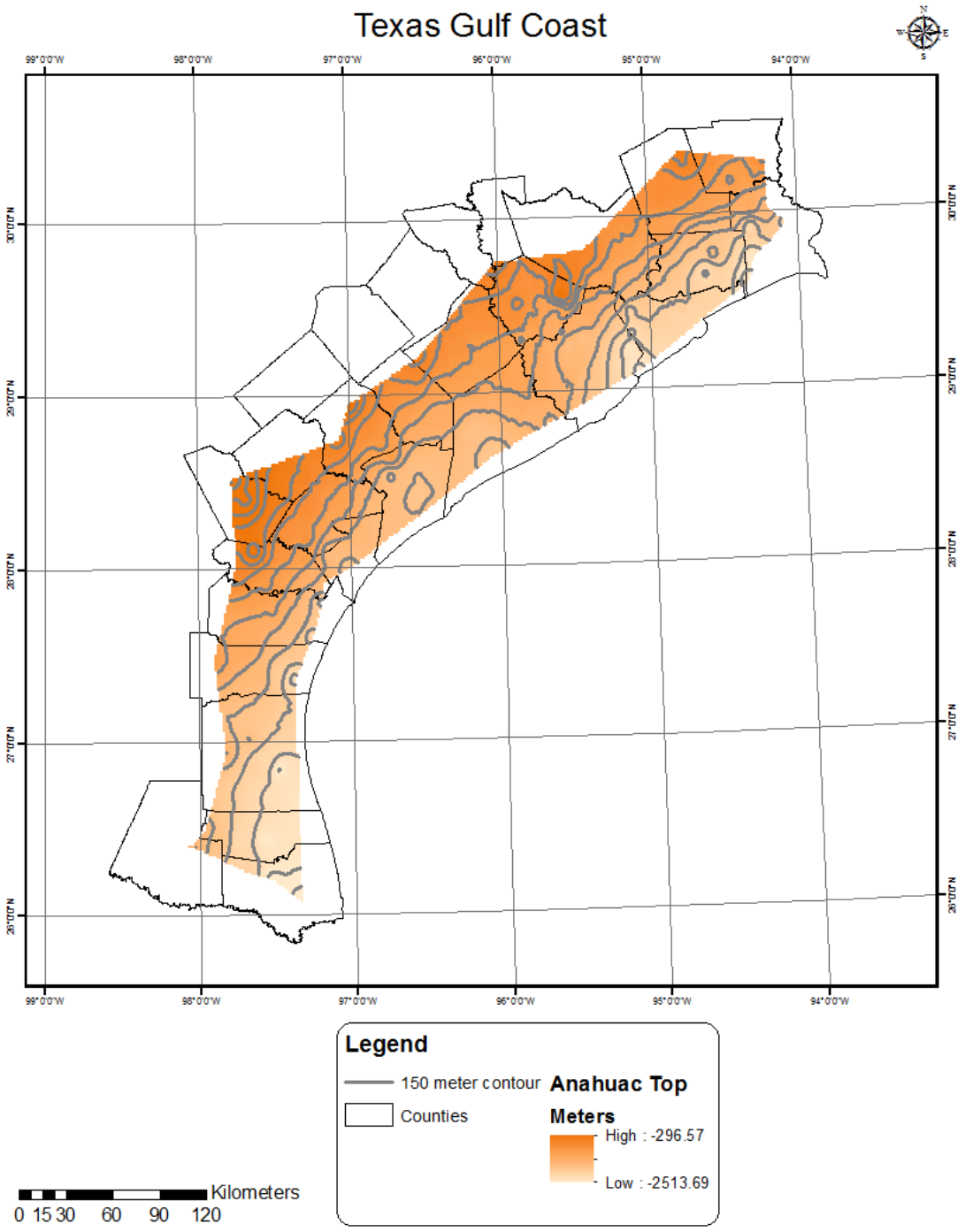

Figure 4-49: Structure contour map of the Anahuac formation as picked from the collected well logs along the Texas Gulf Coast.

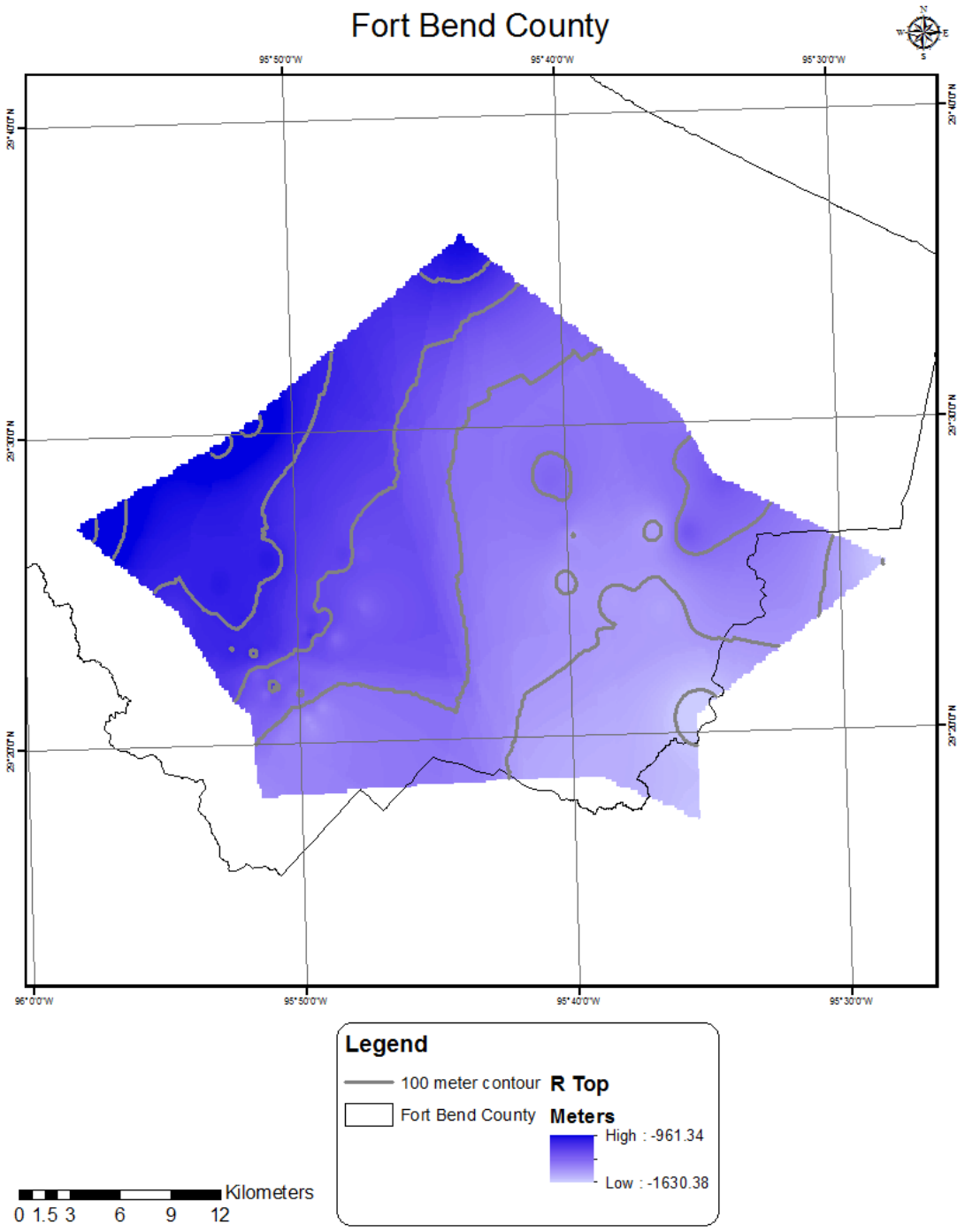

Figure 4-50: Structure contour map of the R formation as picked from the collected well logs in Fort Bend County, Texas.

4.1.6 Gravity

The collected gravity data produced a result that was unexpected, but makes sense. The expectation was for there to be higher gravity on one side of the fault as compared to the other. The result of the gravity survey shows that there are no gravity anomalies on either side of the fault. The gravity values only have a range of less than 0.2 mGal and therefore appear to be very noisy over a distance of 960 meters. It is expected that the gravity value range would be very small on the scale of within 1 mGal due to the soil types in the area, and the lack of great differences in density contrast if salt does not cross a part of the survey. The gravity did produce a positive result in confirming the fault location. This is because the gravity shows only one anomaly, which happens to be a gravity low of approximately 0.05 mGal directly corresponding to the location of the fault. This result can be seen in Figure 4-51, and an elevation profile for the gravity profile can be seen in Figure 4-52.

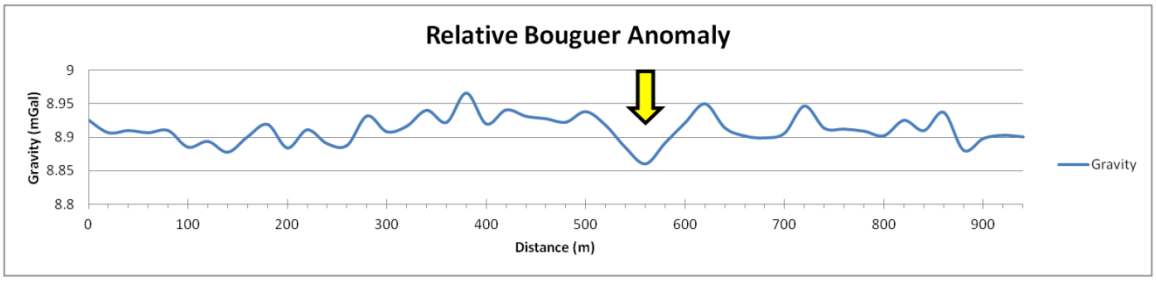

Figure 4-51: Relative Bouguer Anomaly profile along Bushnell Rd. in Needville, Texas. Fault indicated by arrow.

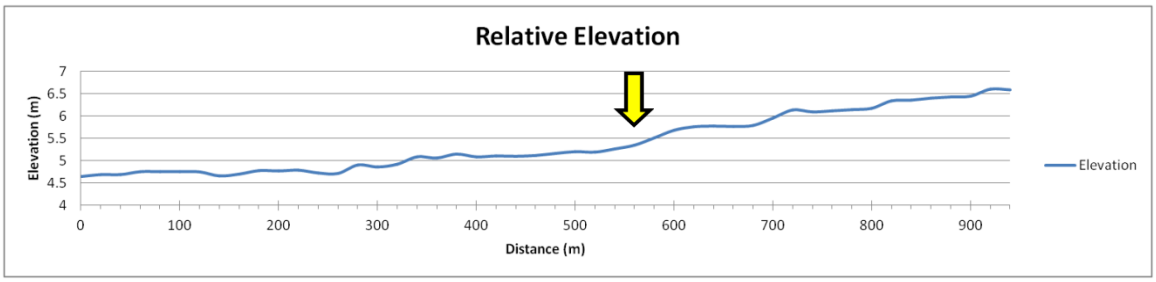

Figure 4-52: Relative Elevation profile along Bushnell Rd. in Needville, Texas.

4.1.7 Combination

All of the techniques used in this study proved to be complimentary in their respective results. The combination of all the data into a single software proved to be a challenge but was a success. This combination allows for a much easier viewing of the data, and therefore reduces the likelihood of interpretation mistakes due to lack of 3D spatial recognition of the interpreter. The fully integrated data can be seen in the attached video. A screen shot of the integrated 3D model can be seen in Figure 4-53.

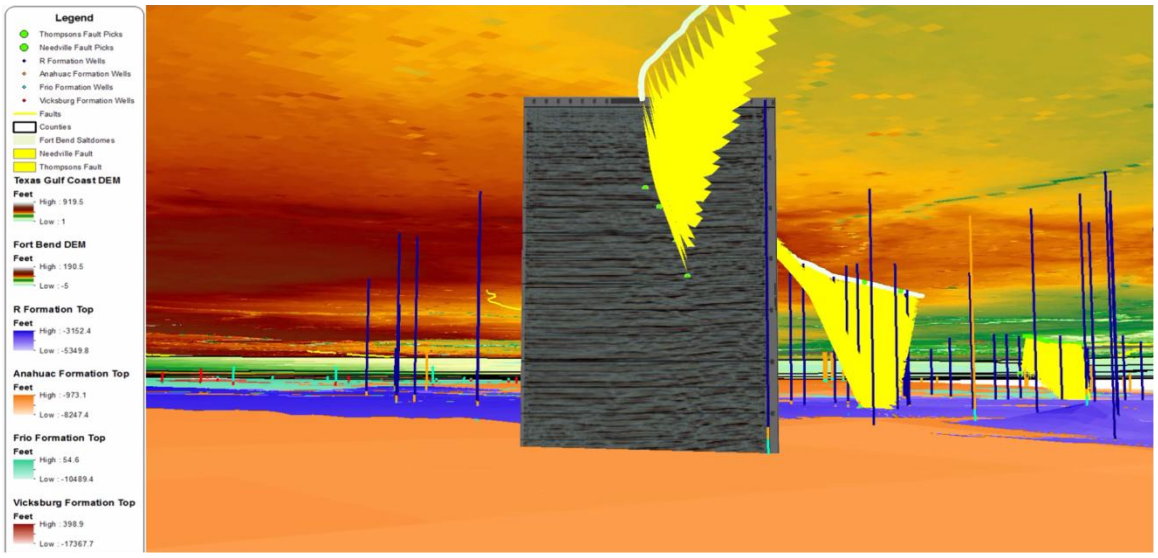

Figure 4-53: Screenshot of the integrated 3D model of Fort Bend County.

Chapter 5

5.1 Conclusions

This study provides a link between older technologies with new technologies in a way that demonstrates that each technology on its own cannot reveal the geologic activity of any area, but by combining multiple technologies a much better understanding can be reached. With the combined technologies the interpreted result is also a lot more reliable than making an interpretation based purely on a single data set. The knowledge that can be gained by combining multiple technologies into a single compilation for easier viewing is a task that should be practiced more often in order to reduce errors in interpretation of data. These blind errors are evident with the interpretation of the GPR data before integrating the GPR data with the other data sets. As more data integration occurs in the future, greater knowledge will be obtained from the same amount and quality of data there is at the present.

The methodologies used in this study proved to be complementary, and work very efficiently together. The LiDAR produced a comprehensive surface model that revealed faulting never recorded before. The GPR while not acquired in the right location did reveal the power it has to link LiDAR to seismic data. The seismic data displayed a comprehensive vertical section that allowed the fault to be interpreted deeper than was possible with the GPR and well logs. The well logs provided a source of

information to produce a widespread subsurface model, while they lack the detail that seismic produces. Then the gravity data were able to confirm that there is an anomaly in the location of the fault. GPS also agreed with there being differences in displacement rates on either side of the fault. With this amount of integration of the technologies in Fort Bend County this study produced a comprehensive 3D model that represents a typical example of how complex the geology is of the passive margin of the Gulf Coast.

Chapter 6 Disclaimer

All of the results featured in this thesis that are construed as my own represent my personal conclusions, and therefore aforementioned companies and individuals should not be held responsible for any conclusions that were drawn from their donated services or data.

Chapter 7 Works Cited

Baker, E. T. (1978). *Stratigraphic and Hydrogeologic Framework of Part of the Coastal Plain of Texas.* Open-File Report 77-712, United States Department of the Interior.

Baker, E. T. (1995). *Stratigraphic Nomenclature and Geologic Sections of the Gulf Coastal Plain of Texas.* Open-File Report 94-461, U.S. Department of the Interior, Austin, Texas.

Bebout, D. G., Luttrell, P. E., & Seo, J. H. (1976). *Regional Tertiary Cross Sections - Texas Gulf Coast.* University of Texas at Austin. Austin: Bureau of Economic Geology.

Boccanera, J. A. (1989). *Investigation of Surface Faulting, Brazoria County, Texas Using Aerial Photography, Field Data, Well Log Data, Seismic Profiles and Fault Modeling.* Masters Thesis, University of Houston, Department of Geosciences, Houston.

Chowdhury, A. H., & Turco, M. J. (2006). Chapter 2: Geology of the Gulf Coast Aquifer, Texas. In R. E. Mace, S. C. Davidson, E. S. Angle, & W. F. Mullican, *Aquifers of the Gulf Coast of Texas: Texas Water Development Board Report 365* (pp. 23-50).

Coplin, L. S., & Galloway, D. (1999). Houston-Galveston, Texas - Managing coastal subsidence. In D. Galloway, D. R. Jones, & S. E. Ingebritsen, *Land subsidence in the United States: U.S. Geological Survey Circular 1182* (pp. 35-48).

Ellisor, A. C. (1994, September). Anahuac Formation Houston, Texas. *Bulletin of the American Association of Petroleum Geologists, 28*(9), 1355-1375.

Engelkemeir, R. (2008). *Evaluating Houston Area Neotectonics Using GIS and Remote Sensing Techniques.* PhD Dissertation, University of Houston, Department of Geosciences, Houston.

Engelkemeir, R. M., & Khan, S. D. (2008). Lidar mapping of faults in Houston, Texas, USA. *Geosphere, 4*(1), 170-182.

Engelkemeir, R., Khan, S. D., & Burke, K. (2010). Surface deformation in Houston, Texas using GPS. *Tectonophysics, 490*, 47-54.

Fjaer, E., Holt, R. M., Horsrud, P., Raeen, A. M., & Risnes, R. (2008). *Petroleum Related Rock Mechanics* (2nd ed., Vol. 53).

Greenman, W. E., & Gustafson, E. E. (1953). *Needville Field Fort Bend County, Texas.* Houston: Goldston Oil Corporation.

GSSI. (2012). Retrieved from Geophysical Survey Systems, Inc.: http://www.geophysical.com/

Harris Galveston Subsidence District. (n.d.). Retrieved 2012, from http://mapper.subsidence.org/

Hovorka, S. D., Holtz, M. H., Sakurai, S., & Knox, P. R. (2003). *Frio Pilot in CO2 Sequestration in Brine-Bearing Sandstones.* Austin: Texas Bureau of Economic Geology.

McCarter, W. B., & O'Bannon, P. H. (1933, November). Sugarland Oil Field, Fort Bend County, Texas. *Bulletin of the American Association of Petroleum Geologists*, 709-733.

Pollack, J. M. (1953). Sugarland Field Fort Bend County, Texas. *Houston Geological Society, 2007*, 153-156.

Ruhl, J. H. (1991). *Identification, Geometry, and Movement History of Active Surface Faults in Fort Bend County, Texas.* Masters Thesis, University of Houston, Department of Geosciences, Houston.

TIGER. (2012). Retrieved from United States Census Bureau: http://www.census.gov/geo/maps-data/data/tiger.html

TNRIS. (2012). Retrieved from Texas Natural Resources Information System: http://www.tnris.org/

Verbeek, E. R., & Clanton, U. S. (1981). Historically Active Faults in the Houston Metropolitan Area, Texas. *Houston Geological Society, 2007*, 28-68.

Chapter 8 Appendix A

The Following figures were were digitized as well logs, and well locations in order to better produce a 3D model of the Texas Gulf Coast.

8.1 (Baker, Stratigraphic and Hydrogeologic Framework of Part of the Coastal Plain of Texas, 1978)

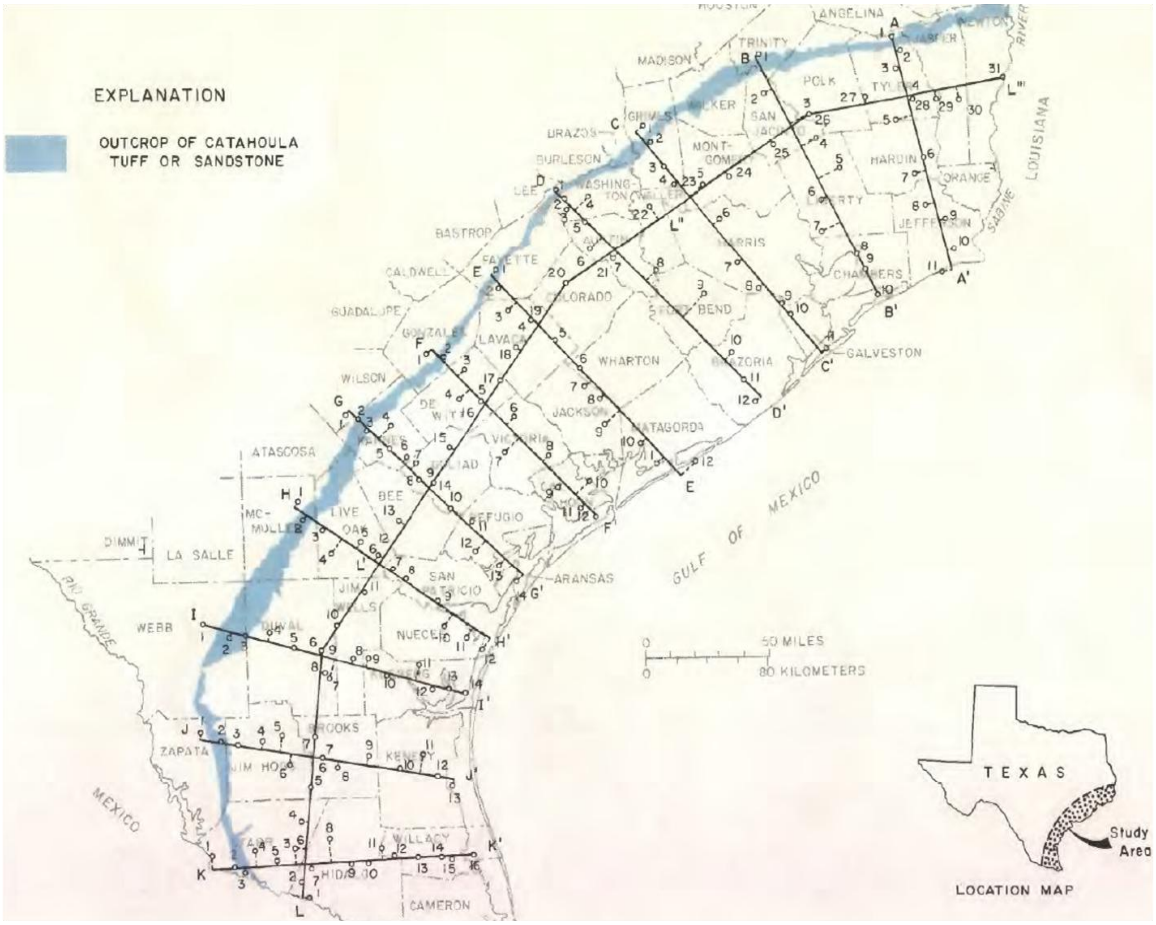

Figure 8-1: Map of the locations of regional cross sections. (Baker, 1978)

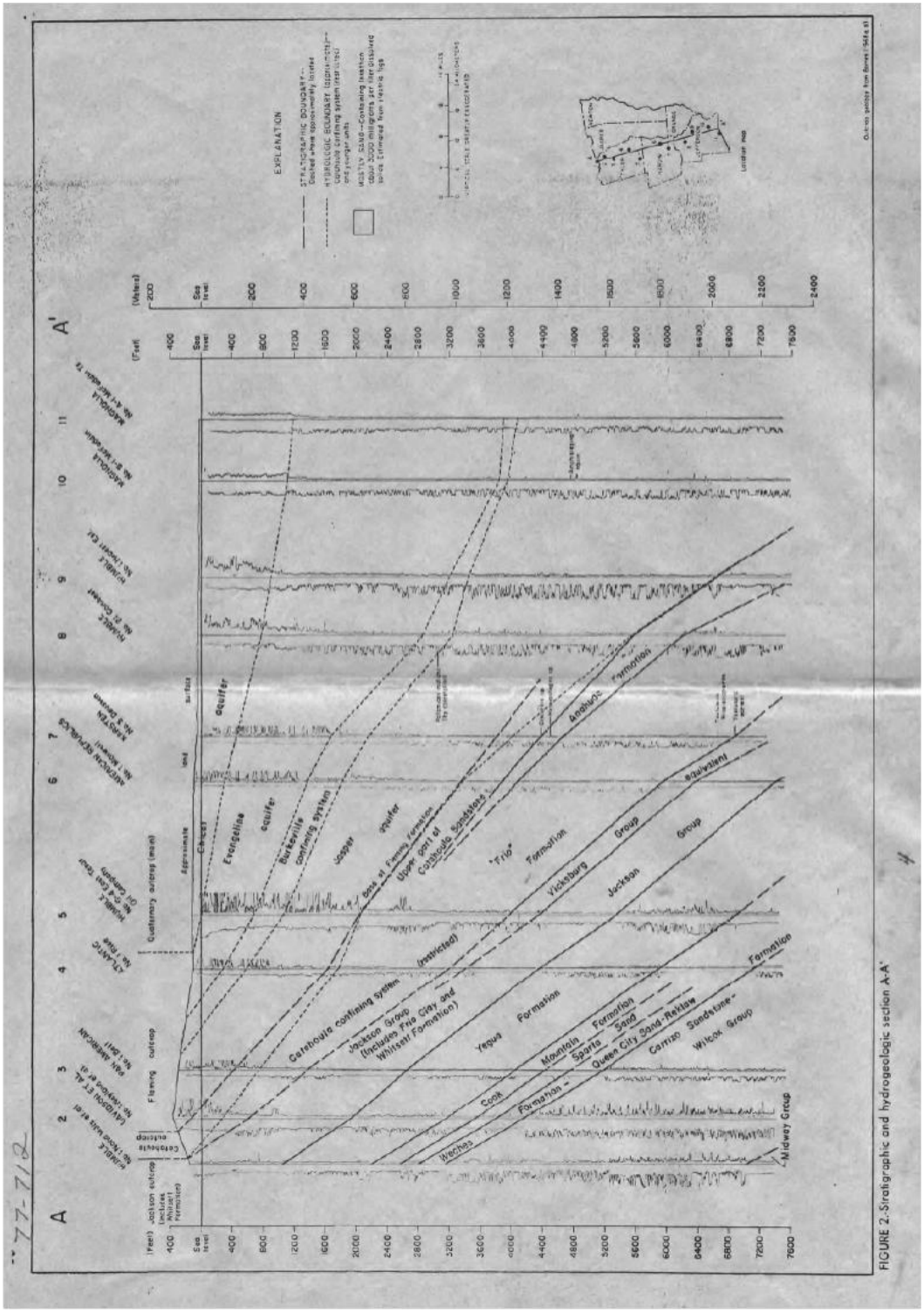

Figure 8-2: Regional cross section A to A'(Baker, 1978)

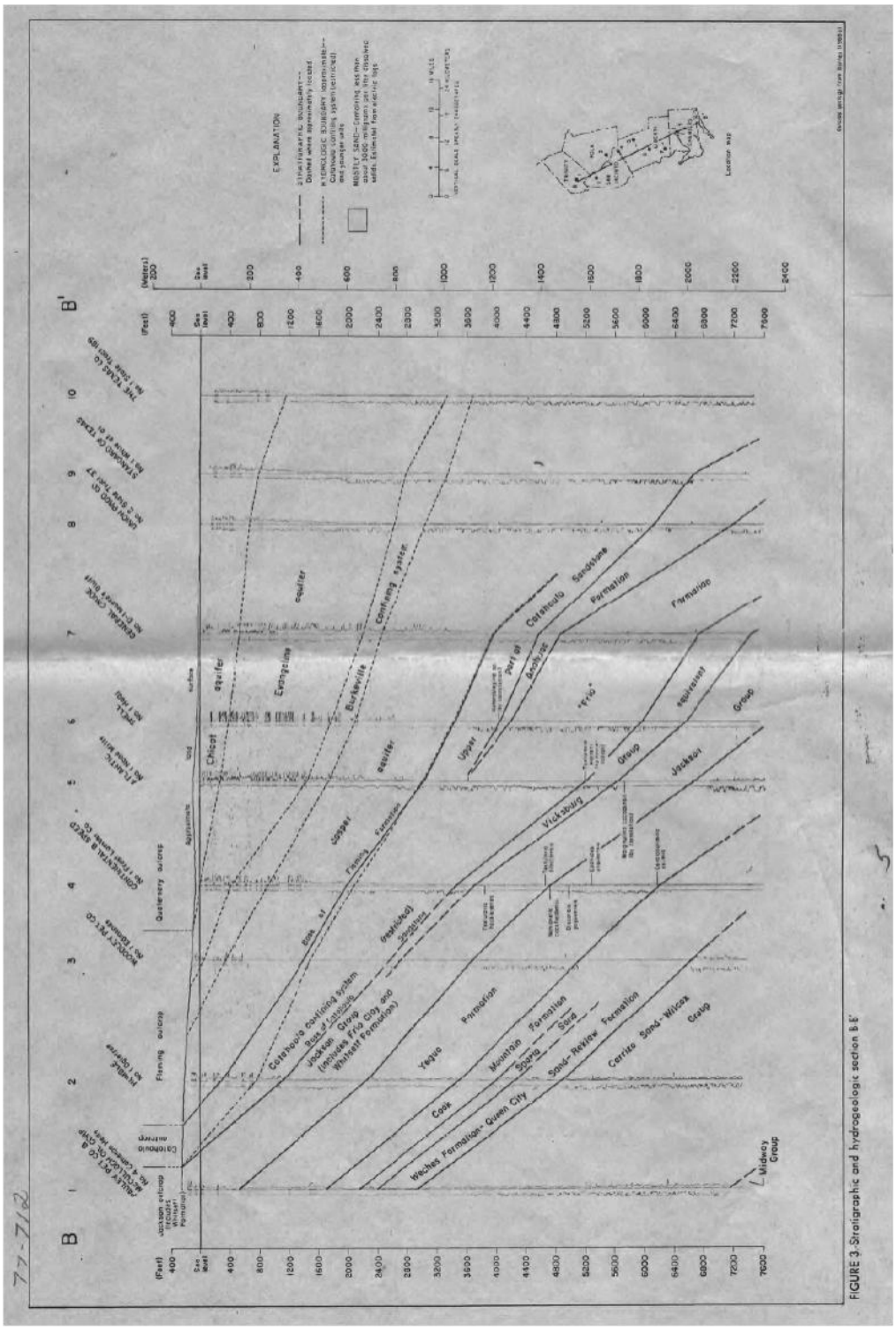

Figure 8-3: Regional cross section B to B'(Baker, 1978)

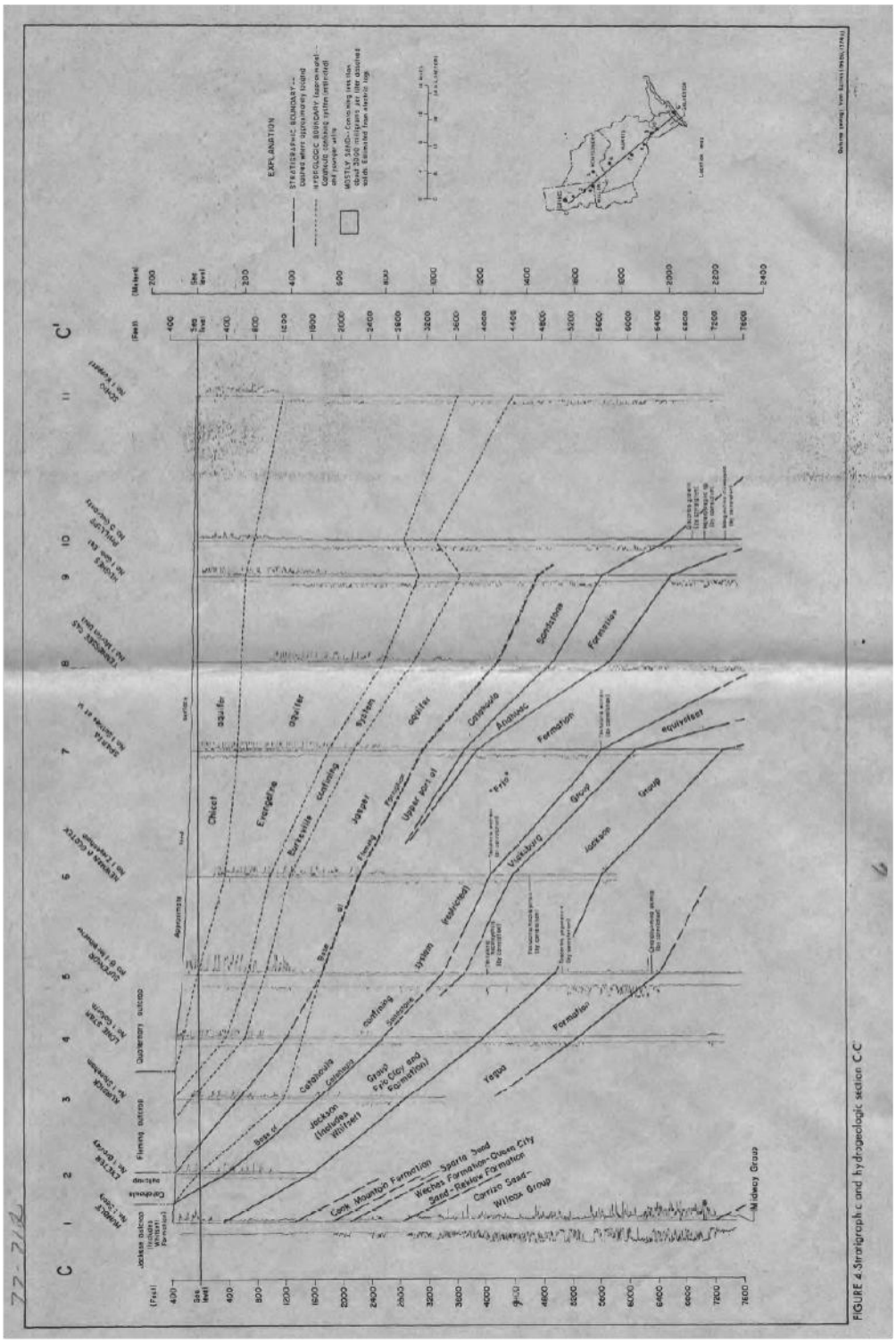

Figure 8-4: Regional cross section C to C'(Baker, 1978)

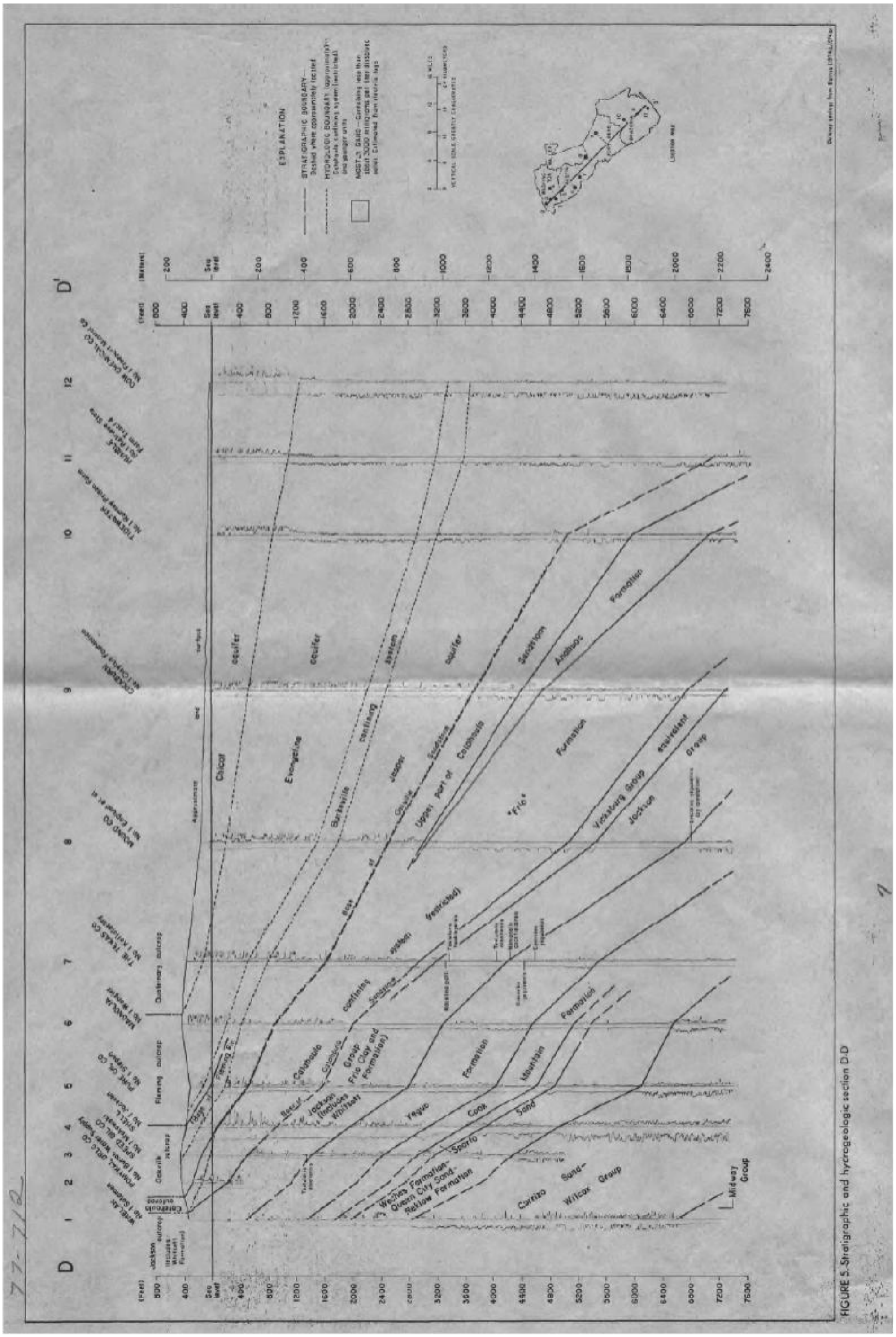

Figure 8-5: Regional cross section D to D’(Baker, 1978)

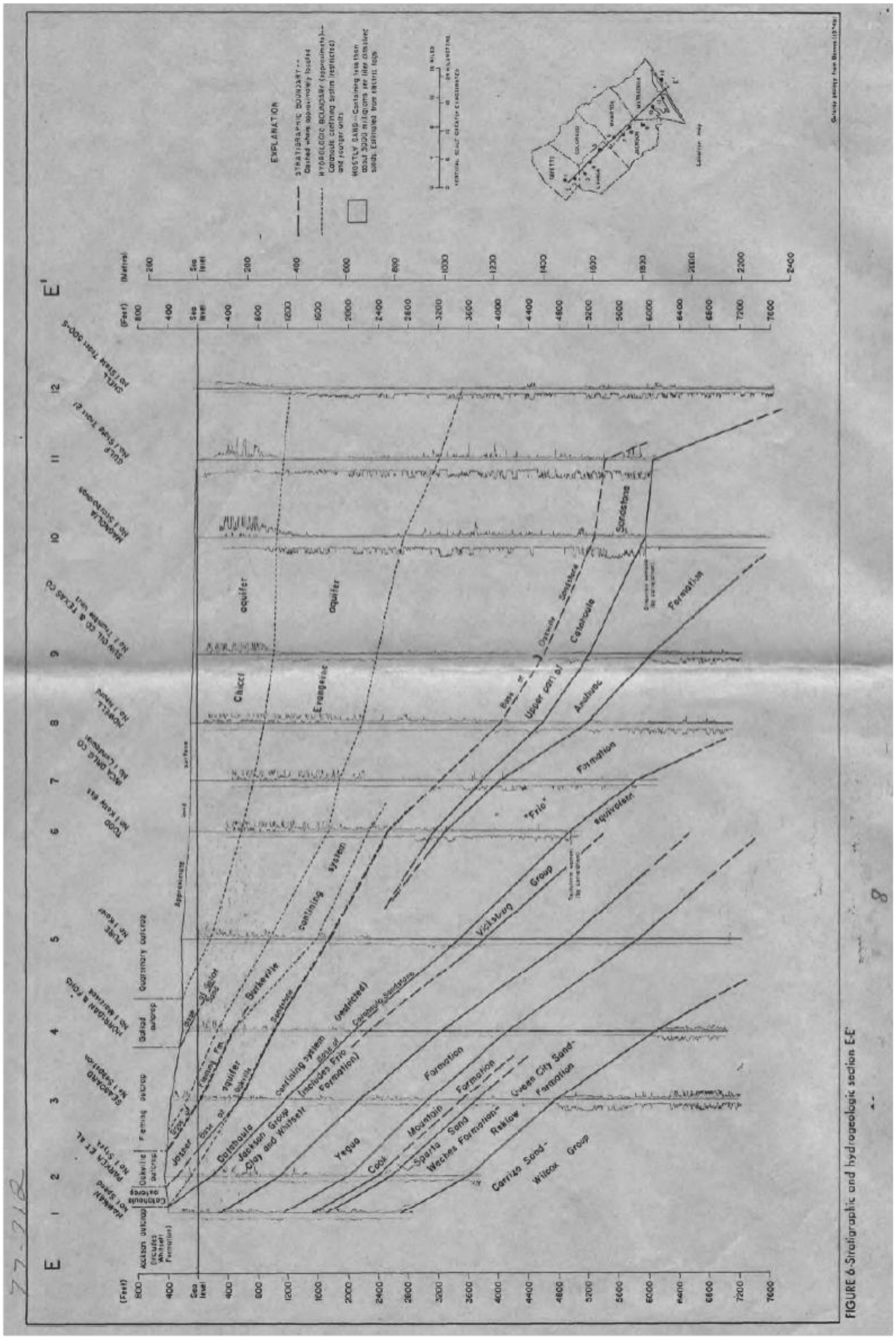

Figure 8-6: Regional cross section E to E'(Baker, 1978)

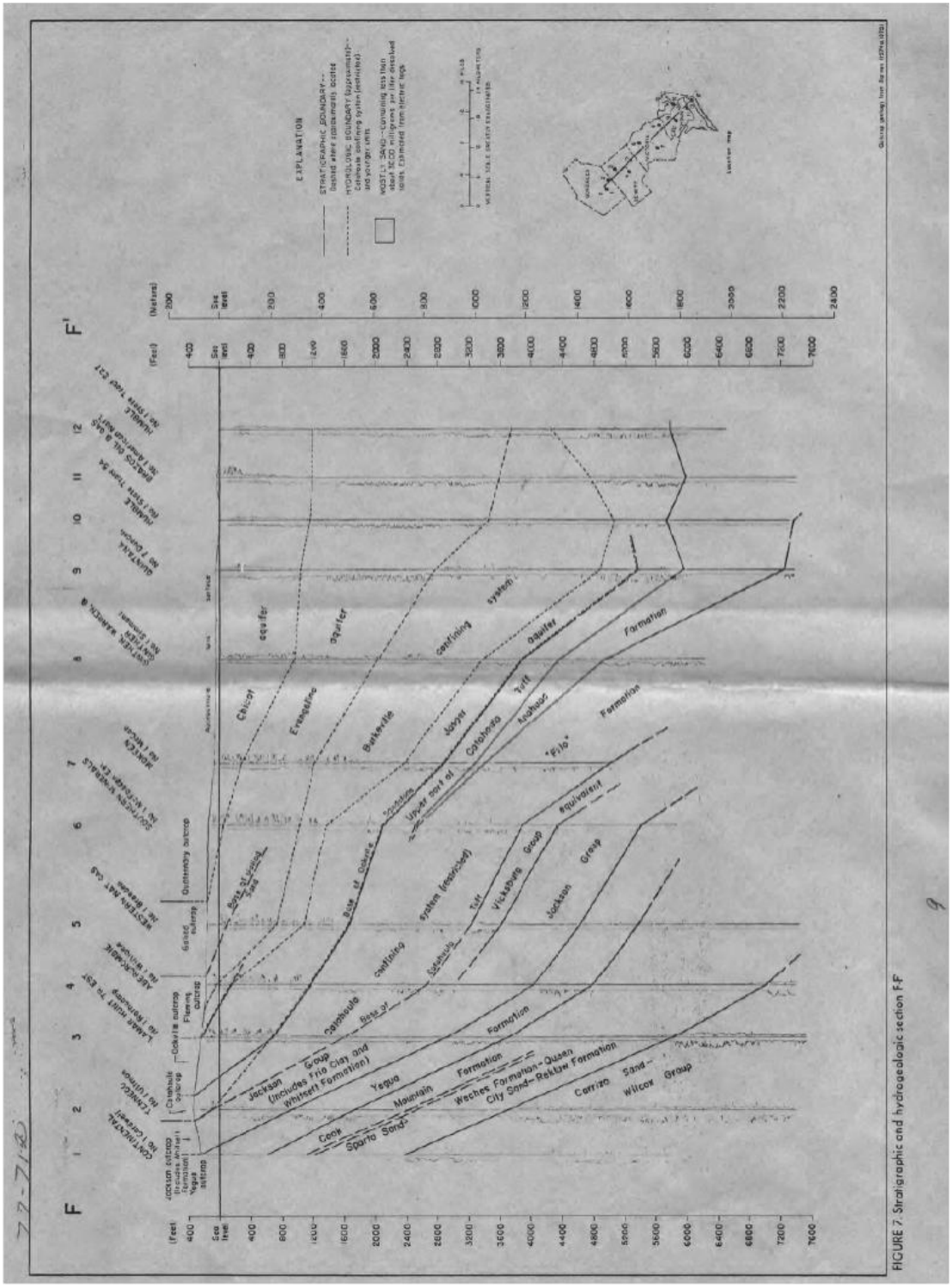

Figure 8-7: Regional cross section F to F'(Baker, 1978)

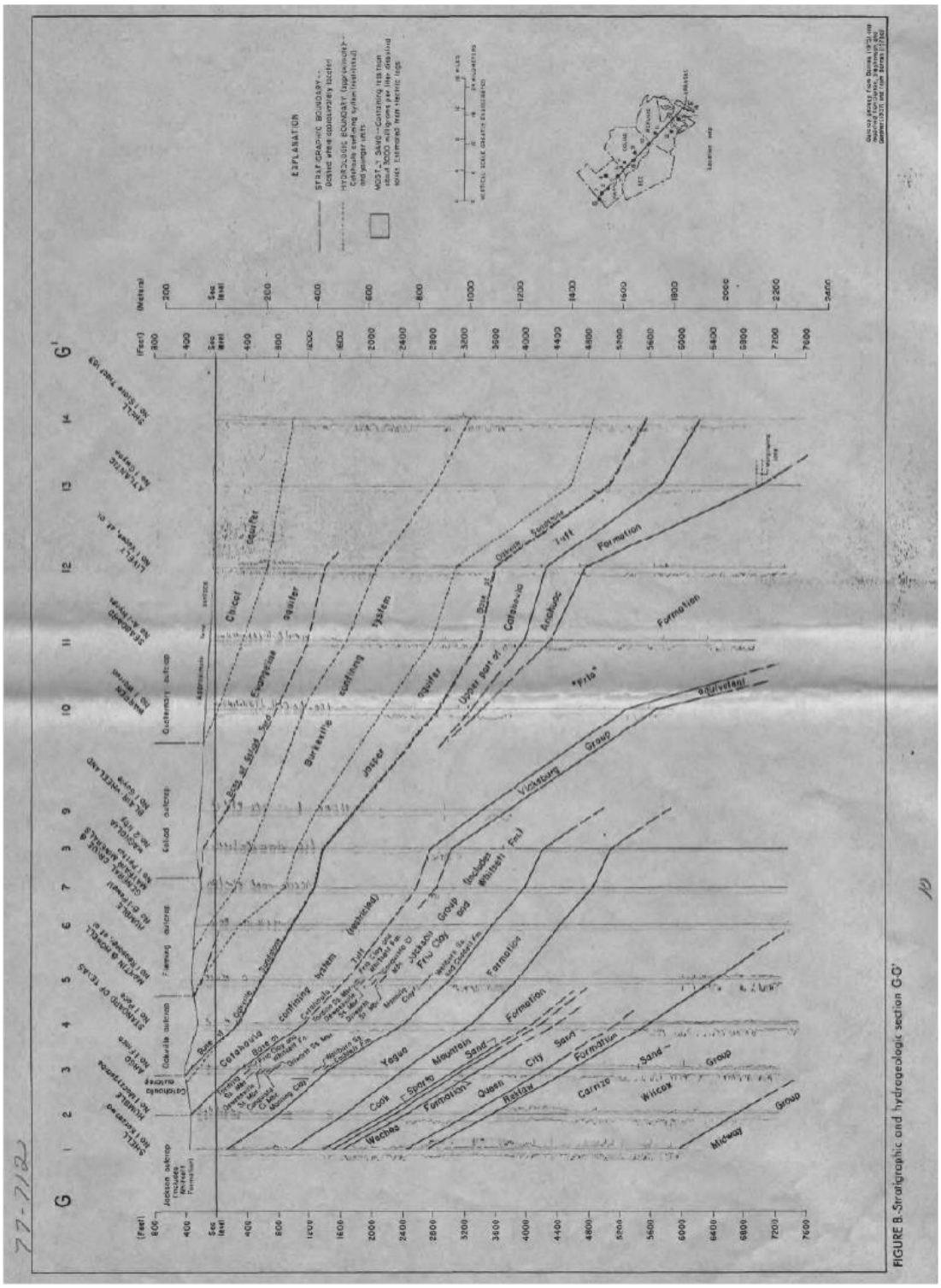

FIGURE 8.-Stratigraphic and hydrogeologic section G-G'

Figure 8-8: Regional cross section G to G'(Baker, 1978)

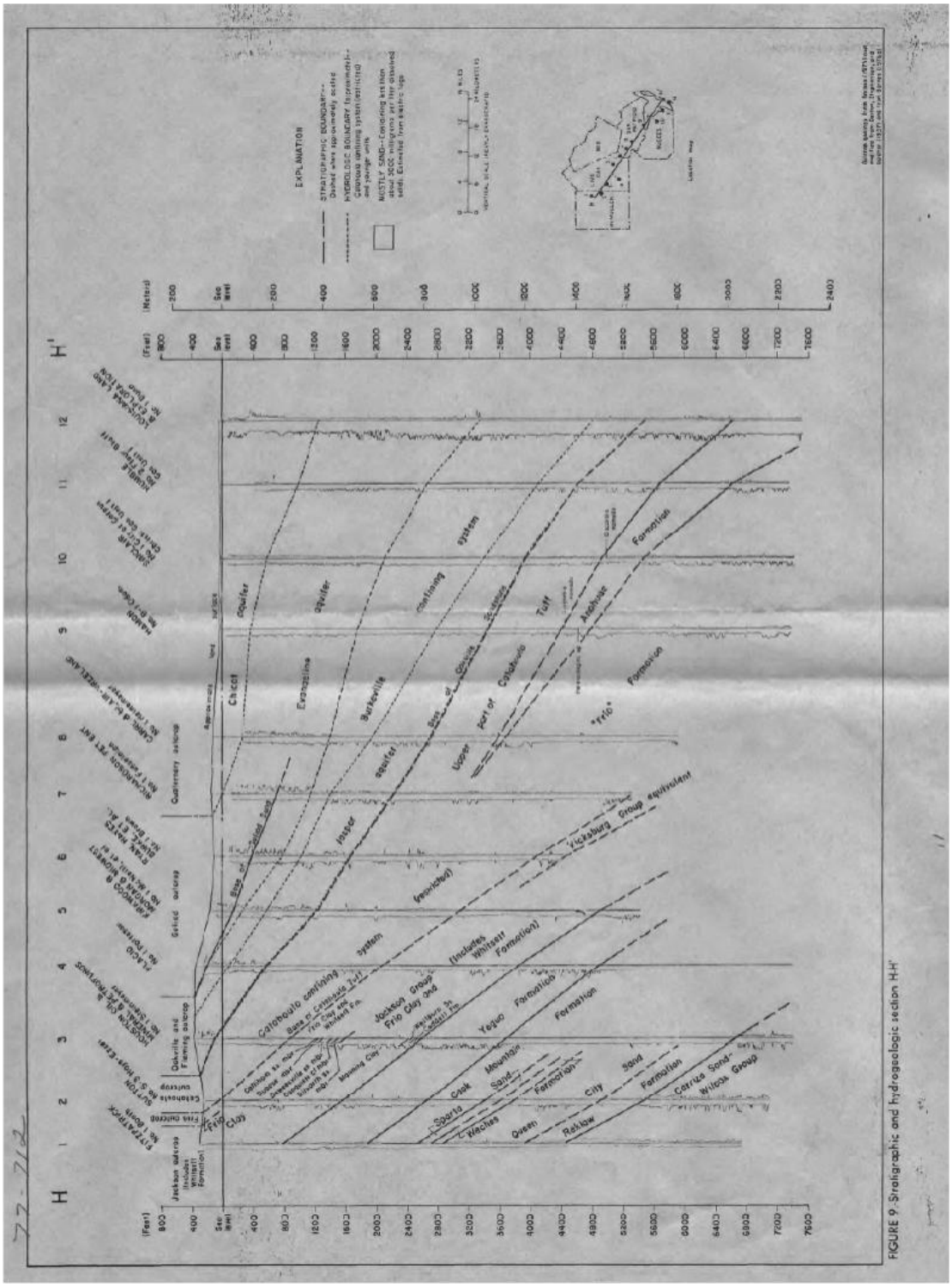

FIGURE 9.-Stratigraphic and hydrogeologic section H-H'

Figure 8-9: Regional cross section H to H'(Baker, 1978)

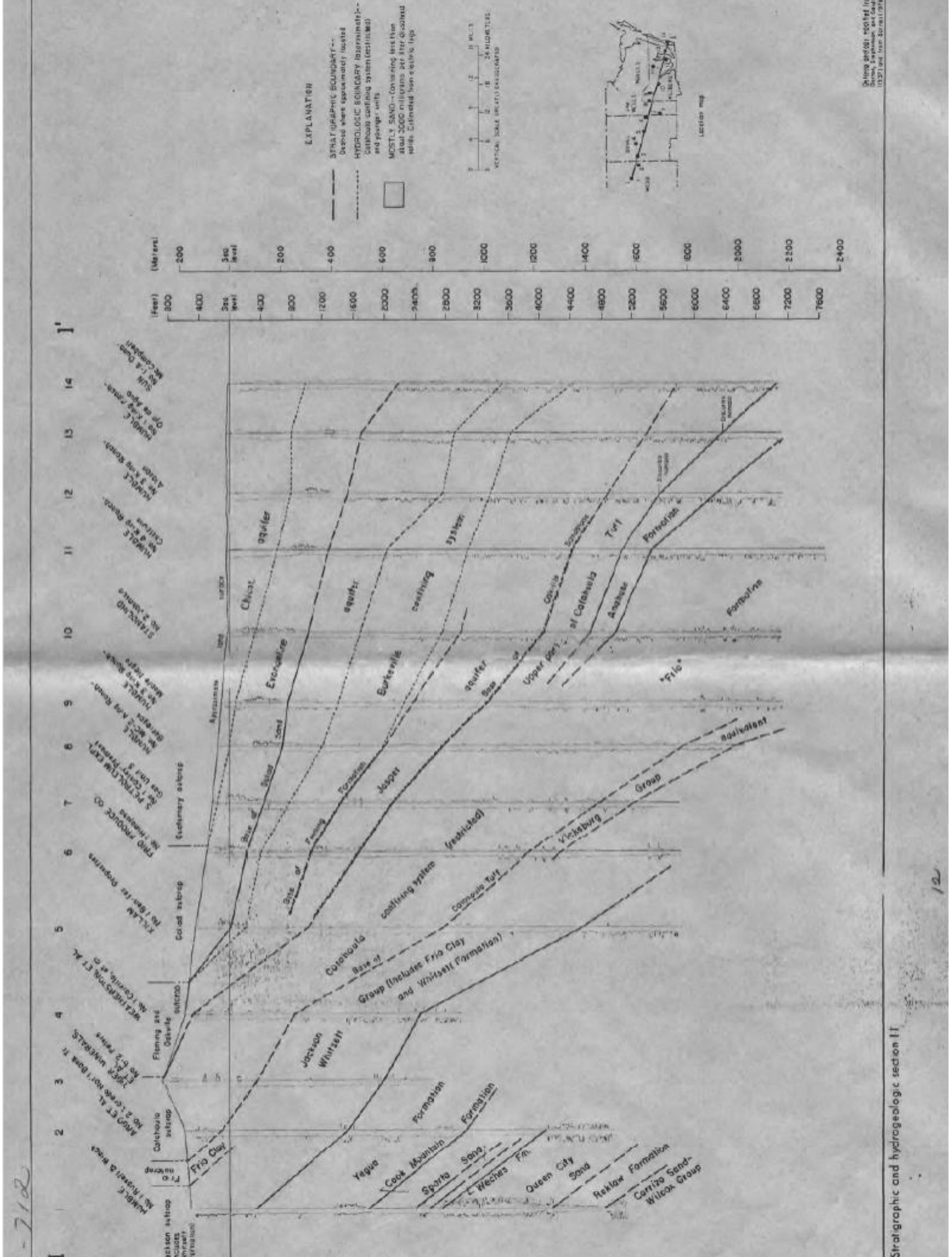

Figure 8-10: Regional cross section I to I'(Baker, 1978)

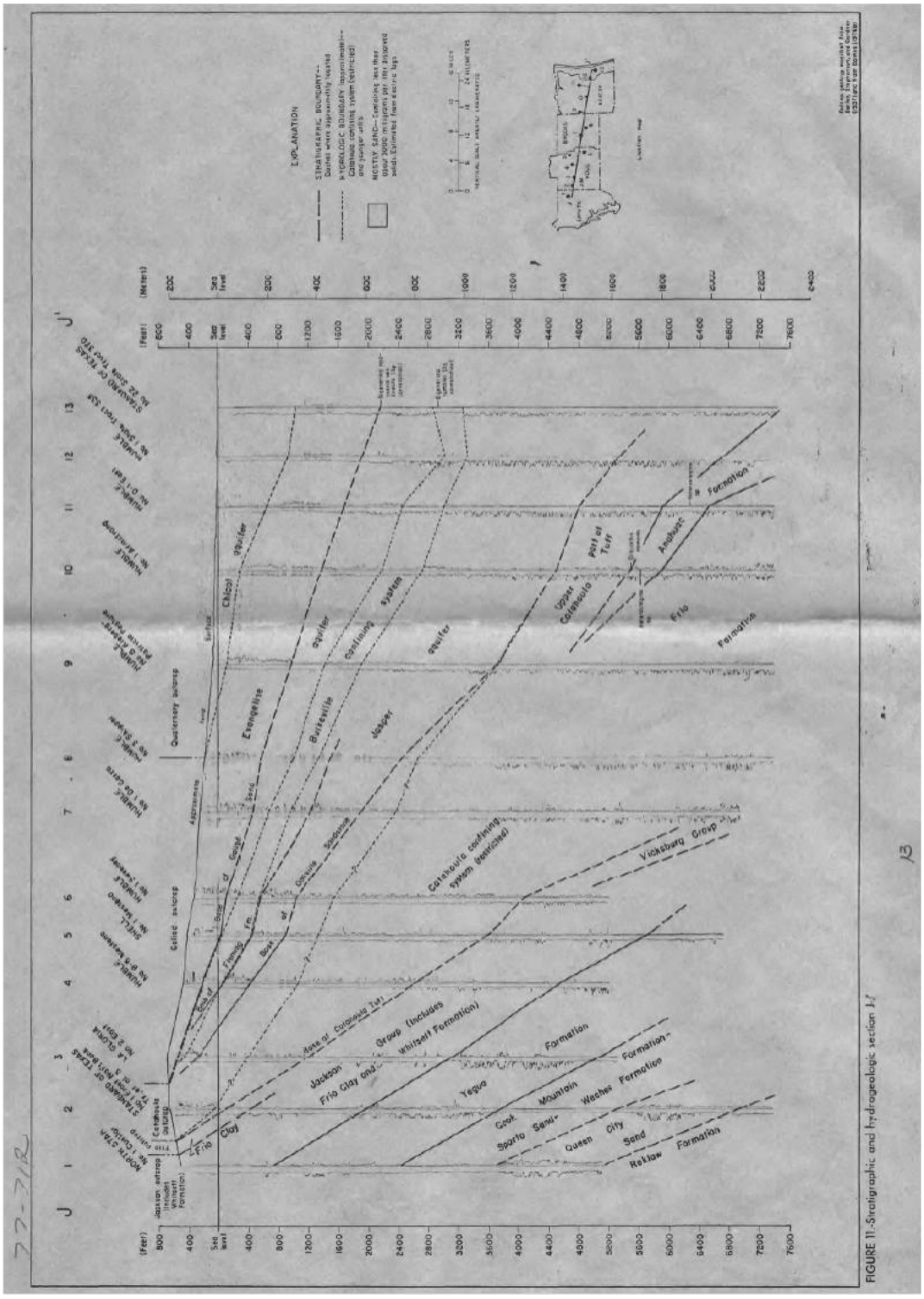

Figure 8-11: Regional cross section J to J'(Baker, 1978)

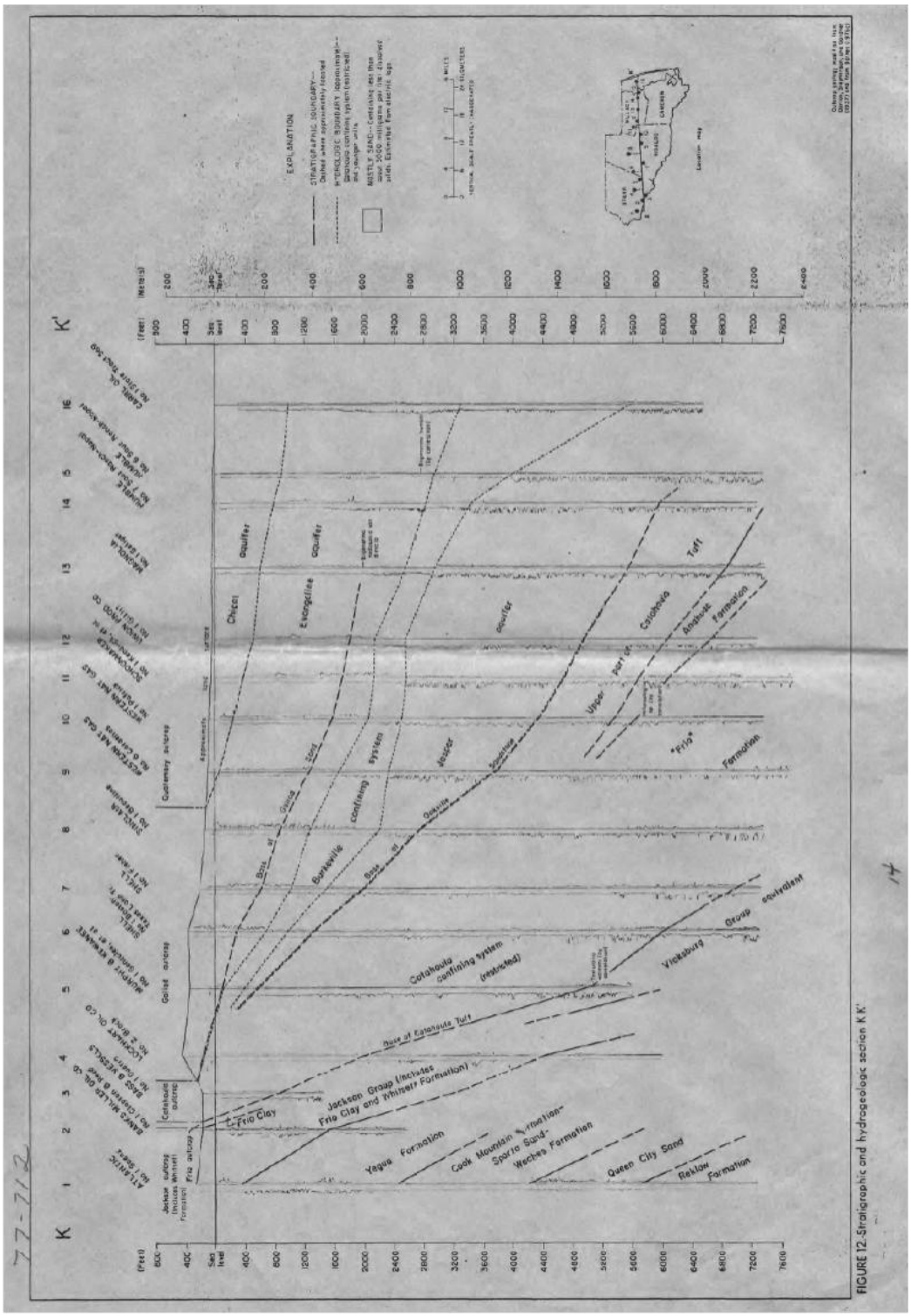

FIGURE 12.-Stratigraphic and hydrogeologic section K-K'.

Figure 8-12: Regional cross section K to K'(Baker, 1978)

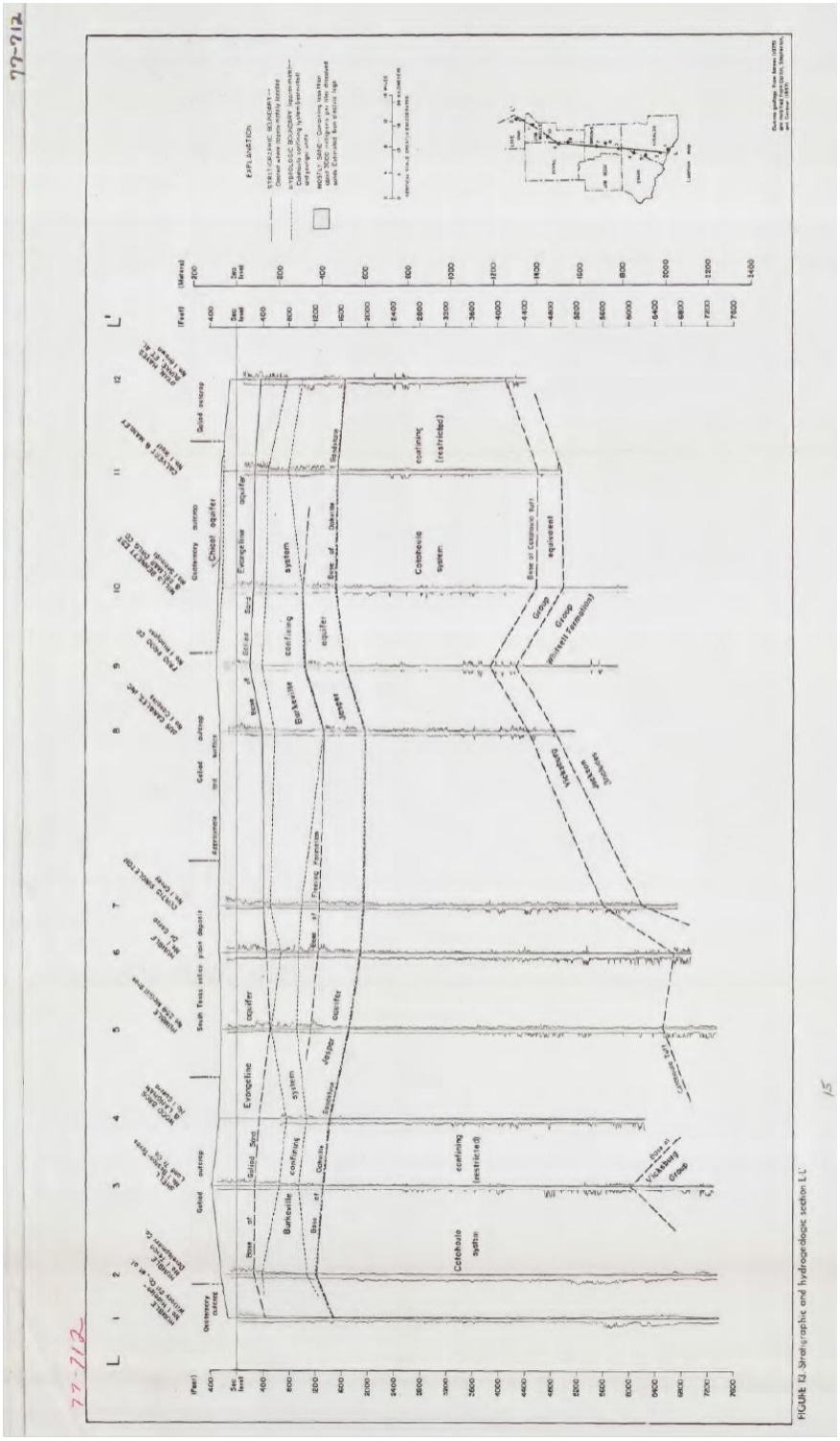

Figure 8-13: Regional cross section L to L'(Baker, 1978)

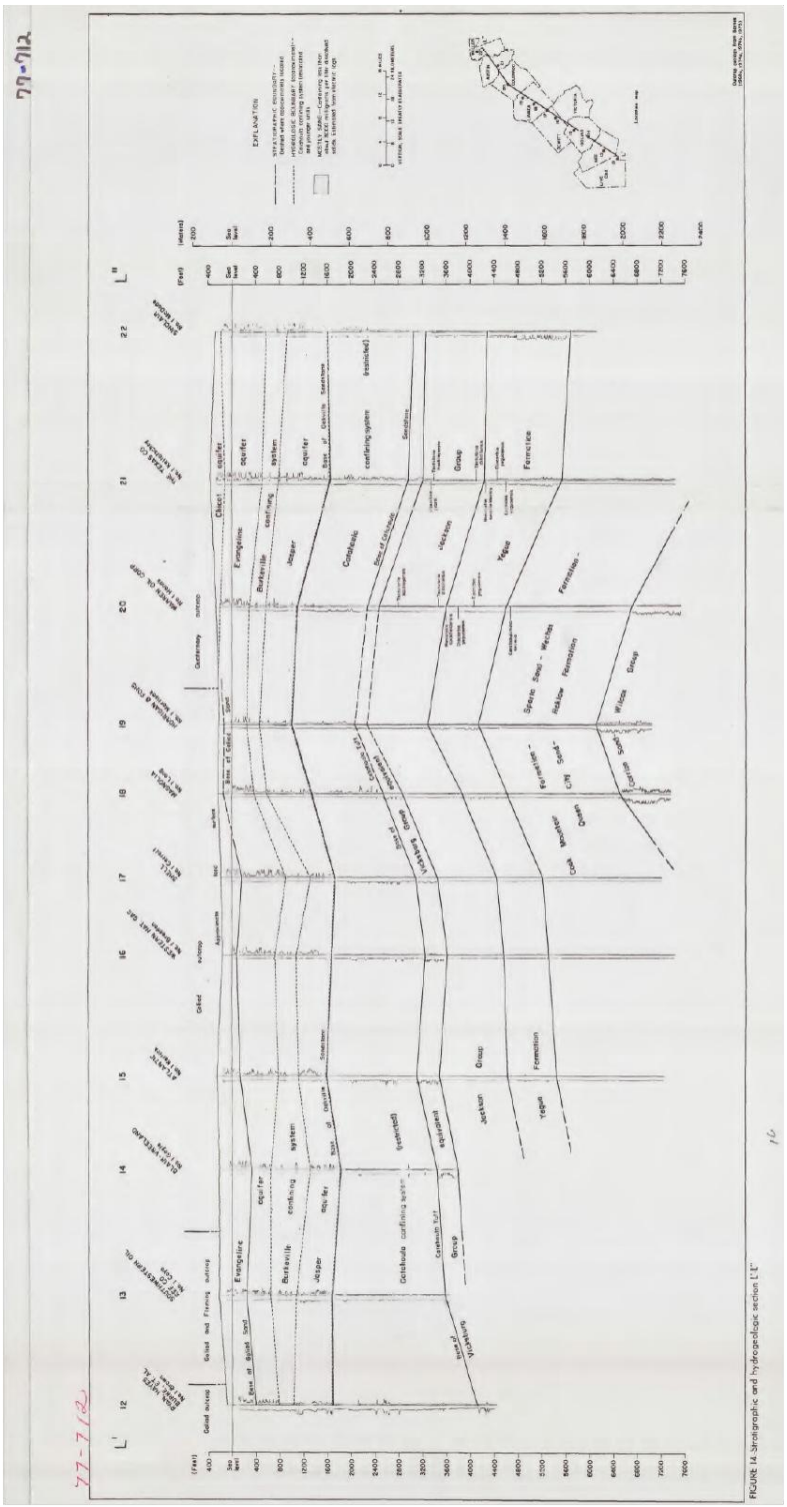

Figure 8-14: Regional cross section L’ to L”(Baker, 1978)

8.2 (Baker, Stratigraphic Nomenclature and Geologic Sections of the Gulf Coastal Plain of Texas, 1995)

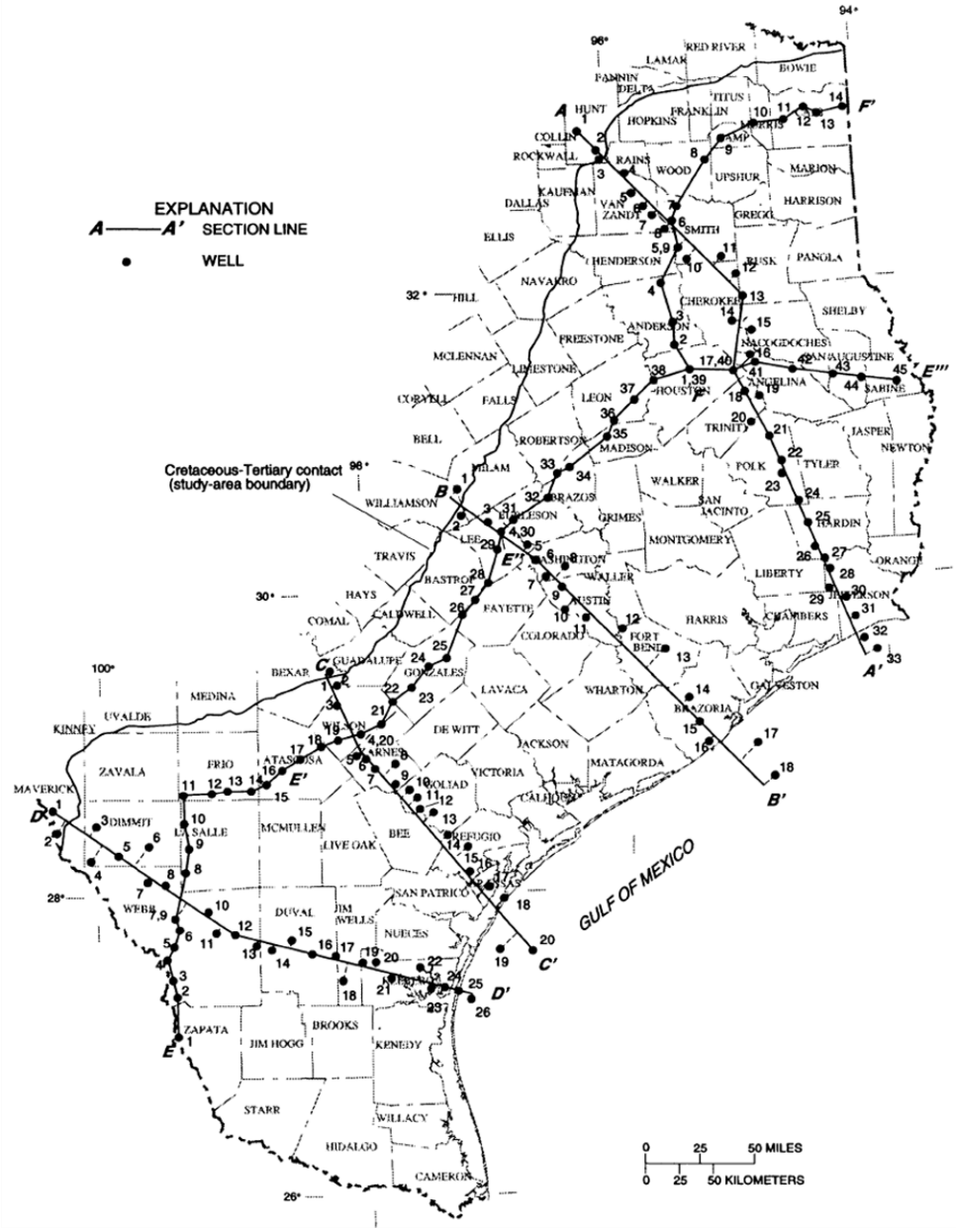

Figure 8-15: Map of the locations of regional cross sections.(Baker, 1995)

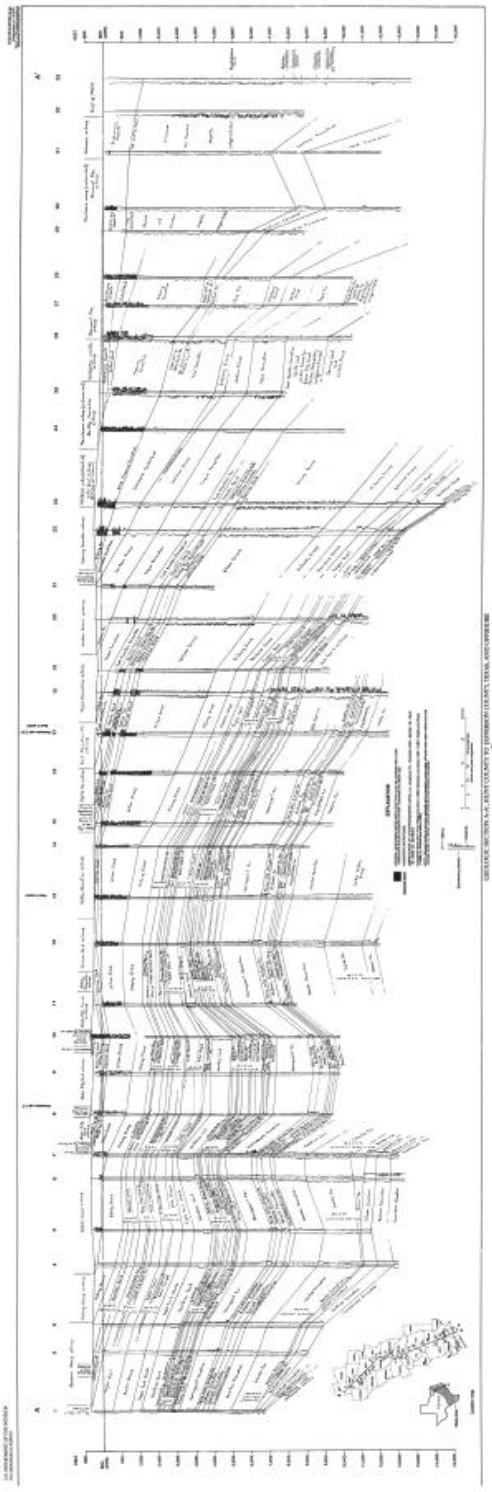

Figure 8-16: Regional cross section A to A’(Baker, 1995)

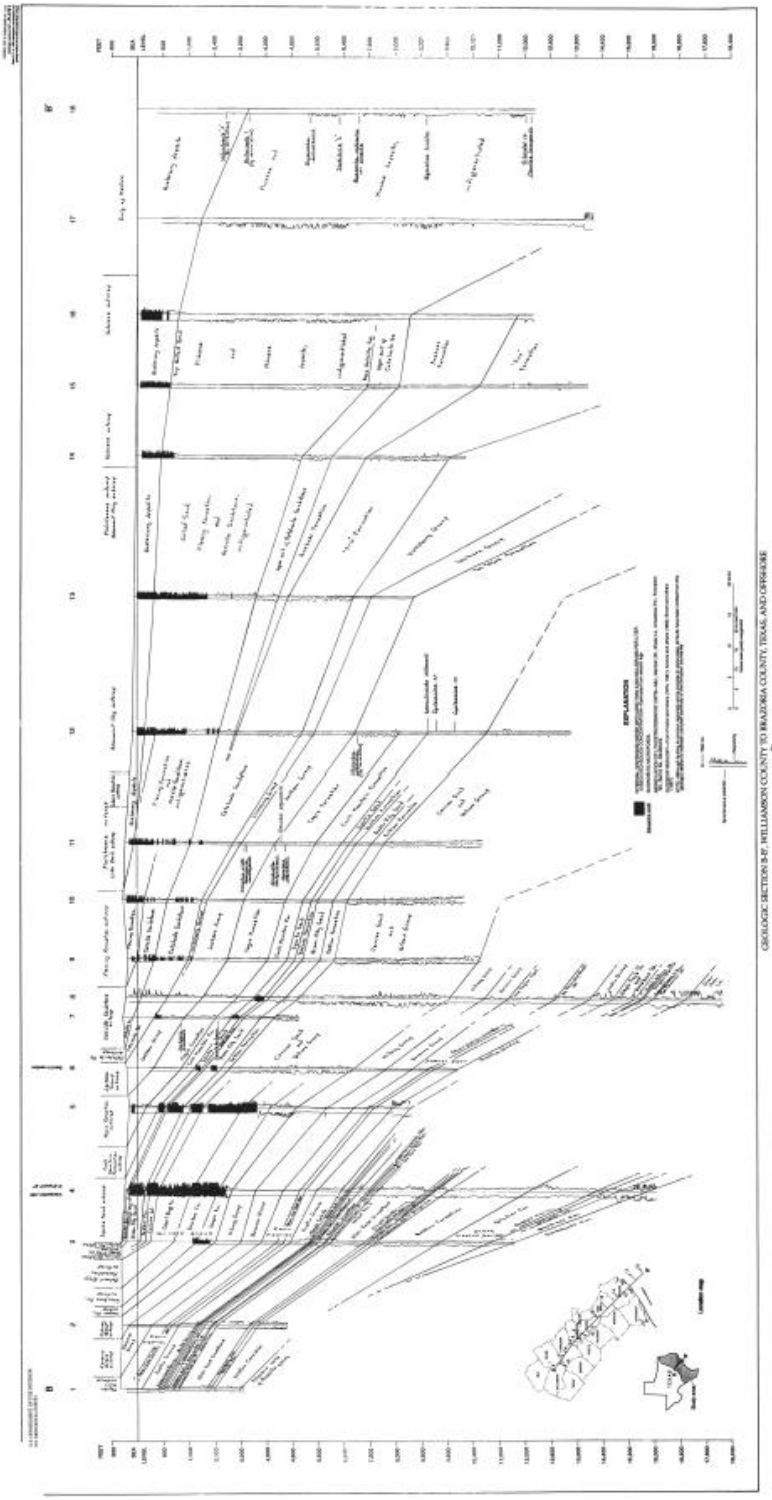

Figure 8-17: Regional cross section B to B'(Baker, 1995)

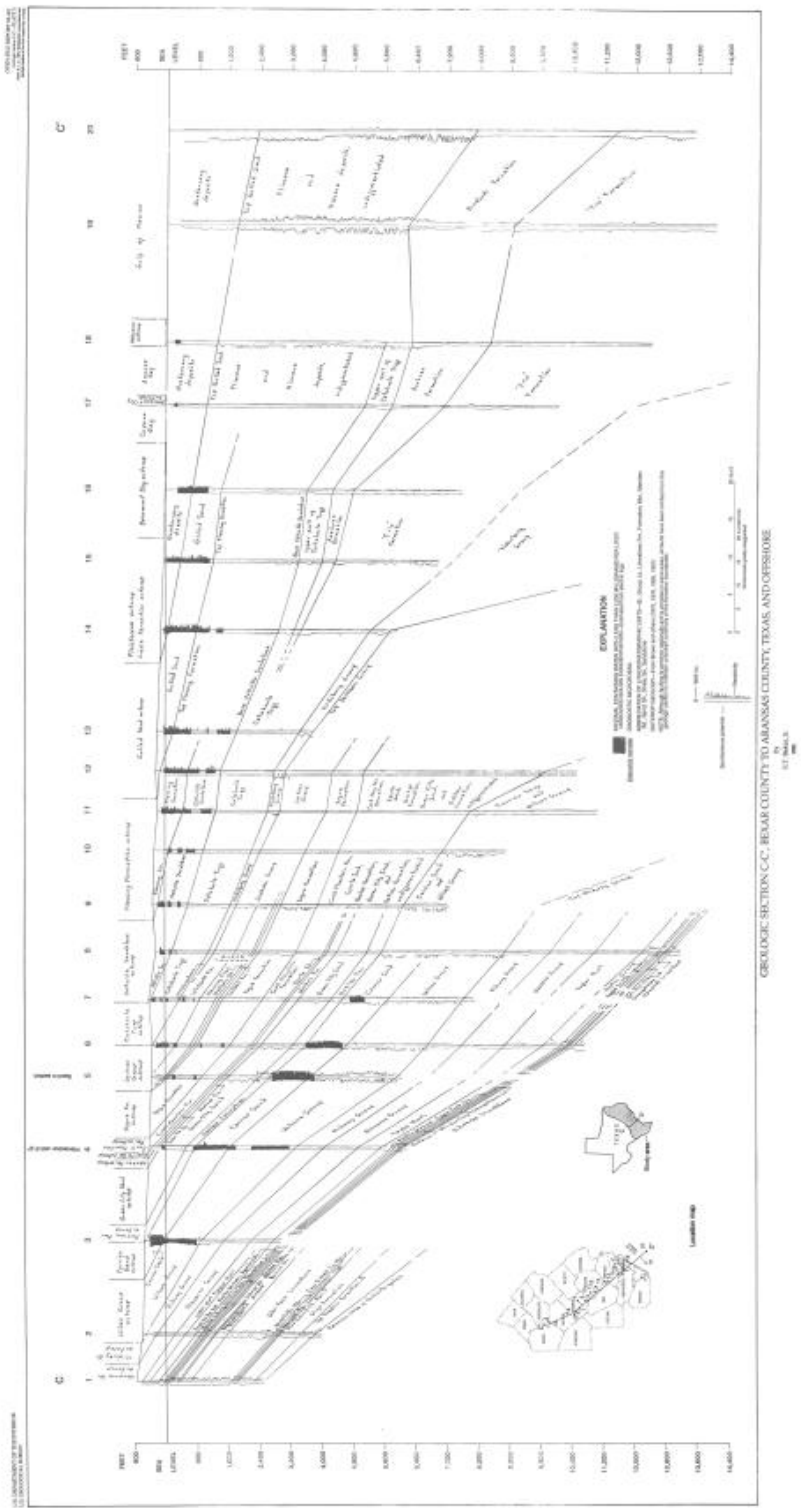

Figure 8-18: Regional cross section C to C'(Baker, 1995)

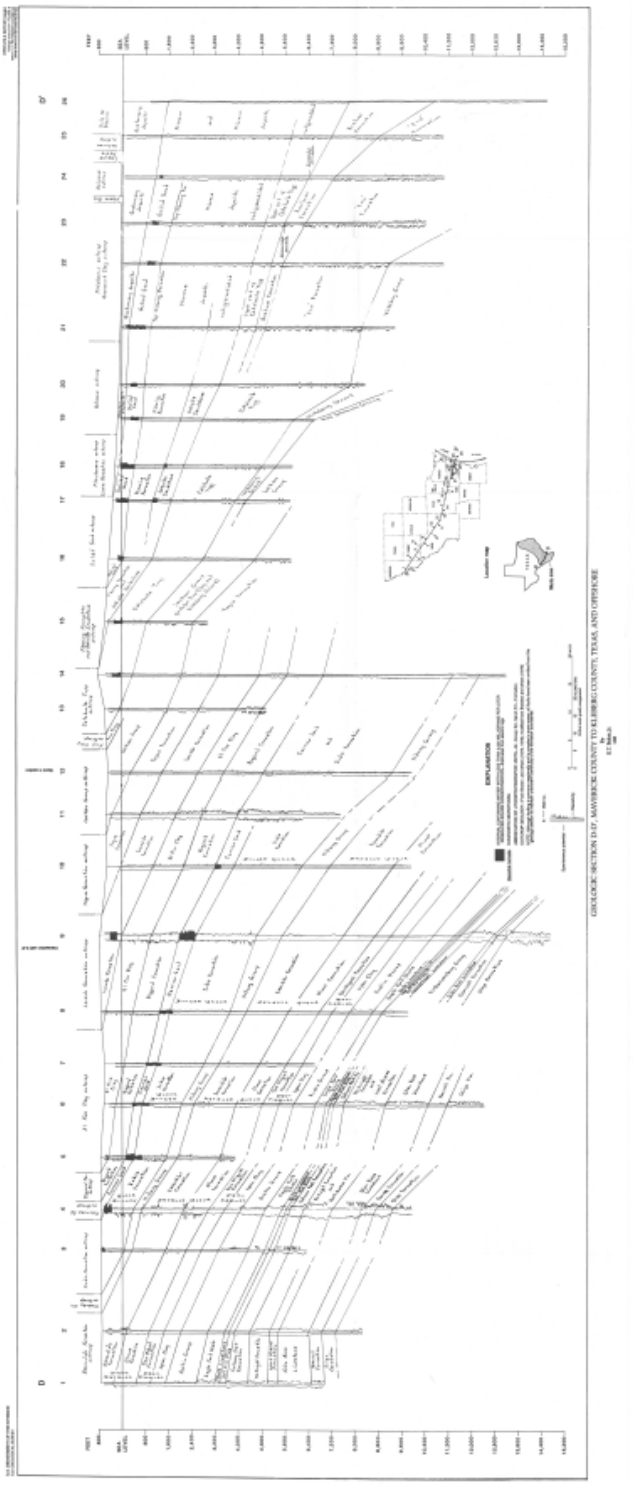

Figure 8-19: Regional cross section D to D’(Baker, 1995)

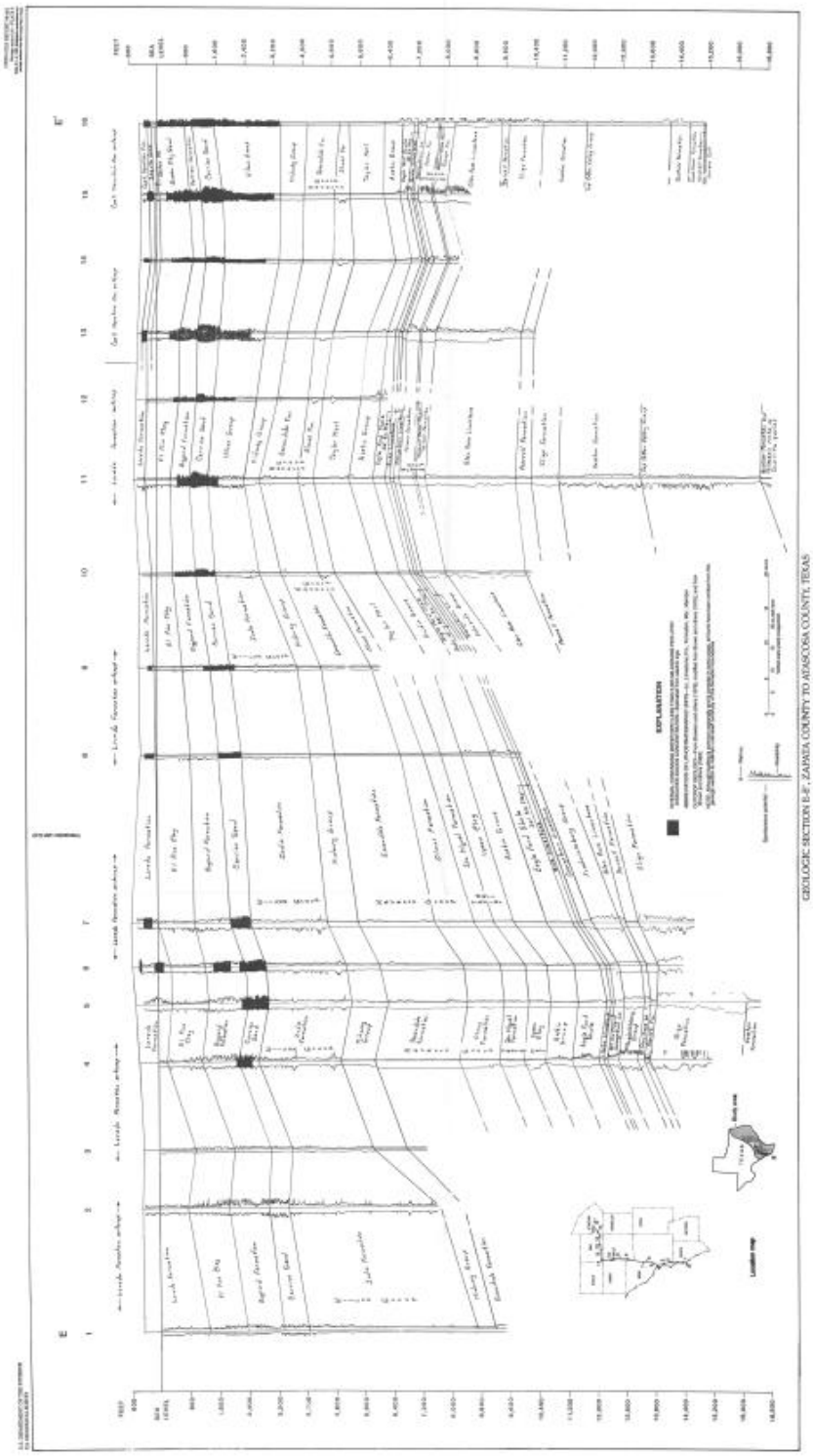

Figure 8-20: Regional cross section E to E'(Baker, 1995)

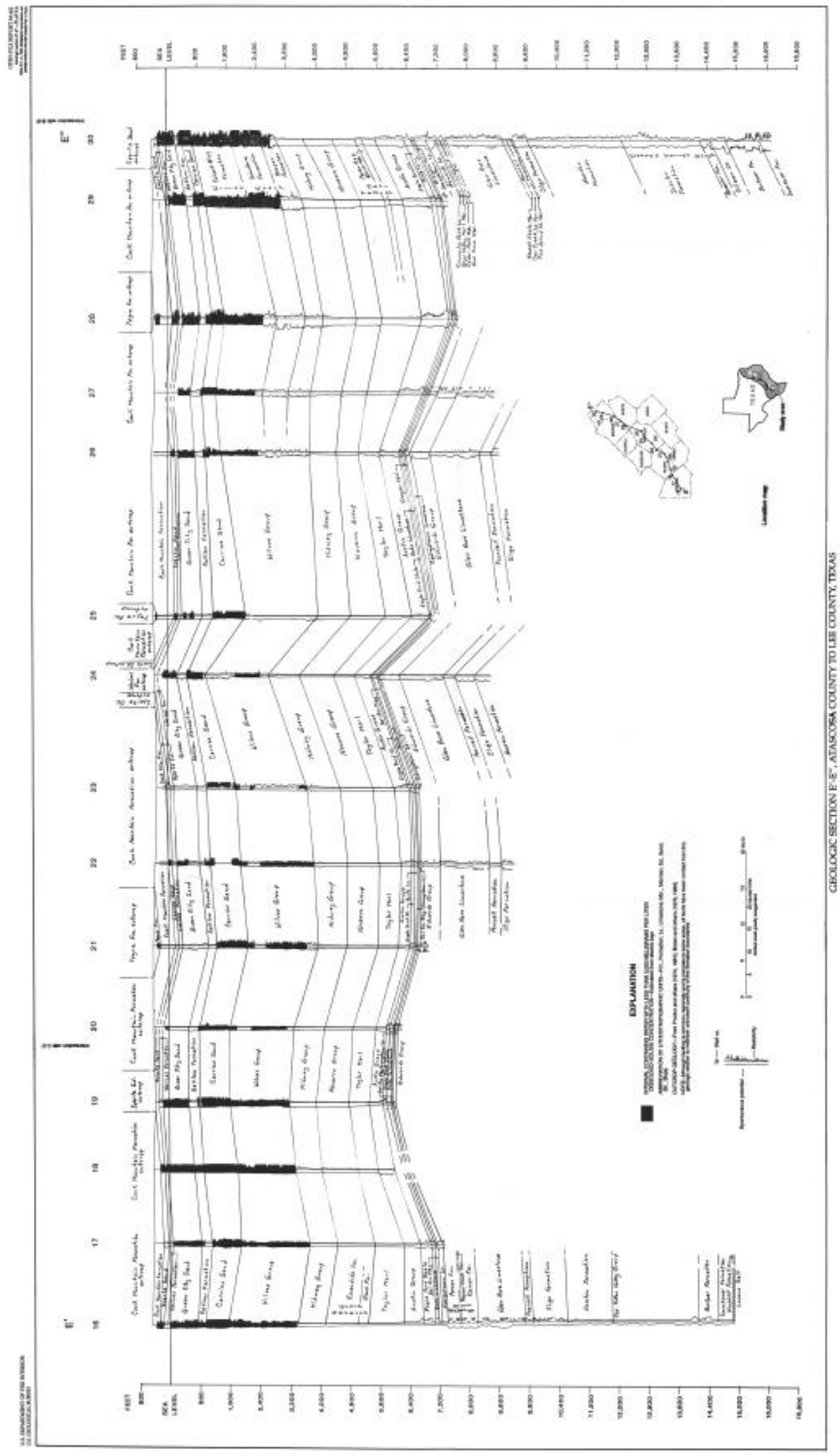

Figure 8-21: Regional cross section E' to E"(Baker, 1995)

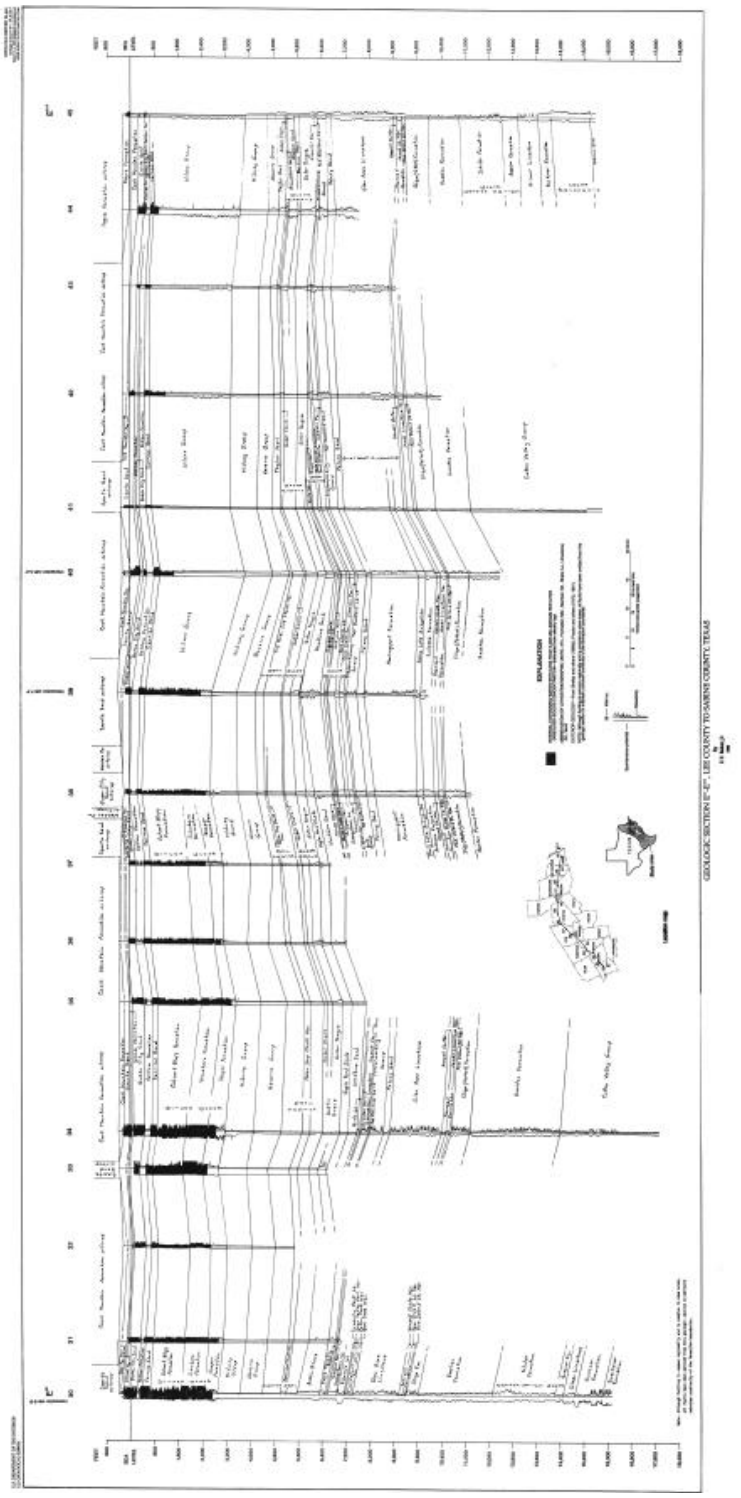

Figure 8-22: Regional cross section E” to E’’’(Baker, 1995)

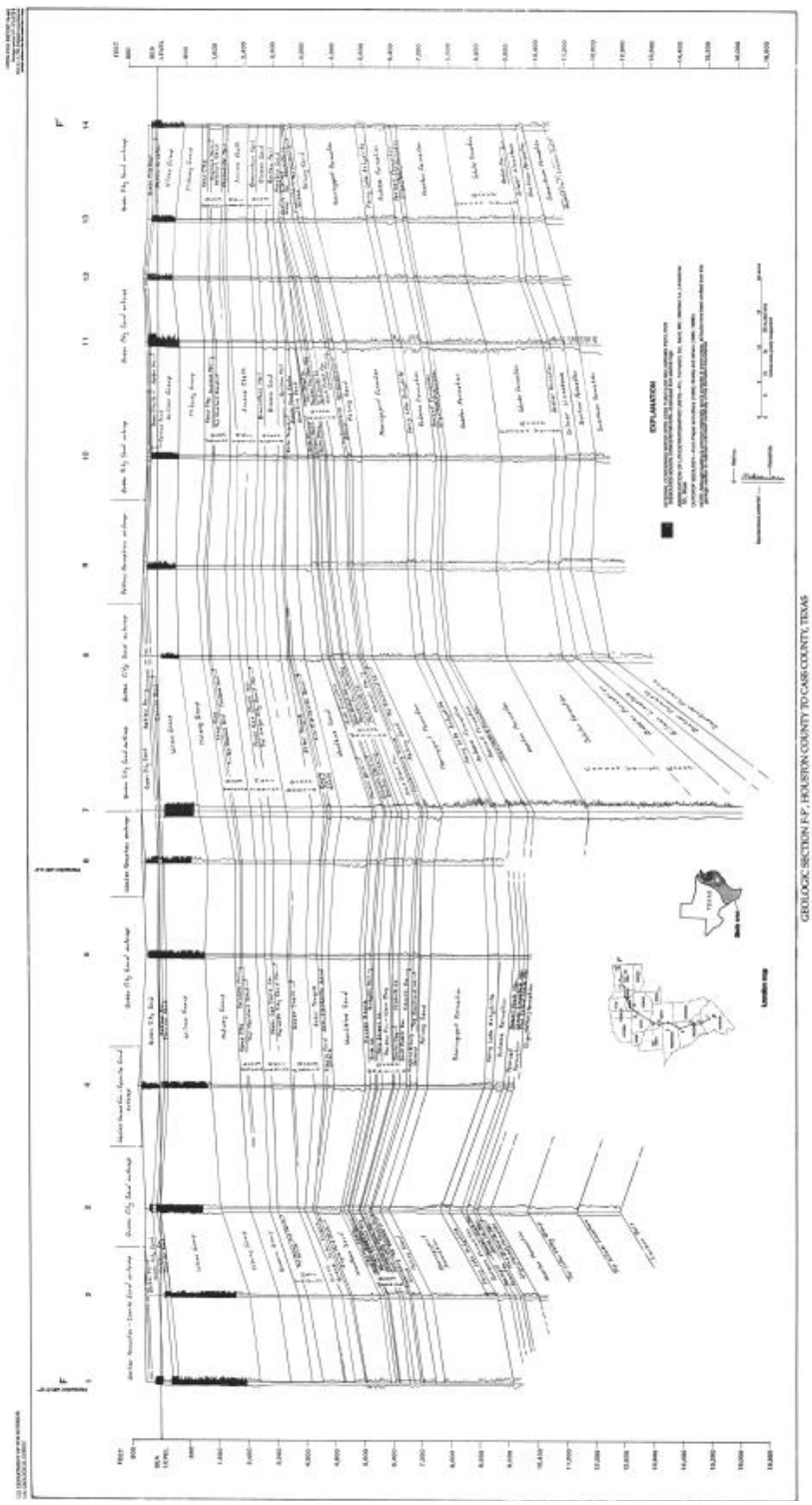

Figure 8-23: Regional cross section F to F'(Baker, 1995)

8.3 (Bebout, Luttrell, & Seo, 1976)

Figure 8-24: Map of the locations of regional cross sections.(Bebout, Luttrell, & Seo, 1976)

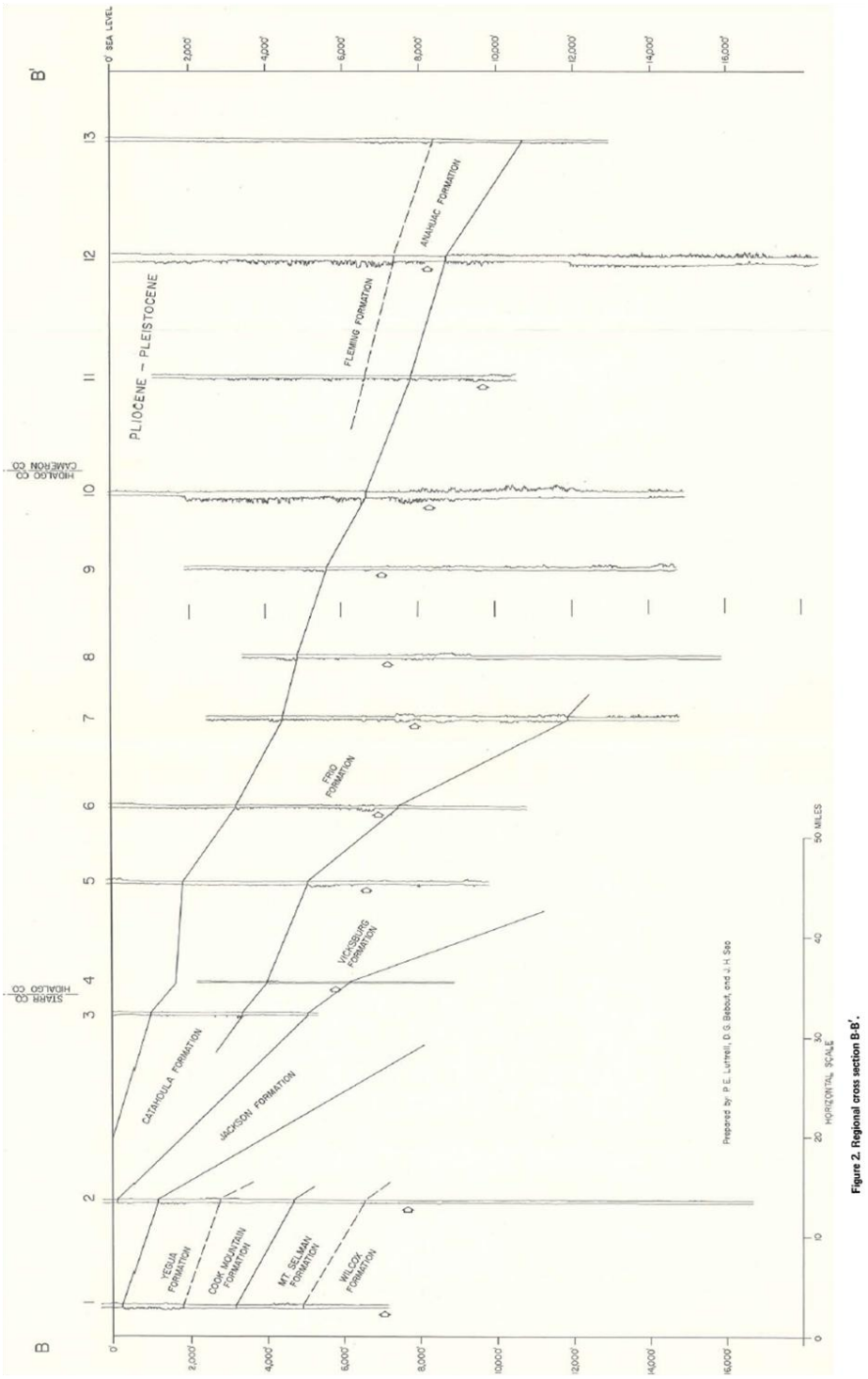

Figure 2. Regional cross section B-B'.

Figure 8-25: Regional cross section B to B'(Bebout, Luttrell, & Seo, 1976)

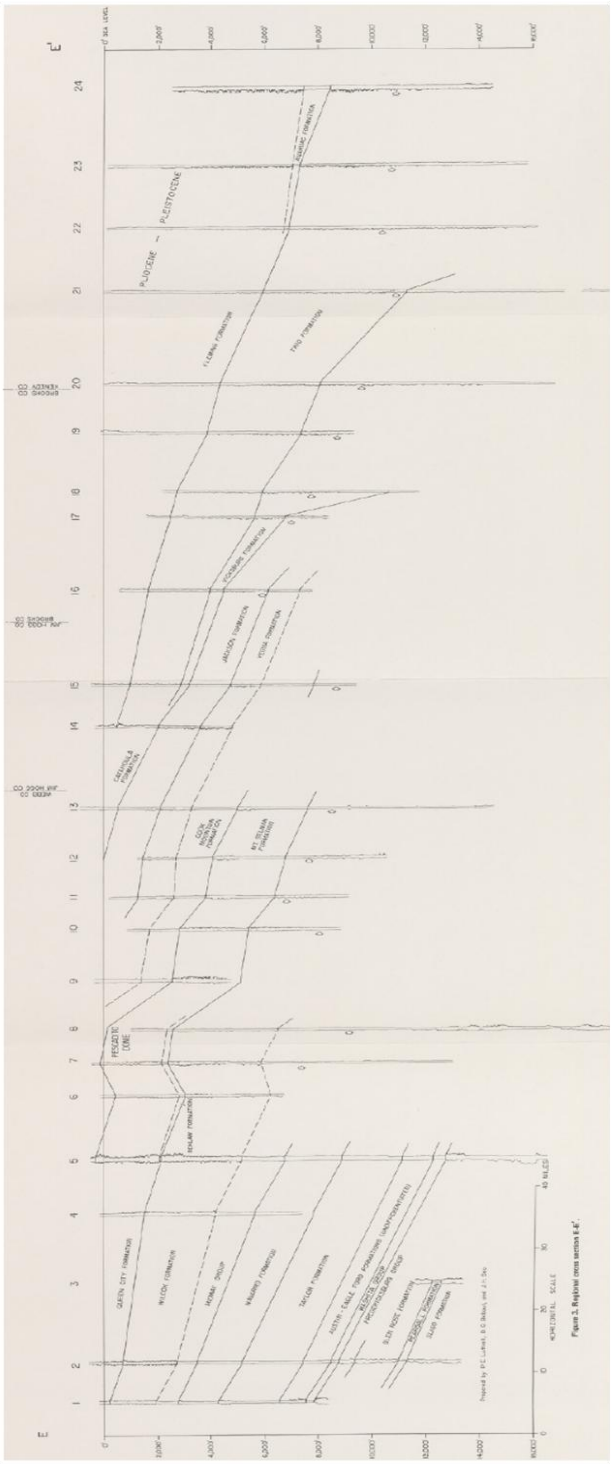

Figure 8-26: Regional cross section E to E'(Bebout, Luttrell, & Seo, 1976)

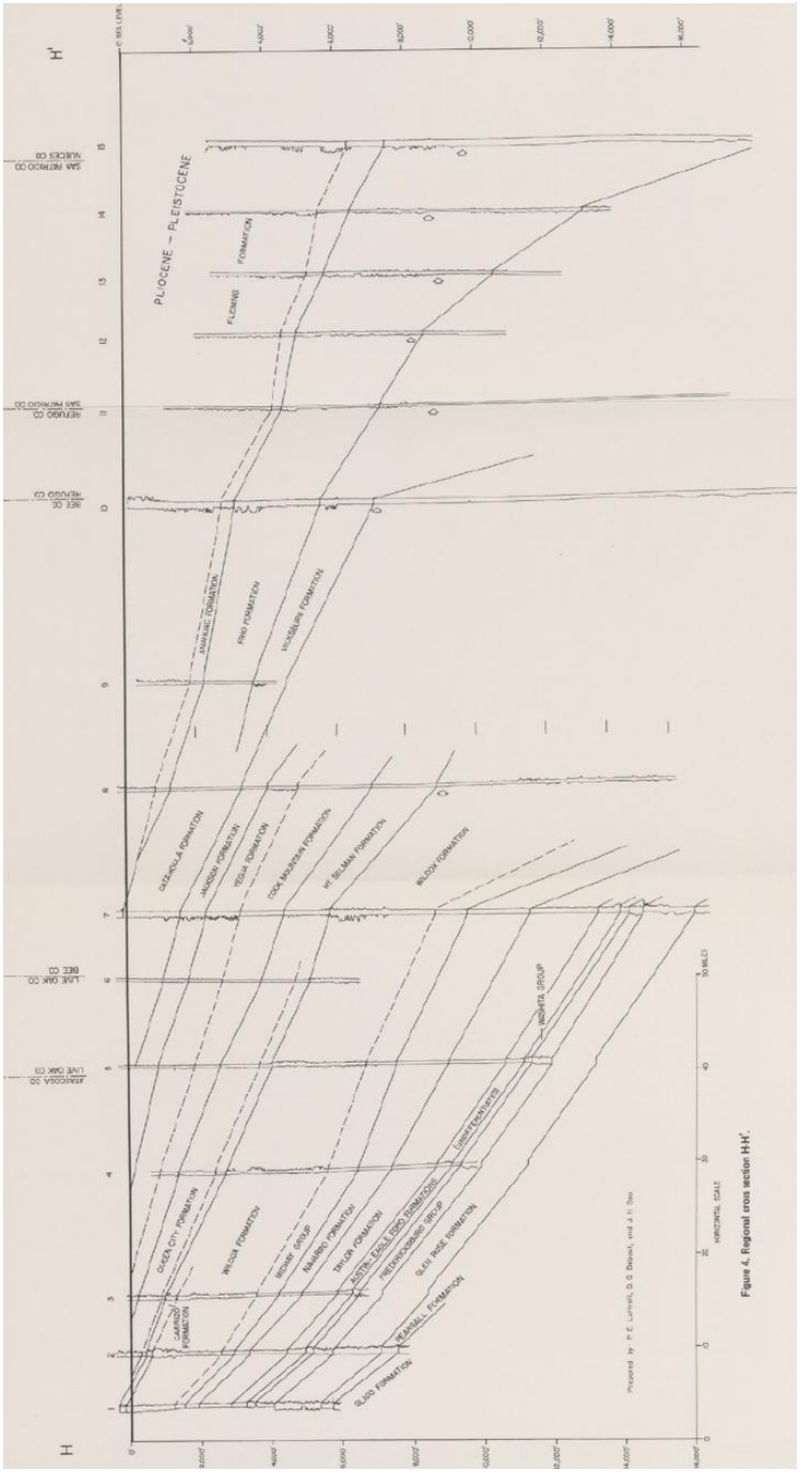

Figure 8-27: Regional cross section H to H'(Bebout, Luttrell, & Seo, 1976)

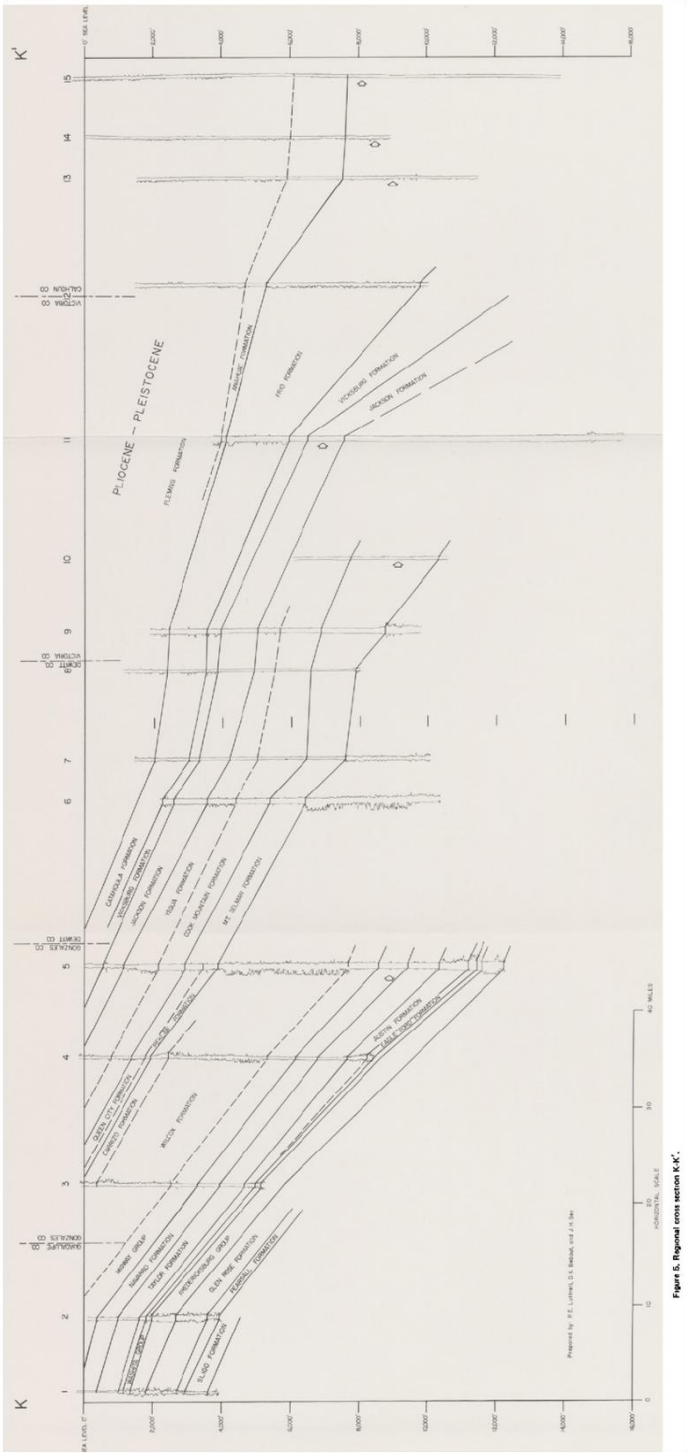

Figure 5. Regional cross section K-K'.

Figure 8-28: Regional cross section K to K'(Bebout, Luttrell, & Seo, 1976)

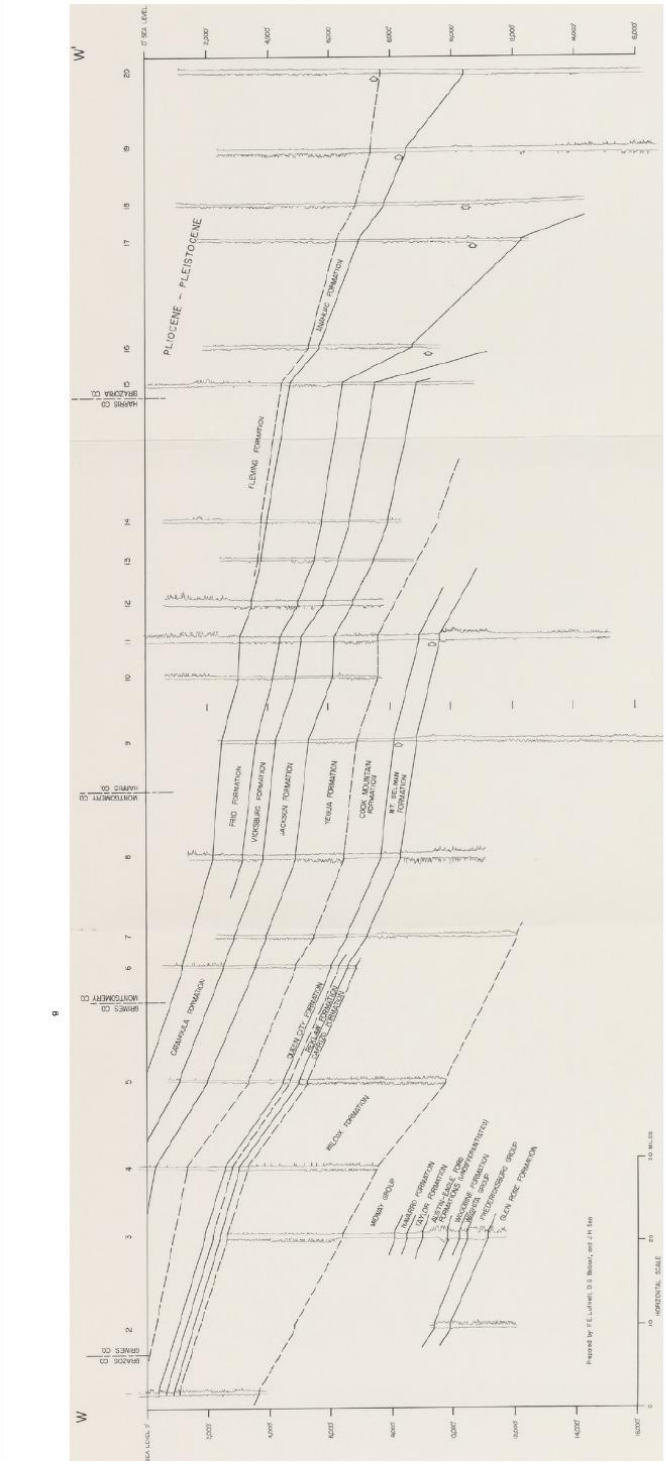

Figure 8-29: Regional cross section W to W'(Bebout, Luttrell, & Seo, 1976)

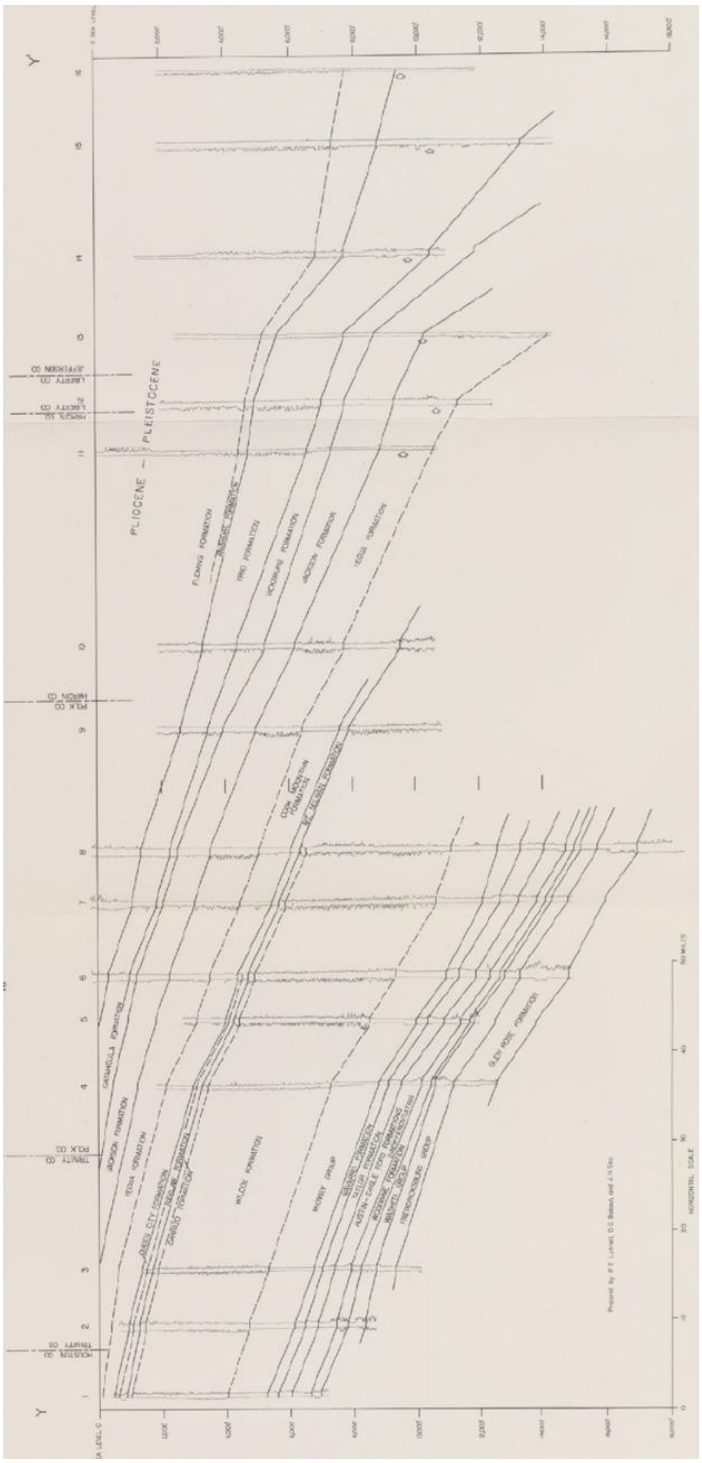

Figure 8-30: Regional cross section Y to Y'(Bebout, Luttrell, & Seo, 1976)

8.4 (Ellisor, 1994)

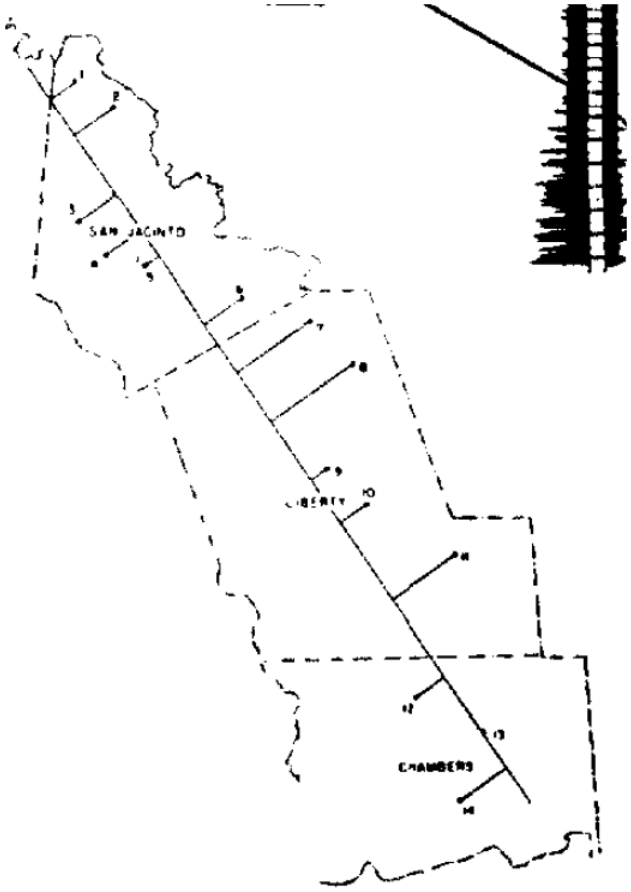

Figure 8-31: Map of the locations of regional cross sections.(Ellisor, 1994)

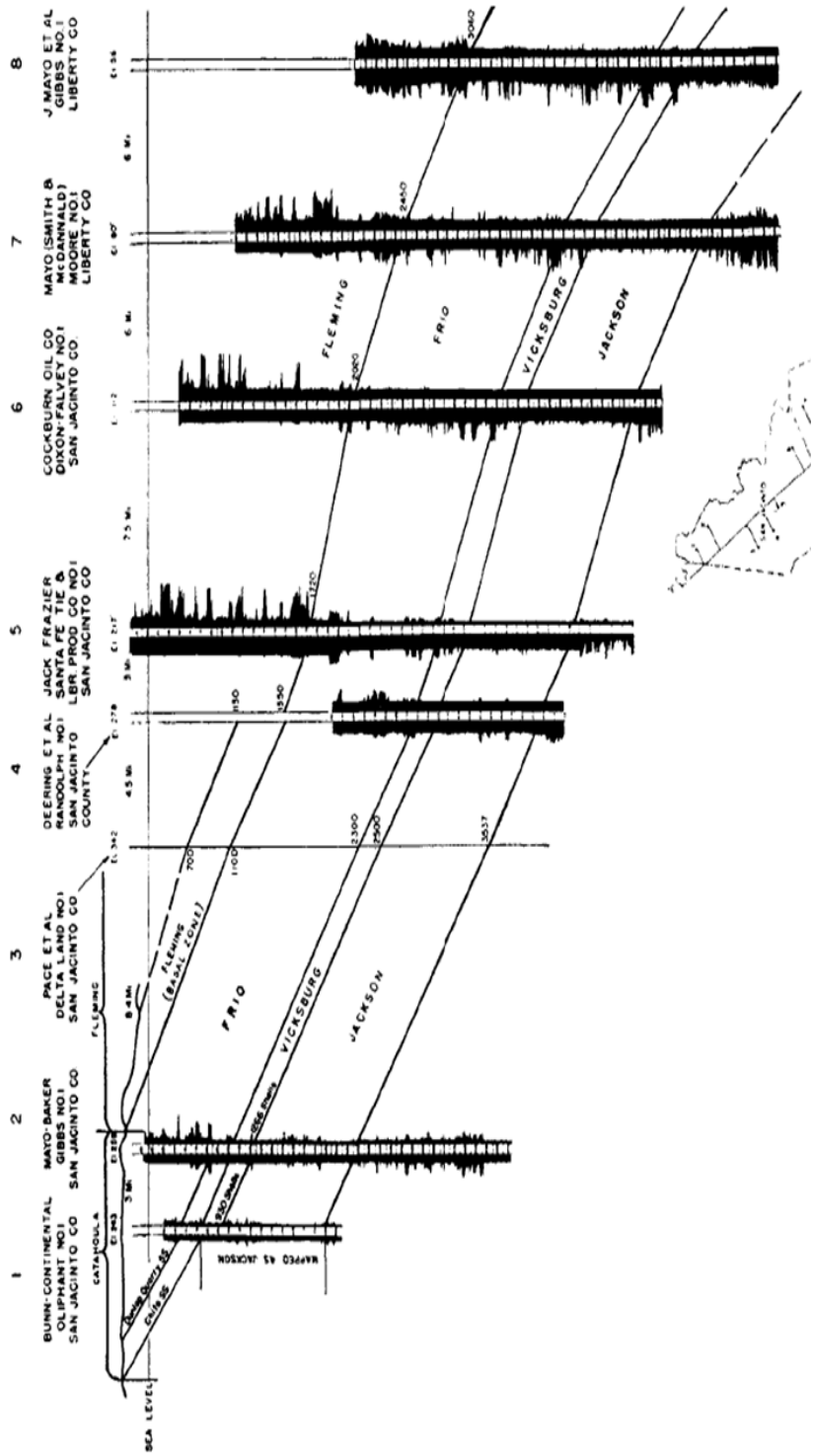

Figure 8-32: Regional cross section from wells 1 to 8(Ellisor, 1994)

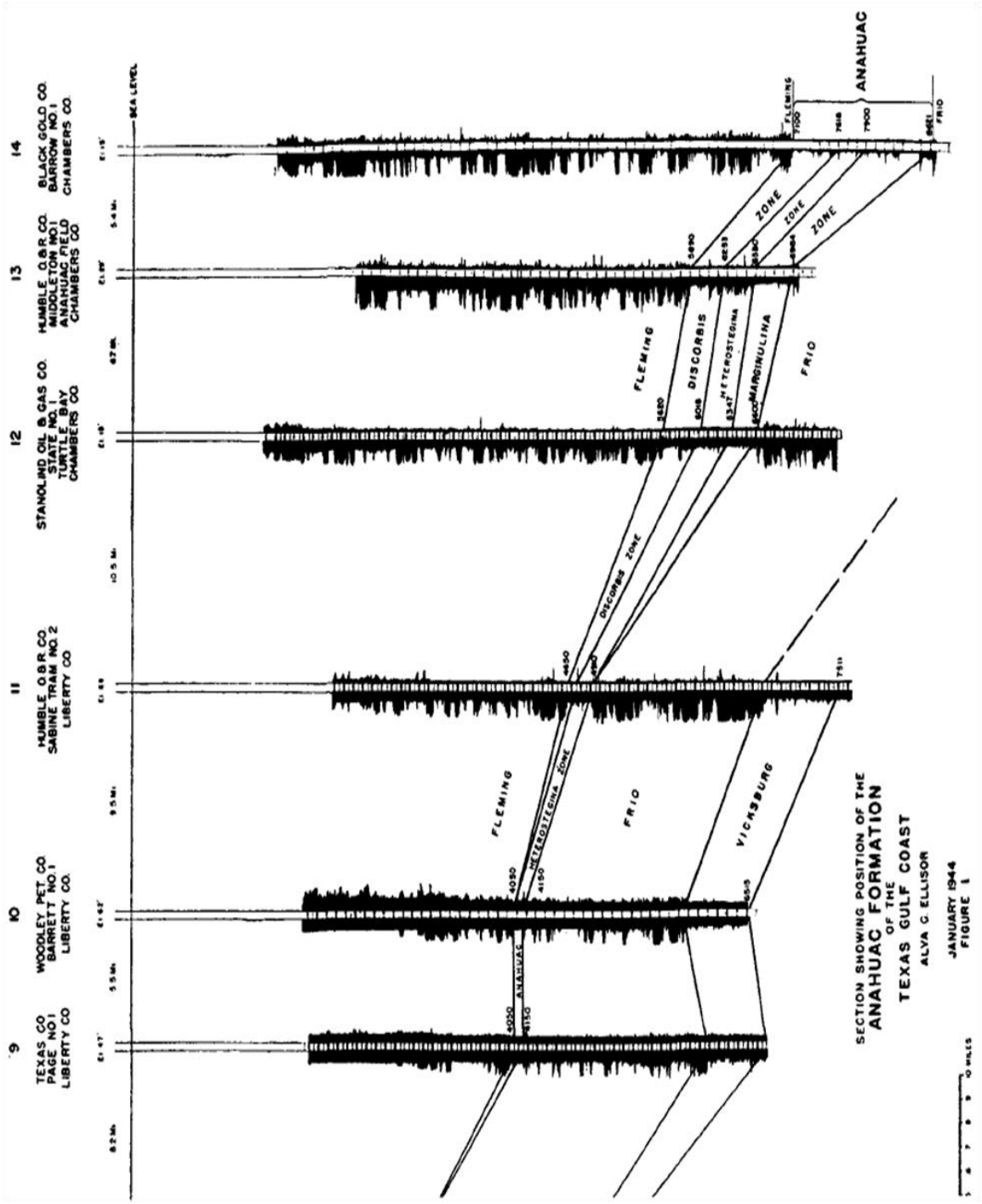

Figure 8-33: Regional cross section from wells 9 to 14.(Ellisor, 1994)

8.5 (Greenman & Gustafson, 1953)

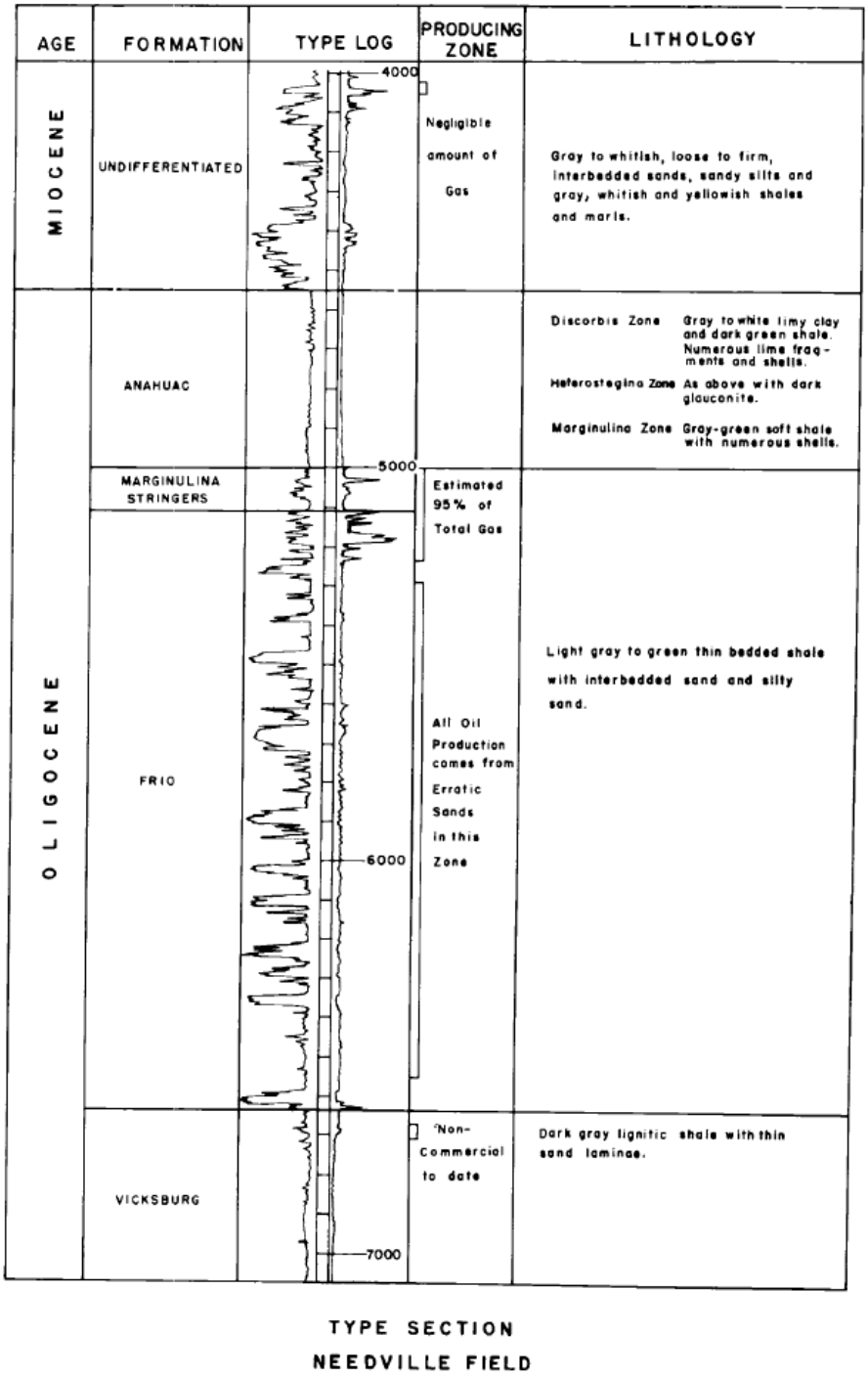

Figure 8-34: Statigraphic section of Needville Field.(Greenman & Gustafson, 1953)

Figure 8-35: Structure Contour of the top of the Frio Formation at Needville Field.(Greenman & Gustafson, 1953)

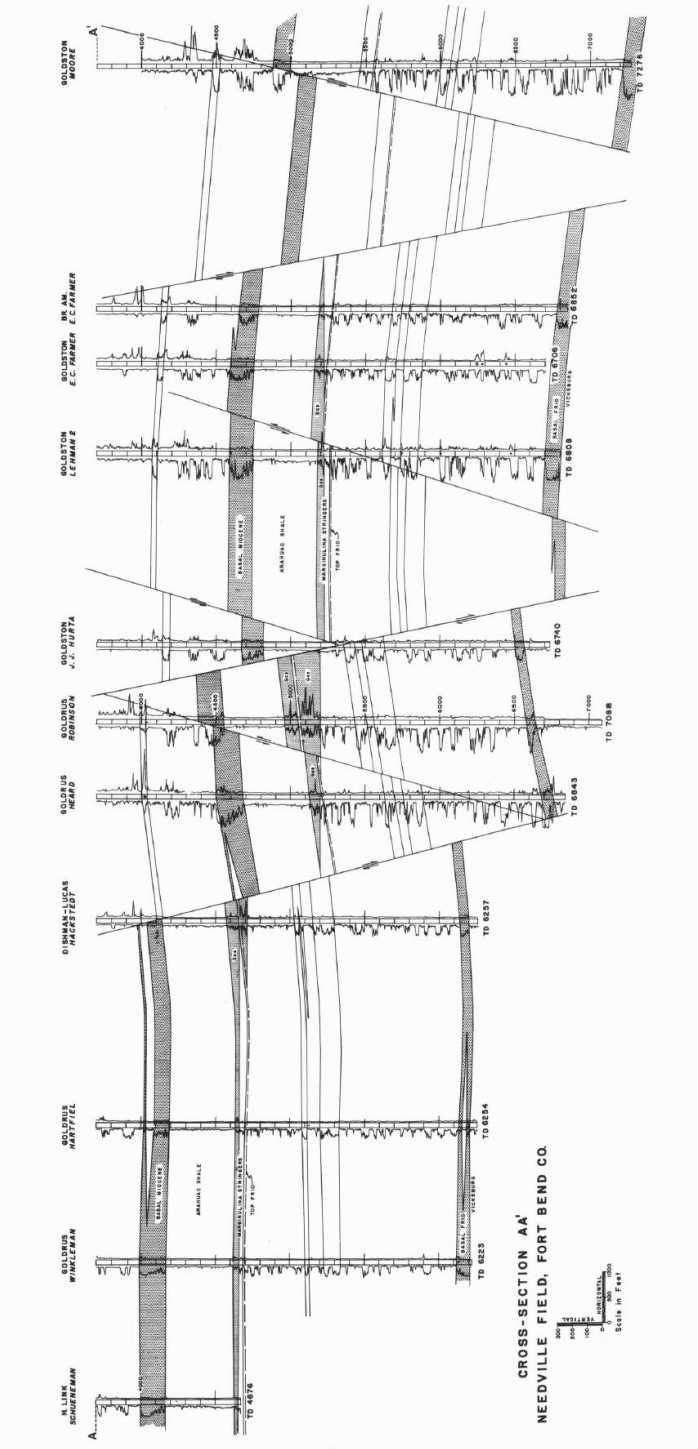

Figure 8-36: Cross section produced from eleven well logs in Needville Field.(Greenman & Gustafson, 1953)

8.6 (Hovorka, Holtz, Sakurai, & Knox, 2003)

Figure 8-37: Location map of cross section.(Hovorka, Holtz, Sakurai, & Knox, 2003)

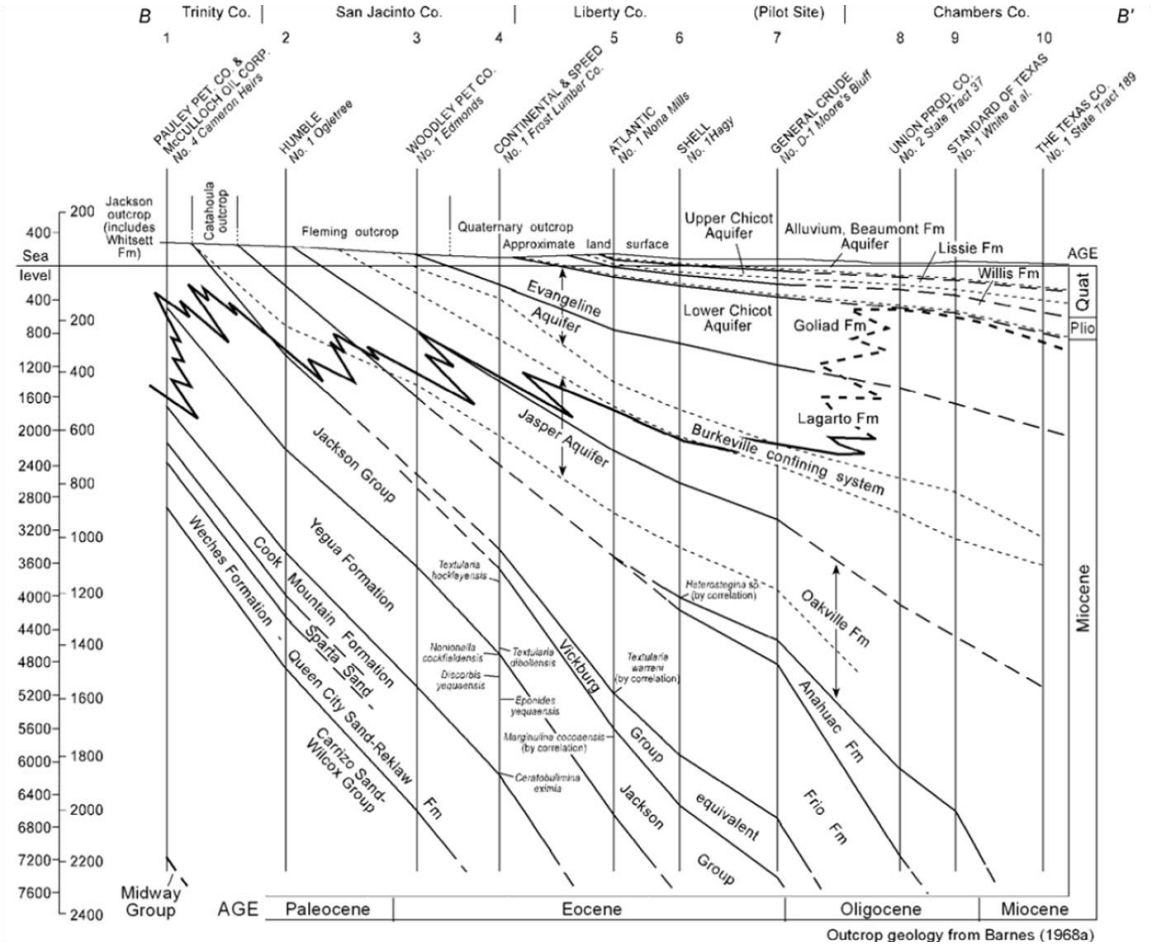

Figure 8-38: Cross section B to B'(Hovorka, Holtz, Sakurai, & Knox, 2003)

8.7 (McCarter & O'Bannon, 1933)

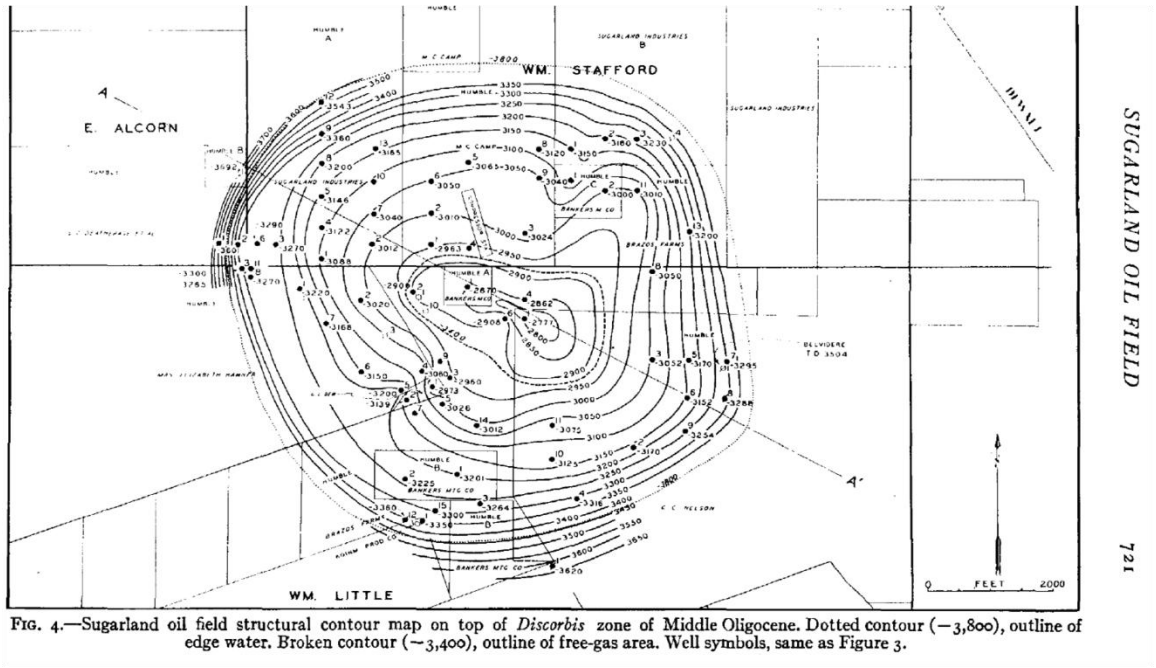

FIG. 4.—Sugarland oil field structural contour map on top of *Discorbis* zone of Middle Oligocene. Dotted contour (−3,800), outline of edge water. Broken contour (−3,400), outline of free-gas area. Well symbols, same as Figure 3.

Figure 8-39: Sugarland field structure contour map. (McCarter & O'Bannon, 1933)

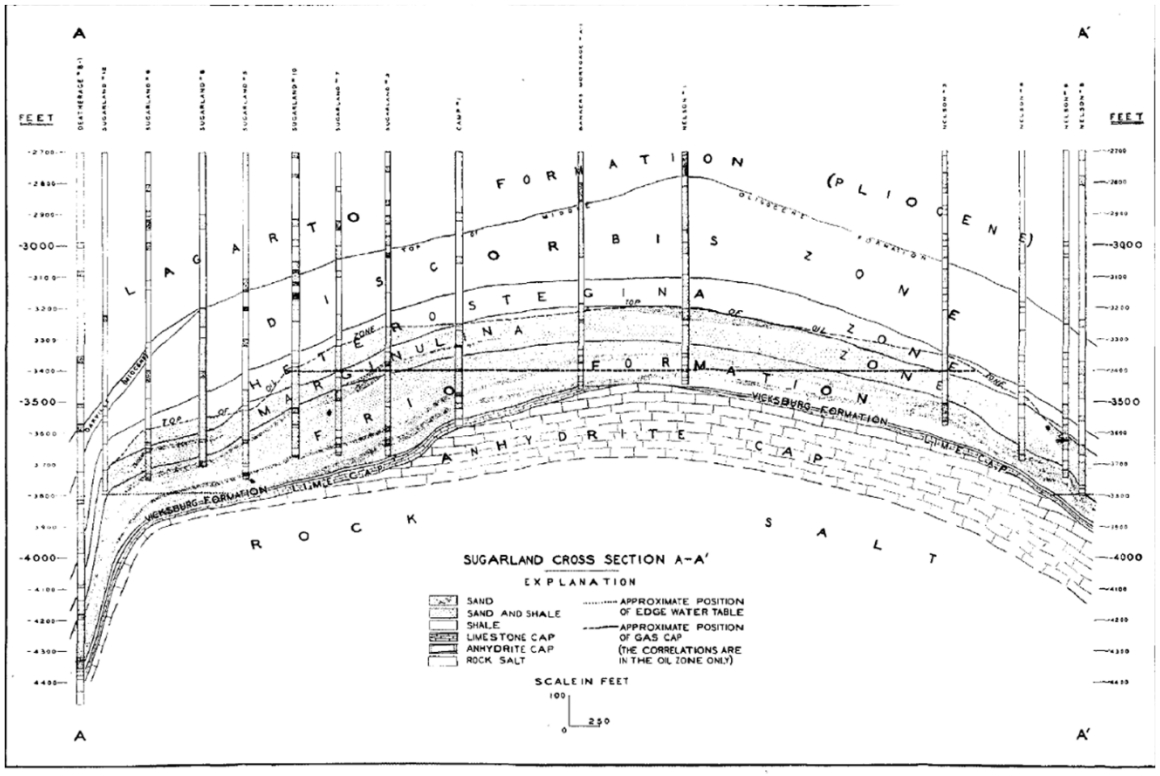

FIG. 2.—Northwest-southeast cross section of Sugarland.

Figure 8-40: Sugarland field cross section A-A'. (McCarter & O'Bannon, 1933)

8.8 (Pollack, 1953)

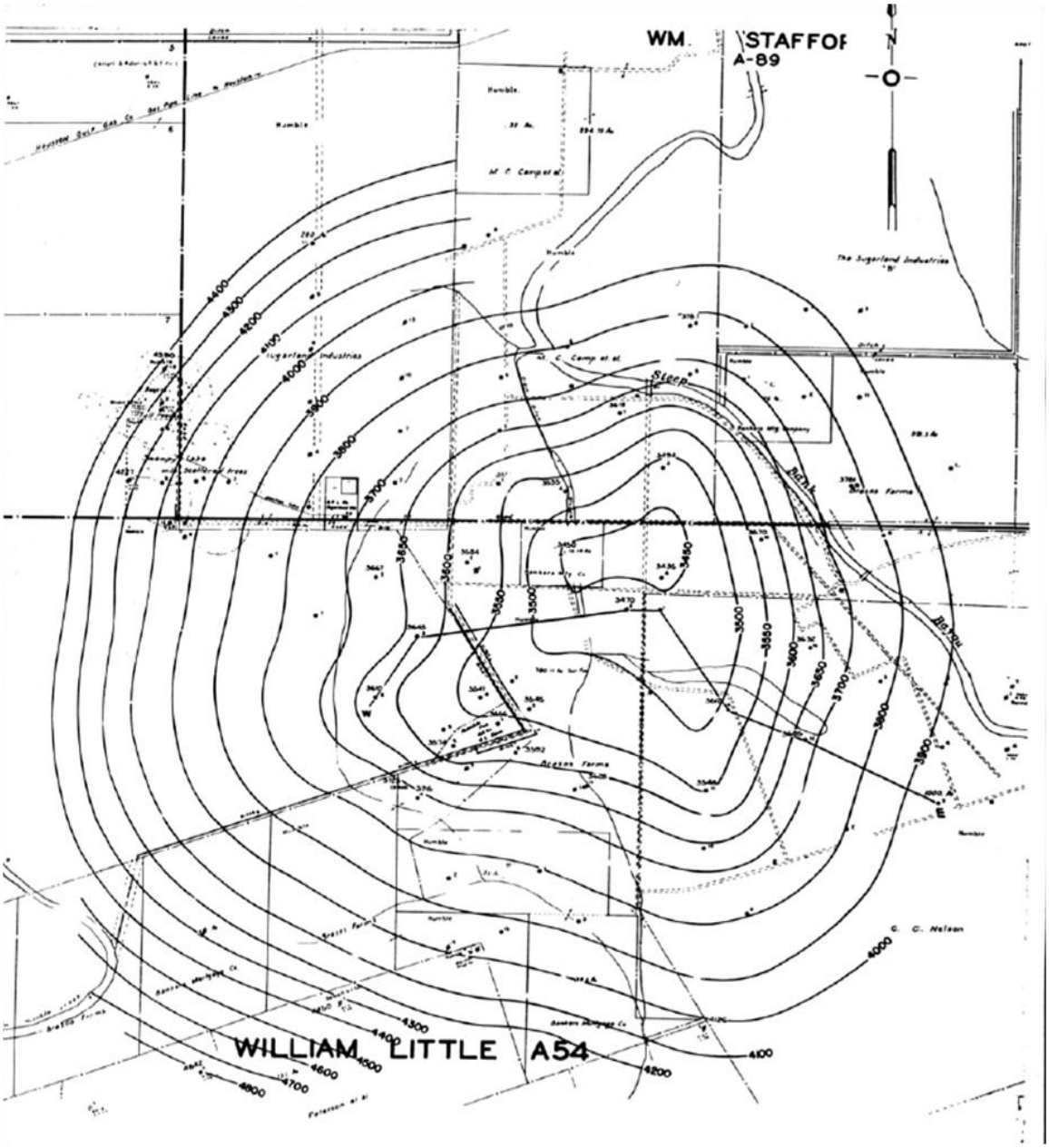

Figure 8-41: Sugarland field structure map. (Pollack, 1953)

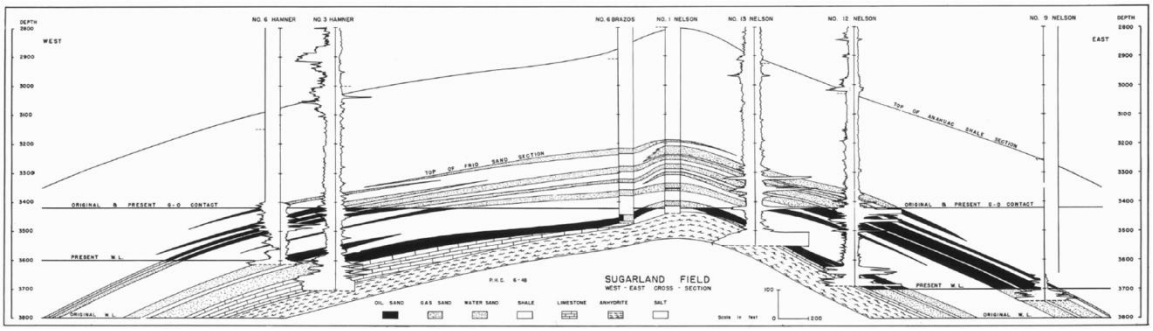

Figure 8-42: Sugarland field cross section. (Pollack, 1953)

Chapter 9 Appendix B

See CD in pocket for video.